The Graduate School

College of Earth and Mineral Sciences

POROMECHANICAL RESPONSE OF NATURALLY FRACTURED SORBING

MEDIA

A Dissertation in

Energy and Mineral Engineering

by

Hemant Kumar

Submitted in Partial Fulfillment
of the Requirements
for the Degree of

Doctor of Philosophy

May, 2014

The dissertation of Hemant Kumar was reviewed and approved* by the following:

Derek Elsworth
Professor of Energy and Geo-Environmental Engineering
Dissertation Co-Advisor
Co-chair of Committee

Jonathan P. Mathews
Assistant Professor of Energy and Mineral Engineering
Dissertation Co-advisor
Co-chair of Committee

Zuleima T. Karpyn
Associate Professor of Petroleum and Natural Gas Engineering

Chris Marone
Professor of Geosciences
Associate Department Head of Graduate Programs

Denis Pone
Special Member
ConocoPhillips, Bartlesville, OK

Luis F. Ayala H.
Associate Professor of Petroleum and Natural Gas Engineering
Associate Department Head for Graduate Education

*Signatures are on file in the Graduate School

ABSTRACT

The injection of CO_2 in coal seams has been utilized for enhanced gas recovery and potential CO_2 sequestration in unmineable coal seams. It is advantageous because as it enhances the production and significant volumes of CO_2 may be stored simultaneously. The key issues for enhanced gas recovery and geologic sequestration of CO_2 include (1) Injectivity prediction: The chemical and physical processes initiated by the injection of CO_2 in the coal seam leads to permeability/porosity changes (2) Up scaling: Development of full scale coupled reservoir model which may predict the enhanced production, associated permeability changes and quantity of sequestered CO_2. (3) Reservoir Stimulation: The coalbeds are often fractured and proppants are placed into the fractures to prevent the permeability reduction but the permeability evolution in such cases is poorly understood. These issues are largely governed by dynamic coupling of adsorption, fluid exchange, transport, water content, stress regime, fracture geometry and physiomechanical changes in coals which are triggered by CO_2 injection. The understanding of complex interactions in coal has been investigated through laboratory experiments and full reservoir scale models are developed to answer key issues.

Chapter I of this dissertation explores the effect of gas pressure and stress on the permeability evolution of coalbed methane (CBM) reservoirs infiltrated by carbon dioxide. Typically the recovery of methane induces coal shrinkage and the injection of CO_2 induces coal swelling respectively increasing or decreasing permeability for constrained coals. Permeability evolution was quantified for moisture equilibrated and partially dried bituminous coal samples together with the transitions caused by sequential

exposure to different gases. The experimental measurements of permeability evolution

was conducted on a coal from the Uinta basin infiltrated by helium, methane and carbon

dioxide under varying gas pressure (1-8 MPa) and moisture content (1-9% by mass)

while subjected to constant applied stresses (10 MPa). Permeability decreases with

increased moisture content for all the gases (He, CH_4 and CO_2). The decrease in He

permeability may be as high as ~100 folds if the moisture content is increased from 1% to

9% by mass. Swelling induced by sorption of CH_4 and CO_2 in the coal matrix reduces

permeability by 5 to 10 fold depending on the gas injected and the moisture content.

Swelling increases with gas pressure to the maximum (strain based estimation 5%) at a

critical pressure (~4.1 MPa) corresponding to maximum adsorption capacity. Beyond this

threshold effective stress effects dominate. Permeability evolution was determined in

bituminous coal for various moisture contents, effective stresses, and gas pressures to

propose a mechanistic model. Also, this model explains the published data for

permeability evolution on water saturated Pennsylvanian anthracite coal. This model was

used to investigate the performance of prototypical ECBM projects. In particular the

effect of the permeability loss examined with the injection of CO_2. This response is

defined in terms of two conditions: reservoirs either above (under-) or below (above-) the

saturation pressure that defines the permeability minima in the reservoir. For

oversaturated reservoirs withdrawal will always result in decreased permeability at the

withdrawal well unless the critical pressure is transited. Similarly permeability will

decrease at the CO_2 injection well unless the pressure increase is sufficiently large to

overcome the reduction in permeability due to CO_2 - typically of order of one to a few

MPa. For undersaturated reservoirs the permeability will always increase at the withdrawal well and can only increase at the injection well if the critical pressure is transited and further exceeded by one to a few MPa. These observations provide a rational method to design injection and recovery strategies for ECBM that account for the complex behavior of the reservoir including the important effects of moisture content, gas composition and effective stress.

Chapter II of this dissertation explores the effect of CO_2 injection on production, permeability evolution and permeability variability using a full scale reservoir model. Enhanced coalbed methane (ECBM) can be recovered by injecting a gas such as carbon dioxide into the reservoir to displace methane. The contrast between density, viscosity, and permeability of the resident and displacing fluids affects the efficiency of ECBM recovery. The prediction of earlier breakthrough becomes complex as the permeability may vary by orders of magnitude during gas injection and methane recovery. Predominantly, the reservoir permeability is modulated by the pore pressure of the sorptive gas (CH_4 and CO_2) and effective stresses. Here we explore the possibility of early breakthrough and its implications for managing coalbed reservoirs during CO_2 assisted ECBM. A coupled finite element (FE) model of binary gas flow, diffusion, competitive sorption and permeability change is used to explore the effect of CO_2 injection on net recovery, permeability evolution and injectivity in uniform and homogeneously permeable reservoirs. This effect is evaluated in terms of dimensionless pressure (p_D), permeability (k_D) and fracture spacing (x_D) on the recovery of methane and permeability evolution for ECBM and non-ECBM scenarios. We have considered

two scenarios (4MPa and 8 MPa) of constant pressure injection of CO_2 for ECBM. The increase in production rate of CH_4 is proportional to k_D but inversely proportional to x_D.

Further, a reservoir with initial permeability heterogeneity was considered to explore the effect of CO_2 injection on the evolution of permeability heterogeneity – whether heterogeneity increases or decreases. The evolution of permeability heterogeneity is investigated for the same two CO_2 injection scenarios. For the specific parameters selected, the model results demonstrate that: (1) The injection of CO_2 in coalbed reservoirs increases the production nearly 10 fold. (2) At higher injection pressures the recovery is rapid and the production increases dramatically - the production increases 2 fold on increasing the CO_2 injection pressure from 4 MPa to 8 MPa (3) However, CO_2 breakthrough occurs earlier at higher injection pressures. (4) The permeability heterogeneity in the reservoir is reduces after a threshold time (~500 days) although the overall heterogeneity is increased relative to the initial condition is overall increased for both non-CO_2 and CO_2 injection scenarios. This indicates that the homogenizing influence of CO_2-sorption-swelling is outpaced by CH_4-desorption-shrinkage and effective stress influences. This leaves the reservoir open to short-circuiting and earlier breakthrough of CO_2 rather than having this effect damped-out by the homogenizing influence of swelling. (5) The cumulative volume of CO_2 produced and stored in the reservoir is proportional to the injection pressure.

Chapter III explores the effect of proppant embedment on permeability evolution. Proppant are often placed in hydraulic fractures to retain the enhanced permeability for longer periods. However, the permeability enhancement may be mitigated due to

proppant embedment into the natural/artificial fractures of coalbed methane reservoirs. The reduction in fracture aperture occurs either when CO_2-induced coal softening causes proppant penetration into the coal fracture surface or coal swelling encroaches into the propped facture during CO_2 assisted enhanced coalbed methane recovery. While coal swelling is a well-established phenomenon, there is limited investigation into coal softening under stressed conditions. Here we investigate permeability transformations at simulated insitu conditions through a suite of laboratory experiments conducted on selected high-rank coals and a granite cores with an artificial saw-cut fracture containing proppant. The permeability of the artificial fracture is measured for both non-sorbing gas (He) and a sorbing gas (CO_2) at constant confining stress of 10MPa. Permeability was also measured with an idealized case of a uniform monolayer of #70-140 mesh proppant sand within the fracture. The increase in He permeability may be as high as ~10 fold if monolayer proppant is sandwiched in the coal or granite fracture. Similar increase is observed in the case of sorptive gas (CO_2) permeability. An exponential increase in permeability is observed with gas pressure for both coal and granite without proppant as expected. However, the permeability decreases due to coal swelling and then increases due to reduced effective stress with gas pressure in case of propped fracture on injection of CO_2. Optical profilometry pre- and post experimental suite is used to quantify proppant embedment, if occurs, in the coal fracture surface. Infrequent and isolated pits, similar to the size of a sand grain, were observed post experimental suite. Sparsely distributed surface indentation on completion of experimental suite, suggests an insignificant contribution of coal softening towards permeability reduction. Thus, a large

reduction in permeability can only be attributed to coal swelling. The increase in surface roughness post exposure to CO_2 by about a fraction of microns indicates a slight irreversible structural rearrangement with CO_2 uptake and loss. A mechanistic model is developed to explain the permeability evolution in a propped artificial fracture on injection of CO_2. The permeability evolution trends alike 'U-shape' with gas pressure at constant confining stress. The excellent fit between model and experimental observations indicates a robustness of the model however more work is needed for the model to run in predictive capacities.

Chapter IV reports measurements of permeability evolution in shales infiltrated separately by non-sorbing (He) and sorbing (CO_2) gases under varying gas pressures, confining stresses and deviatoric stresses. Experiments are completed on Pennsylvanian shales containing both natural and artificial fractures under non-propped and propped conditions. We use observations for permeability evolution in other sorbing media (coal, Kumar et al., 2012) to codify the response for shale. It is observed that for a naturally fractured shale, the He-permeability increases by ~15% as effective stress is reduced by increasing the gas pressure from 1 MPa to 6 MPa at constant confining stress of 10 MPa. Conversely, the CO_2-permeability reduces by a factor of two under similar conditions. Permeability of the core recovers to the original magnitude when the core is resaturated by a non-adsorbing gas, despite prior CO_2 exposure. A second core is split with a fine saw to create a smooth artificial fracture and the permeabilities measured for both non-propped and propped fractures. The He-permeability of a monolayer sand-propped artificial fracture is ~2-3 fold that of a non-propped fracture. Upon increasing the gas

pressure, the He-permeability of the propped fracture increases under constant confining stress. Conversely, the CO_2-permeability of the propped fracture decreases by between one-half to one-third as the gas pressure increases from 1 to 4 MPa at a constant confining stress. We attribute the reduction in permeability to sorption-induced swelling in the organic material of the shale. The permeability of the non-propped shale fracture increases with gas pressure, at constant confining stress, due to the absence of rock bridges that commonly occur in naturally fractured samples. Although the permeability evolution of non-propped and propped artificial fractures in shale are found to be similar to those observed in coal, the extent of permeability reduction by swelling is much lower in shale due to its lower organic content. The surface roughness and peak-to-valley differential for the artificial fracture surfaces are quantified by optical profilometry. Initial values of surface roughness and peak-to-valley differential height are 4.1 μm and 77.9 μm, respectively, which increases to 6.1 μm and 122.4 μm at completion of experiments - indicating the significant influence of proppant indentation into the surface of the fracture in shale. A mechanistic model representing permeability evolution in sorbing media is applied to describe permeability evolution in shale. This model characterizes the 'U-shaped' variation of permeability with gas pressure typical for sorbing media and apparent for shales.

The chapters of this dissertation correspond with a series of four papers either published or in preparation. By order of chapter appearance, these papers are:

1) Kumar, H., Elsworth, D., Liu, J., Pone, D., Mathews, J.P., 2012. Optimizing enhanced coalbed methane recovery for unhindered production and CO_2 injectivity. International Journal of Greenhouse Gas Control 11, 86-97.

2) Kumar, H., Elsworth, D., Liu, J., Pone, D., Mathews, J.P., 2013. Effect of CO_2 Injection on Homogeneously and Heterogeneously Permeable Coalbed Reservoirs. Submitted to Fuel.

3) Kumar, H., Elsworth, D., Liu, J., Pone, D., Mathews, J.P., 2013. Permeability evolution of propped artificial fractures in coal. Submitted to International Journal of Coal Geology.

4) Kumar, H., Elsworth, D., Mathews, J.P., Marone, C., 2013. Permeability evolution in sorbing media: Analogies between organic-rich shale and coal. In preparation to Geofluids.

Table of Contents

List of Tables

List of Figures

Acknowledgments

I express my sincere gratitude towards my Ph.D. thesis advisor Dr. Derek Elsworth. Without his continuous support, motivation, patience, knowledge and effort to ensure the highest quality in research, my walk through these few important years of my life wouldn't have been as enthusiastic and fulfilling. Also, my gratitude extends to my co-advisor Dr. Jonathan P. Mathews for his guidance and help throughout my graduate studies starting from the time I joined him for my Masters degree. I would like to thank my Ph.D. committee members: Dr. Zuliema Karpyn and Dr. Chris Marone for their time, encouragement and insightful comments.

I would also like to thank the Department of Energy and Mineral Engineering for their carefully designed course structure for the Petroleum degree which provided me the relevant industrial skills in this field. The 'Integrative Design' course in particular was most helpful in shaping me as a team player. I am thankful to ConocoPhillips and ExxonMobil for their financial support which made this work possible.

I am very grateful to my friends and colleagues at G^3 Centre and Rock Mechanics Lab as well as my fellow lab mates: Baisheng, Divya, Gan, Ghazal, Roozbeh, Shugang, Taha and Tom who also provided me considerable support. My special thanks to Steven Swavely, Research Support Technician at Rock Mechanics lab, for his readiness to help and keeping the lab a safe and enjoyable place.

My time at Penn State was made enjoyable in large part due to the emotional support and care of my friends Sarmishtha, Rakesh, Yasharth, Manu, Satyam, Sumit,

Bajpai and Swati who became my family away from home during both good and difficult times.

Lastly, I would like to thank my father Shri Hari Prakash Sharma and Late Smt. Kamlesh Sharma for their blessings. I dedicate this thesis to my grandfather Late Shri Nandlal Sharma and my grandmother Late Smt. Radha Devi without whose encouragement during the last few years, completion of my degree would have been a distant dream. It is unfortunate that I cannot share this moment of accomplishment with them.

Chapter 1 : Optimizing Enhanced Coalbed Methane Recovery for Unhindered Production and CO$_2$ Injectivity

Abstract

We explore the effect of gas pressure and stress on the permeability evolution of coalbed methane (CBM) reservoirs infiltrated by carbon dioxide (CO$_2$). Typically the recovery of methane induces shrinkage and the injection of CO$_2$ induces swelling respectively increasing or decreasing permeability for constrained coals. Permeability evolution was quantified for moisture equilibrated and partially dried bituminous coal samples together with the transitions caused by sequential exposure to different gases. We report experimental measurements of permeability evolution in a coal from the Uinta basin infiltrated by helium (He), methane (CH$_4$) and CO$_2$ under varying gas pressure (1-8 MPa) and moisture content (1-9% by mass) while subjected to constant applied stresses (10 MPa). Permeability decreases with increased moisture content for all the gases (He, CH$_4$ and CO$_2$). The decrease in He permeability may be as high as ~100 folds if the moisture content is increased from 1% to 9%. Swelling induced by sorption of CH$_4$ and CO$_2$ in the coal matrix reduces permeability by 5 to 10 folds depending on the gas injected and the moisture content. Swelling increases with gas pressure to a maximum (strain based estimation 5%) at a critical pressure (~4.1 MPa) corresponding to maximum adsorption capacity. Beyond this threshold effective stress effects dominate. We use permeability evolution in bituminous coal for various moisture contents, effective stresses, and gas pressures to propose a mechanistic model. Also, we showcase this

model to explain the published data for permeability evolution on water saturated Pennsylvanian anthracite coal. We use this model to investigate the performance of prototypical ECBM projects. In particular we examine the effect of the permeability loss with injection of CO_2. We define response in terms of two conditions: reservoirs either above (under-) or below (above-) the saturation pressure that defines the permeability minima in the reservoir. For oversaturated reservoirs withdrawal will always result in decreased permeability at the withdrawal well unless the critical pressure is transited. Similarly permeability will decrease at the CO_2 injection well unless the pressure increase is sufficiently large to overcome the reduction in permeability due to CO_2 - typically of order of one to a few MPa. For undersaturated reservoirs the permeability will always increase at the withdrawal well and can only increase at the injection well if the critical pressure is transited and further exceeded by one to a few MPa. These observations provide a rational method to design injection and recovery strategies for ECBM that account for the complex behavior of the reservoir including the important effects of moisture content, gas composition and effective stress.

1 Introduction

Full scale exploration in the Uinta basin began in the 1990s. This basin has 10 trillion cubic feet of recoverable CBM reserves (EPA, 2004). There were 500 CBM wells in the basin with cumulative production of 75.7 billion cubic feet in 2000 (EPA, 2004). The Uinta basin has high CH_4 content ranging from 250 to 400 scf/ton (US-DOE, 2004) with the highest recovery factor amongst all the basins at 89% (Reeves, 2003). Injection of CO_2 in unmineable coal seams provides 'value-added' sequestration with benefits such as enhanced coalbed methane recovery with lower net-cost (Reeves, 2003), making unmineable coals potentially attractive sequestration sites. Coalbeds are commonly self-sourcing and low permeability (on the order of fractions of milliDarcies) gas reservoirs with recovery enabled through reservoir pressure depletion by water removal (Rogers, 1994). Various studies on laboratory and pilot plant scales demonstrate that geomechanical processes coupled with gas uptake or loss evolution during the ECBM recovery process affect the dynamic permeability and hence production (Gu and Chalaturnyk, 2005; van Bergen et al., 2009).

Coal shrinkage and swelling with gas desorption/adsorption has an important influence on the evolution of permeability (Bustin et al., 2008; Cui et al., 2007a; Harpalani and Chen, 1995; Kelemen et al., 2006; Seidle and Huitt, 1995b). Coal swells with adsorption of CO_2 and develops compactive stresses if mechanically constrained (Day et al., 2010; Pone et al., 2010; Reucroft and Patel, 1986; Siemons and Busch, 2007). Coal swelling has been implicated as observed reductions in permeabilities during ECBM operations at pilot plant scale (Durucan and Shi, 2009; Kiyama et al., 2011; van Bergen et

al., 2006). Gas adsorption and related swelling is largely impacted by sorption capacity, coal rank and the composition of the permeating gas (Chikatamarla et al., 2004b; Chikatamarla et al., 2004a; Levine, 1996; Pone et al., 2010). The uptake of gas by coal at various pore pressures is often represented by the sorption isotherm (Kelemen et al., 2006; Levine, 1996). The preferential sorption of CO_2 over CH_4 results in net swelling of the coal matrix (Chikatamarla et al., 2004a; Gu and Chalaturnyk, 2005; Levine, 1996) that closes or reduces the aperture of existing cleats and result in a net reduction in permeability during CO_2 injection for constrained coals. At higher gas pressures, this reduction in permeability is counteracted by dilation in fractures due to elevated pore pressures and reduced effective stress (Palmer and Mansoori, 1998a).

The presence of water in cleat/micropores may also change its mechanical and chemical interaction. There are three types of water forms present in the organic portion of coal, namely, free water, bound water and non-freezing water (Norinaga et al., 1997). The water present in the coal matrix which does not crystallize under subzero conditions is referred as non-freezing water (Norinaga et al., 1997; Unsworth et al., 1988). Presumably, they influence gas transport differently. Free water may inhibit the flow of gas by blocking cleats and external surfaces, while bound water may reduce the adsorption capacity for sorbing gas in micropores. Moisture often swells coals and reduces adsorption capacity for CH_4 and CO_2 (Day et al., 2008; Joubert et al., 1974; Kelemen et al., 2006; Levy et al., 1997; Pan et al., 2010; van Bergen et al., 2009). The presence of elevated water content is thought to reduces the sorptive capacity of CH_4 and CO_2 by plugging the microstructures (Levine, 1991; Pan and Connell, 2012) reducing capacity and the extent of sorption-induced swelling. However, the bulk water can hold

dissolved CO_2 increasing its capacity (Chikatamarla et al., 2009). The moisture in coal is dependent on the rank, oxygen functionality, and pore size distribution/fracture network. This can vary widely over the rank, for example, Australian lignite coals often containing up to 60% moisture by mass with much lower values for bituminous coals (Durie, 1991). The bulk water present in the meso- and macropores/fractures may significantly influence the permeability. While, the bound water associated with the oxygen functionality of the coal often in micropores may influence the gas capacity. Moisture in the micropores is thought to be particularly important in the blocking of access to CO_2 gas to the preferential sorption sites (Prinz and Littke, 2005; Radliński et al., 2009). The moisture content reduces the capacity of CH_4 in bituminous coal up to a critical point, with additional moisture having little effect (Joubert et al., 1973, 1974).

Coal permeability is also a function of net effective stress (Brace et al., 1968; Gash et al., 1993). Cleat closure can occur with increasing effective stress resulting in the closure of smaller cleats, and a reduction in permeability as the interconnections between pores and cleats are reduced (Soeder, 1991). Empirical relationships between permeability and effective stress have been proposed (Bai et al., 1995; Durucan and Edwards, 1986; Min et al., 2009; Seidle et al., 1992; Somerton et al., 1975) including the role of stress cycling on permeability loss (Harpalani and Chen, 1995; Somerton et al., 1975).

Given the complexity of the processes various models have been suggested to predict permeability transformations. These models may be divided into analytical and numerical coupled flow models (Palmer, 2009). Analytical models are further divided into stress based (Bai et al., 1993a; Durucan and Shi, 2009; Liu et al., 2010a; Palmer,

2009; Palmer and Mansoori, 1998a; Pan et al., 2010; Shi and Durucan, 2005; Shi and Durucan, 2008) and strain based (Clarkson et al., 2010; Gu and Chalaturnyk, 2006; Harpalani and Chen, 1995; Levine, 1996; Liu et al., 2010b; Liu et al., 1997; Ouyang and Elsworth, 1993) models. Until recently, most models described the permeability empirically as a function of sorption induced swelling and effective stress. Such analytical models are simple, easy to use with acceptable accuracies and have demonstrated acceptable fits for San Juan basin methane production data. However, the understanding of cumulative or lumped effect of physical processes (sorption induced swelling, effective stress and moisture-influenced swelling effects) remains limited. Coupled flow models have received increased attention because of their ability to deconvolve important first order processes that contribute to permeability evolution (Gu and Chalaturnyk, 2005; Liu and Rutqvist, 2010a; Liu et al., 2010b; Liu et al., 2011; Mazumder and Farajzadeh, 2010; Pan and Connell, 2007; Pan et al., 2010; Robertson and Christiansen, 2007; Siriwardane et al., 2009b; Wu et al., 2010a; Wu et al., 2010b; Wu et al., 2010c), but unfortunately the processes are not well constrained.

In this work the evolution of permeability is explored for Uinta basin bituminous coal to account for the important first order effects of effective stresses, gas pressure, and moisture content on permeability evolution. These characterizations are constrained by laboratory observations, fit to appropriate mechanistic models (Izadi et al., 2011; Min et al. 2009) and applied to the optimized recovery of CH_4 from coalbeds under CO_2 injection during ECBM recovery.

2 Experimental Methods

We complete forced fluid percolation experiments on eight cylindrical samples stressed to in situ conditions. These experiments use He, CH4, CO2 as permeants and allow the role of swelling on the dynamic evolution of permeability to be examined.

2.1 Samples

A block sample of coal was collected from an underground coal mine from the subbituminous/bituminous region of the Uinta basin (Colorado, USA). The calorific value of this coal on a dry basis was 12000 BTU/lb (ASTM D388, 2005). The fixed carbon, volatile material and ash yield on the dry basis were determined as 56.99%, 38.31% and 4.70% (ASTM D7582, 2010) indicating bituminous rank. Eight cylindrical core samples of 2.5cm diameter and 5cm length were sampled horizontally (into the bedding plane) from immediately adjacent lithographic similar sites. The natural fracture network (butt and face cleats) had approximately uniform spacing in these samples (~10mm). Moisture content, defined as the mass of water present per mass of coal, was 5% by mass for the as-received sample (ASTM, 2010). Coal can have equilibrium moisture values as high as 60% for Australian Brown coals depending on rank and mineral matter contributions (Durie, 1991). Porosity of the as-received sample, including the fracture and cleat network, was 16% using He as the injecting fluid. The methane sorption capacity of dry coal core under 10MPa of constant confining stress was 0.12 mmol/gm. Two samples were kept in a vacuum at 70˚C for a few hours followed by immersion in 105˚C dry air for an hour to achieve lower moisture contents. Cleats within

the other samples were pre-saturated by flow-through of moisture for 24 hrs at a rate 0.1

ml/sec prior to emplacement into a humidifier containing a saturated solution of K_2SO_4 to

maintain 97% relative humidity (ASTM, 2007). Six samples were left in the desiccators

for few months (1-4) at 40˚C, depending on the desired moisture content (up to ~9% by

mass). The moisture content in each core was determined from the core-cuttings taken

from the core prior to the experiments and assumed to be the representative of the

volumetric moisture content. Moisture equilibrated cores were used immediately, other

cores were kept in laminated argon-filled bags to limit deterioration (Glick et al., 2005).

The samples were wrapped in aluminum foil before loading into the permeability cell to

prevent any adsorption or diffusion (of CO_2 and CH_4) through the rubber jacket during

the permeability experiments. The absence of leakage and external adsorption was

confirmed by the constant equilibrium pressure profile after pulse test.

 ## 2.2 Apparatus

Experiments were completed using a simple triaxial apparatus capable of applying

defined effective stress paths and concurrently measuring permeability and sortive

capacity (Figure 1.1). All experiments were performed in a 'free expansion/shrinkage

under constant stress' mode. The apparatus comprises a tri-axial cell to confine the

sample at prescribed stresses, an axial strain gauge to monitor the shrinkage or swelling

in the axial direction, ISCO syringe pumps to apply stresses and to measure volume

strains (axial and confining), pressure transducers to monitor the upstream and

downstream reservoir pressures and a data acquisition system (DAS). The volumes of the

upstream and downstream reservoir were 17.36 and 3.1 cm^3 respectively. Additional

details of the equipment are described elsewhere (Wang et al., 2011). Pumps, transducers,

strain gauges and reservoir volumes were calibrated prior to the experiments. A transient

pulse test method (described in section 2.4) was used to determine the permeability of the

samples. The volumes of the reservoirs are significantly higher than the total adsorption

capacity of the coal cores used in the experimental suites. Pulse test gas reservoirs were

kept in a water-bath at room temperature (~20˚C) to avoid rapid temperature fluctuations.

The temperature was assumed to be constant for the duration of each pressure pulse (<30

min.). Evenly grooved end-platens enforce uniform flow in the specimen during flow

tests. Permeability was evaluated from the rate of pressure decay/gain in the

upstream/downstream reservoirs (Brace et al., 1968) assuming no sorption during the

short duration (<30 min) pulse decay experiments where the effective diffusion from the

cleats would reach of the order of 0.1mm into the 5mm cleat blocks. System was

calibrated and tested against known permeability sandstones Berea (~300md) and Crab

Orchard (~0.01md).
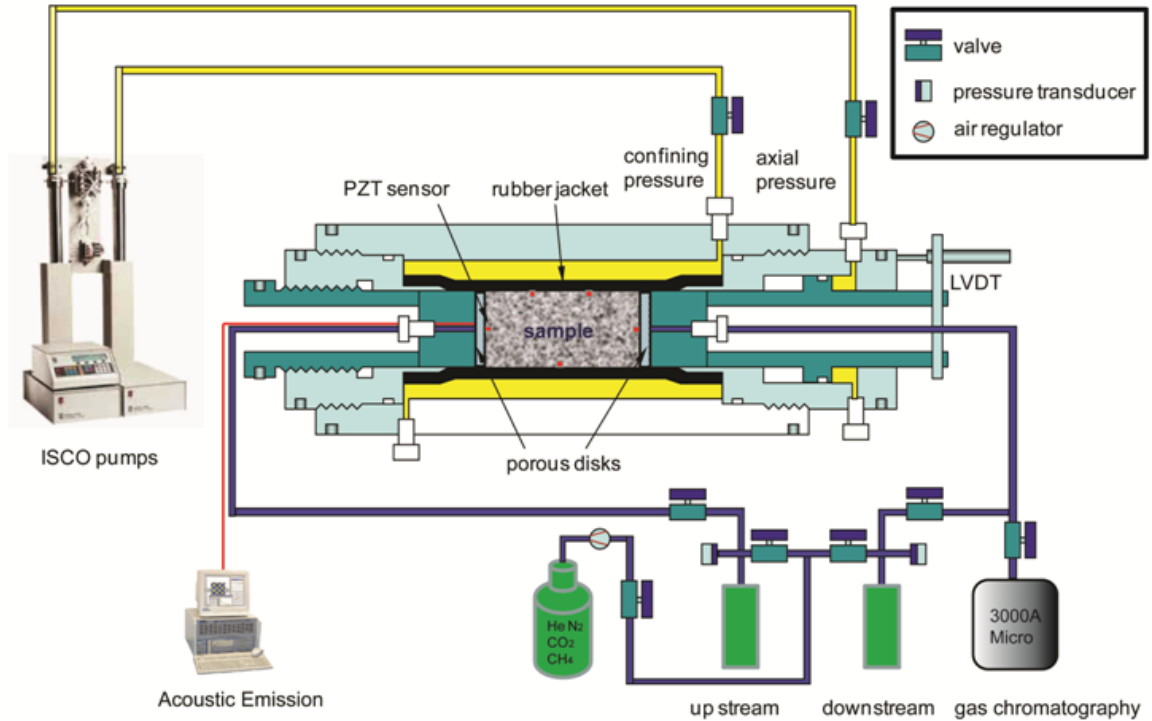
Figure 1.1: Schematic of pulse test transient system.

2.4 Procedures

Coal cores were placed within the triaxial core holder and stresses were applied. A suite of experiments was conducted to identify the critical ECBM processes. Table 1.1, provides the ranges of experimental variables and measured outputs. Experiments were completed to explore the role of gas pressure, effective stress and moisture content on the evolution of permeability for sequential sweeps of He, CH_4 and CO_2. The following experimental sequence was adopted for a given sample under constant isotropic stress with incremental gas pressures:

1. *He permeability*: He was circulated in the sample to measure baseline permeability. Here He has been considered as a non-adsorbing fluid, which is consistent with the majority of the literature.

2. *CH$_4$ permeability*: The sample was exposed to a predetermined pressure of CH$_4$ and saturation was assumed to have been achieved when the pressure transducer reading plateaued with time. The Typical time taken to achieve majority of saturation is ~4 hours. Permeability was then measured by pulse test at different gas pressures (2-8 MPa).

3. *CO$_2$ assisted sweep of CH$_4$*: The sample was sealed at the completion of step (2) and permeability was measured with the upstream reservoir charged with CO$_2$ and the downstream reservoir evacuated. This represents the process of ECBM recovery and explores the competitive exchange CO$_2$ for CH$_4$. At completion the gas mixture (CO$_2$+CH$_4$) was released from the system.

4. *CO$_2$ permeability*: The sample was vented for 12h aided by a mild vacuum (~25mm Hg). The desorbed sample was resaturated by CO$_2$ and permeability was measured.

5. *He permeability*: The sample was vented to atmospheric pressure for 12h followed by mild vacuum. The time allowed for CO$_2$ venting (three times of the saturation time) prior to He injection was deemed to be sufficient to remove majority of CO$_2$ from step 4. Then, He is recirculated through the sample to measure post-sweep permeability.

The removal of gas is required to reuse the coal core for the next permeability test in the experimental sequence. Here it may be noted that the pulse decay is not likely to result in the loss of significant moisture due to small gas-volume used for injection. The treatment used for removing the gases may have had some effect on moisture content of the coal. However, the moisture is more likely to be retained in the matrix due to its higher affinity. We do not quantify the retained gas sorption for various gases in this work. The comparison of the initial He permeability to the permeability following sorption and removal of CH_4 and CO_2 shows similar trends but with a lower permeability (~20%) indicating a combination of moisture retention that was desirable and some undesirable CO_2 retention hence the order of experimentation was kept as noted above.

All experiments were conducted at a mean total stress of 10 MPa (equivalent to and effective stress at ~1000m or ~3500 feet depth). The evolution of permeability is measured under the influence of: (i) effective stress, (ii) gas pressure and (iii) water content (S_w).

Table 1.1: Suite of variables and prescribed ranges utilized in the experiments, for gas pressure P_p, permeability k, axial stress σ_1, confining stress σ_3, and axial strain ε_a.

Experimental variables	Experimental Range	Measured Outputs
Temperature	Constant	N/A
Gas pressure	1 to 8 MPa	P_p
Moisture content	Dry (1%) to Moist (9%)	N/A
Axial stress σ_1	10 MPa	σ_1
Confining stress σ_3	10 MPa	σ_3
		ε_a
Gas type	He, CO_2, CH_4	N/A

2.5 Procedures

Coal permeability was evaluated by the transient pulse test method (Brace et al., 1968). In a typical run, a coal core is packed and placed under axial and radial stress in the triaxial apparatus as shown in Figure 1.1. A mild vacuum was applied to evacuate the air from the sample reservoir system. The core was saturated with gas (He, CH_4 or CO_2) to an equilibrium pressure before applying a pressure pulse. A pressure pulse is allowed to flow through the core from the upstream reservoir to the downstream reservoir until the pressure reaches equilibrium i.e. upstream and downstream pressures are approximately equal. This equilibrium pressure has been referred to as gas pressure. The

13

pressure pulse is significantly smaller (<10%) than the initial gas pressure in the system. We have assumed that there is insignificant additional adsorption with less than 10% increment in gas pressure. The pressure loss in the upstream reservoir and pressure gain in the downstream reservoir are recorded with time. This process is repeated until the predetermined value of gas pressure is achieved. The pressure-time profile from the experiment was used to obtain permeability, k (Brace et al., 1968).

$$\mathbf{k} = \frac{\gamma \cdot \mu \cdot L \cdot V_{up} V_{down}}{P_{eq} \cdot A \cdot (V_{up} + V_{down})} \tag{1}$$

Where permeability $k(m^2)$ is calculated from the decay parameter $\gamma(s^{-1})$ for a known gas viscosity $\mu(Pa.s)$, sample length $L(m)$, equilibrium pressure at the end of the experiment $P_{eq}(N/m^2)$ and cross sectional area of the specimen $A(m^2)$ relative to upstream/downstream reservoir volumes $V_{up/down}(m^3)$, measured initial pressure $p_{up/down0}(N/m^2)$ and transient upstream/downstream reservoir pressures $p_{up/down}(N/m^{2.})$.

$$\gamma = \frac{\log \left(\frac{d(p_{up} - p_{down})}{(p_{up0} - p_{down0})} \right)_t}{dt} \tag{2}$$

The value of γ is the slope of the line obtained from a $\log \left(\frac{d(p_{up} - p_{down})}{(p_{up0} - p_{down0})} \right)$ versus time straight line plot. This method yields a single value of permeability for a single pulse.

Pressure-decay in the upstream reservoir and complementary pressure-gain in the downstream reservoir for a typical pulse test in moist coal with non-adsorbing (He) gas is

14

shown in Figure 1.2. Pulse-decay data are reduced for $dP_o = p_{up^o} - p_{down^o}$, $dP_t = p_{up} - p_{down}$ and P_{eq}. A typical set of observations was used for the calculation of percentage error in the permeability. Uncertainties in measured pressure and length are ±0.03MPa and ±0.01mm respectively with a conservative assumption of 1% relative error in volume measurements. From these presumed errors, all values for permeability are accurate to within 9% determined conservatively for equation (1). Errors were calculated using an 'error propagation' method utilizing a Jacobian matrix (Wolfram Mathematica 7.2, 2009).
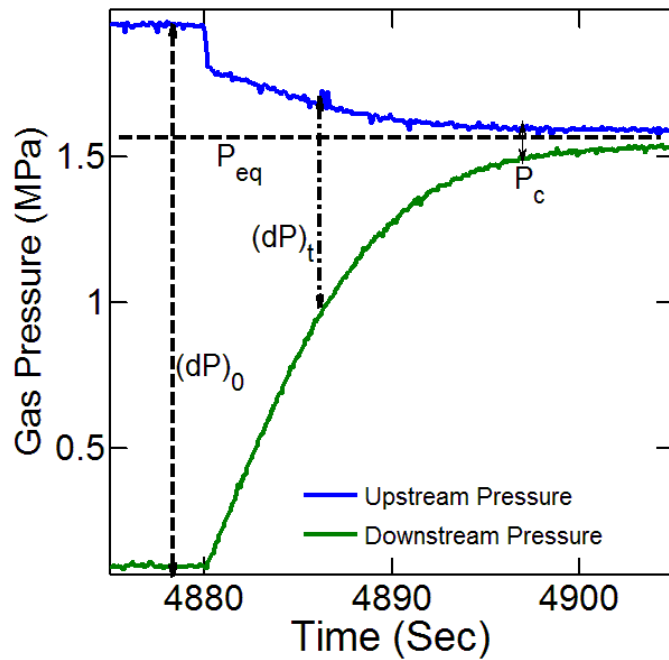
Figure 1.2: Typical pressure-pulse decay in moist coal with non-adsorbing gas (Helium) during a transient pulse decay permeability test.

3 Results and Discussions

Forced sequential injections of He, CH_4 and CO_2 were performed in coal cores at various moisture contents and gas pore pressures. Permeability was modulated by the effects of gas pressure, effective stress and moisture content. These three principal processes are further investigated below.

3.1 Influence of Gas Sorption

We record the evolution of permeability to sweeps of non sorbing He, and sorbing gases (CH_4 and CO_2). Permeability increased as the He gas pressure increased under constant confining stress (Figure 1.3). This is consistent with the dilation of fractures as effective stresses reduce as gas pressures are elevated. Conversely, permeability was reduced for both CH_4 and CO_2, with increasing gas pressure with the reduction being more significant for CO_2 (Figure 1.3). The reduction in permeability coincides with swelling strains. Presumably, observed dilational strains are the measured surplus strain after the interior closing of cleats has occured and resulted in net reduction of permeability even as effective stresses have reduced. For example, the permeability at 2 MPa is approximately six times of the minimum permeability observed at ~4 MPa in a 7% moisture saturated coal. The rate of change of permeability with pore pressure of sorptive gas (CH_4 or CO_2) is higher in dry coal in comparison to the moist coal (Figure 1.3) as expected based on sorption capacity influences (Joubert et al., 1974). The water molecules have tendency to block the sorption sites for gases resulting in inhibited sorption of gas (Prinz and Littke, 2005). The reduction in adsorption decreases the rate of

change of permability change with sorption as presented in Figure 1.3. When either CH_4

or CO_2 desorbs by reducing gas pressure then the permeability partly recovers to the

baseline permeability ($k/k_0 \sim 1$) (not shown in Figure 1.3). Note that k_0 has a value of

$5.44 \times 10^{-15} m^2$. However this recovery was limited by the rate of desorption of the gas

from the matrix blocks and into the fractures. A percentage of the original He

permeability is retained in the sample implying that the core moisture content has not

varied significantly during the experimental suite.

3.2 Influence of Effective Stress

There was an increase in permeability with increased gas pressure of He at

constant confining stress for (1%, 5%, 7% and 9 % by mass) moisture saturated coals

(Figure 1.3). This is consistent with the closure of microfractures as effective stresses

increase. Conversely, for the moderately sorbing CH_4 and more strongly sorbing CO_2, the

permeability decreases with an increase in gas pressure. This is the result of the dominant

swelling response of the coal relative to the inhibited dilation due to decreased effective

stresses at gas pressures below the pressure at which maximum swelling strain occurs.

Interestingly, for various moisture content level coals, permeability ratios follow similar

trends under constant confining stress but for varying gas pressures (Figure 1.3). For non-

sorbing He, permeability was dominated by the effective stress response while for

sorbing gases, the role of swelling was more prominent.

3.3 Influence of Moisture Content

The permeability of bituminous coal decreases with an increase in moisture

content of the coal. Moisture contents varying from (1-9 % by mass) have been

considered for this study. Samples with the higher moisture contents exhibit the lowest

permeability with the injection of sorbing or non-sorbing gas, Figure 1.3. The presence of

moisture in fractures will inhibit the flow of gas by occluding pore-space. Additionally,

the moisture in the micro- and meso-pores will influence flow tortuosity and out compete

for sorption sites (Day et al., 2008; Fry et al., 2009). The moisture loading in coal swells

the matrix to a degree (Fry et al., 2009; Robertson, 2005). Water occupying the fracture

system is not expected to result in significant swelling while water in the matrix is more

likely to result in matrix swelling depending on the pore size distribution. Presumably,

the swelling developed in the matrix decreases the fracture aperture that further reduces

the permeability. Shrinkage measurements on the Argonne suite show that the contraction

of powdered coal on drying can range from 34 to 8% (Kelemen et al., 2005). The

volumetric strains induced by moisture loading in bituminous/subbituminous coal blocks

are in the same order of magnitude (~5%) (Fry et al., 2009) with low-rank having

potentially much higher strains 12% (Czerw, 2011). The differences between the

permeabilities to He, CH_4, CO_2-sweep and CO_2 are reduced most significantly in the

moist coal (7% moisture content) relative to the dry coal (1% moisture content), Figure

1.3. These observations are consistent with inhibited swelling in the moist coals (van

Bergen et al., 2009). The presence of moisture in coal reduces the diffusion coefficient,

ultimate adsorption capacity and sorption-induced swelling (Day et al., 2011; Pan et al.,

2010). Hence the reduction in permeability for dry coals is much higher than that of the

moist coals (compare Figure 1.3a & 1.3b). This is consistent with observations for

bituminous coal (Wang et al., 2011). In the case of a constant head permeability test, an

increase in permeability is expected in the moist coal experiments as the coal continues to

dry with the flow of large volumes of various gases (Mathews et al., 2011). However, the

transient pulse test approach minimizes this moisture loss over the more invasive fluid

flow testing approaches and helps retain the integrity of the sample.
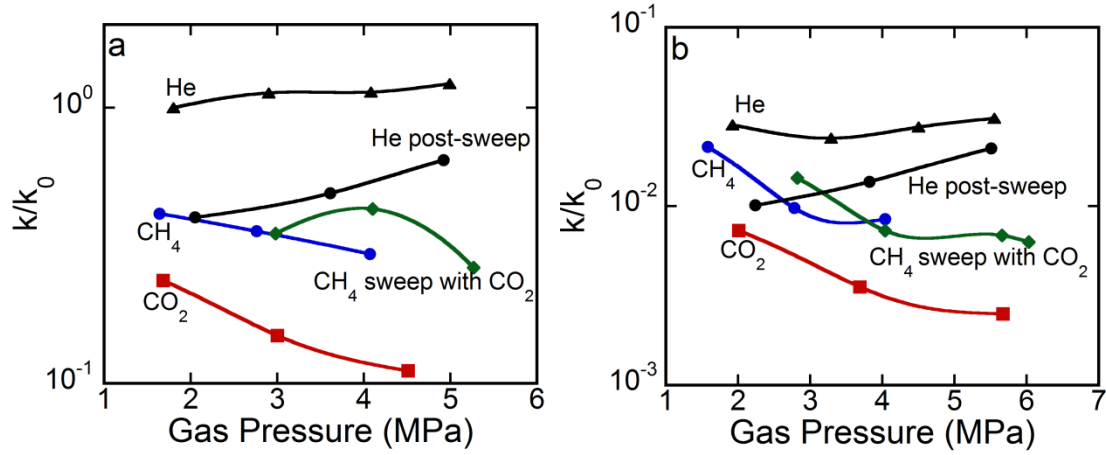
Figure 1.3: a. Evolution of permeability ratio with increasing pore pressure in a. partially

dry (1-2% moisture content by mass) and b. for moist (7% moisture) coal. Computation

error in the permeability values is within $\pm 10\%$. k0= 5.44×10^{-15} m^2

3.4 Mechanistic Model

Observations of permeability evolution were used to develop a mechanistic model

for permeability evolution in stress-constrained coal. As in the other experimental (Han et

al., 2010) studies the cleat permeability is orders of magnitudes higher than the matrix

permeability. We consider a model where individual cleats of finite length are embedded

within a coal matrix (Izadi et al., 2011) and the processes (sorption/desorption) resulting

in swelling/shrinkage occurring in the matrix directly affect the cleat permeability by

changing the cleat aperture (Izadi et al., 2011; Wang et al., 2012). The rock-bridge model

is based on matrix-fracture interaction (Izadi et al., 2011). This model was used to

explore the changes in porosity and permeability that accompany gas sorption under

conditions of constant applied stress and for increments of applied gas pressure. The

influence of gas pressure, effective stress, and moisture content were evaluated to

separately identify the individual effects on permeability. A single parameter was varied

while other parameters being held constant. This approach allowed addressing the

important aspects of permeability evolution.

3.4.1 *Gas Sorption*

The permeability evolution data were fit to a model representing the evolution of

permeability on coals subjected to prescribed stress boundary conditions (Izadi et al.,

2011). This model identifies the change in permeability in the swelling regime.

The dynamic permeability of a cracked system may be represented as,

$$\frac{k}{k_0} = \left(1 + \frac{\Delta b}{b_0}\right)^3 \tag{3}$$

If external boundaries have zero displacement, the swelling strain is defined as

$$\varepsilon_v = \frac{\Delta b.a}{s.s} \tag{4}$$

Volumetric strain due to swelling ε_v may be expressed as Langmuir type curve

(Robertson, 2005)

$$\varepsilon_v = \varepsilon_L \frac{p}{p+p_L} \tag{5}$$

Using Equation 4 and 5, the relative aperture change may be calculated as

$$\frac{\Delta b}{b_0} = \left(\frac{\varepsilon_L s^2}{ab_0}\right)\frac{p}{p+p_L} \tag{6}$$

Combining equation 3 and 5, the change in permeability may be recovered as

$$\frac{k}{k_0} = \left(1 + \frac{\Delta b}{b_0}\right)^3 = \left(1 + \left(\frac{\varepsilon_L s^2}{ab_0}\right)\frac{p}{p+p_L}\right)^3 \tag{7}$$

If an arbitrary variable C is such that

$$C = \left(\frac{\varepsilon_L s^2}{ab_0}\right) \tag{8}$$

then equation 7 may be rewritten as

$$\frac{k}{k_0} = \left(1 + C\frac{p}{p+p_L}\right)^3 \tag{9}$$

where permeability k, initial permeability k_0, initial fracture aperture b_0, change in fracture aperture Δb, fracture length a, fracture spacing s, volumetric strain ε_v, peak Langmuir strain ε_L, gas pressure p, Langmuir pressure p_L and assumed fitting constant $C = \left(\frac{\varepsilon_L s^2}{ab_0}\right)$ define the response. Here peak Langmuir strain is defined as the maximum strain that occurs due to gas adsorption at infinite pressure (Robertson, 2005). It may be noted that the parameter 'C' represents lumped response of swelling induced strain by both moisture and sorptive gas. Although, it is desirable from a scientific point of view to deconvolve the individual effect of moisture and sorption (CH_4 and CO_2) induced strain on permeability, we have specifically chosen not to separate the two components. This is for two reasons: first, to avoid increasing the number of free parameters in the model and second since it is non-trivial to separate

the effect of moisture and gas-induced strain as the presence of moisture also influences the gas capacity hence the magnitude of swelling.

This formulation allows the evolution of normalized permeability to be represented by the analytical curves of (Figure 1.4) where the magnitudes of C are evaluated from the best fit as indexed by the coefficient of correlation (R^2). These identify acceptable fits in the swelling dominant region for CH_4, CH_4-swept with CO_2 and for uptake of CO_2.
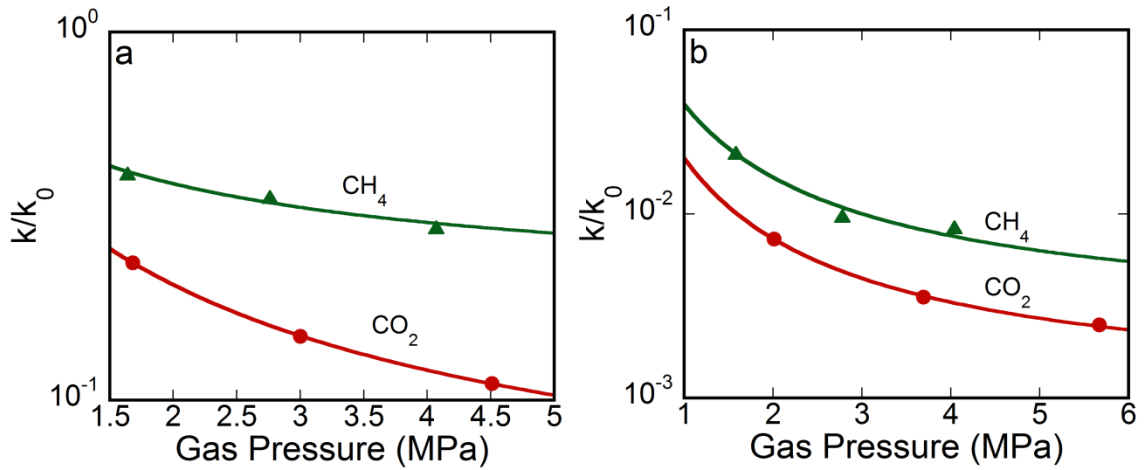
Figure 1.4: Analytical fits of equation (9) to the measured permeability evolution for a.) dry (1% moisture) and b.) moist (fracture saturated) coal. R^2 fit for all curves are >90%.

3.4.2 Effective Stress

Many permeability models or empirical correlations index permeability as a function of effective stress (Durucan and Edwards, 1986; Jasinge et al., 2011; Somerton et al., 1975). We note (Figure 1.5a) the log-linear trend in permeability with effective

stress with a goodness of fit of 99%, supported by similar observations for various coals

(Jasinge et al., 2011). This correlation may be represented as,

$$\frac{k}{k_0} = \alpha e^{-\beta\sigma'}$$ (10)

where permeability k, initial permeability k_0, Effective stress

$\sigma' = confining\ stress - pore\ pressure$, and the arbitrary material-specific constants α

& β define response.

The slope of the permeability versus effective stress response line β (MPa^{-1})

represents the inverse of Young's modulus. The comparison of permeability evolution in

dry and moist coals indicates that dry coals have higher modulus than moist coals (Figure

1.5a). This means that the dry coals are less sensitive to effective stress compared to

moist coals (Figure 1.5a). Permeability decreases by two orders of magnitude with an

increase in effective stress from 4MPa to 8MPa in the moist coals. It is clear from Figure

1.5a that permeability decreases with an increase in effective stress for the dry coal but

that the magnitude of this decrease is much smaller than that of the other higher moisture

saturated coal. The Young's modulus decreases as the moisture content increases in

Australian bituminous coals which indicates coal hardening when losing moisture content

(Pan et al., 2010). Alternatively, coal becomes less stiff with addition of moisture. The

decrease in stiffness results in a greater sensitivity of aperture change to the applied stress

and thereby a greater sensitivity of permeability change to stress change (Ouyang and

Elsworth, 1993). The slope of the permeability-effective stress linear relationship is

greater in moist coals than the dry coal (Figure 1.5a), which indicates that the coals at

higher moisture contents are less stiff. The permeability evolution data for high moisture

content coal show scatter at higher effective stresses suggesting the existence of a lower-bound value of permeability. However, as observed, the coal samples with lower moisture content do not show this behavior at least in the range of 9 MPa. The lower-bound permeability values correspond to the scenario when fracture aperture reaches a threshold and does not change further with effective stress (Min et al., 2009). These values however seem to be dependent on moisture content of coal as shown by dotted line in the Figure 1.5a.

3.4.3   Moisture Content

Permeability evolution for the infiltration of He gas was observed to be log-linear with moisture content. An exponential decrease in permeability is observed with increasing moisture content of the coal (Figure 1.5b). The decrease in He permeability may be as high as ~100 folds if the moisture content is increased from 1% to 9% (Figure 1.5b). It is important to note that only non-adsorbing gas holds a log-linear relationship with increasing moisture content (Figure 1.5b). We explain this behavior on the basis of coal fracture-wall swelling (Day et al., 2011; Day et al., 2008) and the occlusion of micropores (Day et al., 2008) by the water molecules. The infiltrating water first occupies high energy water adsorption sites (Busch and Gensterblum, 2011) and the ease of access to a suitable-site for water-molecules becomes exponentially more difficult (Menon et al., 1991). Presumably, the water molecules then begin occupying free space in the matrix and the fracture when the majority of the adsorption sites are filled. This process reduces effective space allowing the flow of the injected gas. Hence, the exponential reduction in

permeability is observed with the loading of moist in coals (Chikatamarla et al., 2009).

Typical correlations shown in Figure 1.5b may be represented as,

$$\frac{k}{k_0} = \gamma e^{-\delta S_w} \tag{11}$$

where permeability k, initial permeability k_0, moisture content S_w and the arbitrary coal characteristics constants γ and δ define behavior. The higher values of parameter δ indicate a greater sensitivity to interaction between coal and a particular gas in the presence of moisture. The moist coals swell less than dry coals in the presence of a sorbing gas. However, the moist coals show lower permeability than the dry coal because of the cumulative effect of moisture and of the sorbing gases.
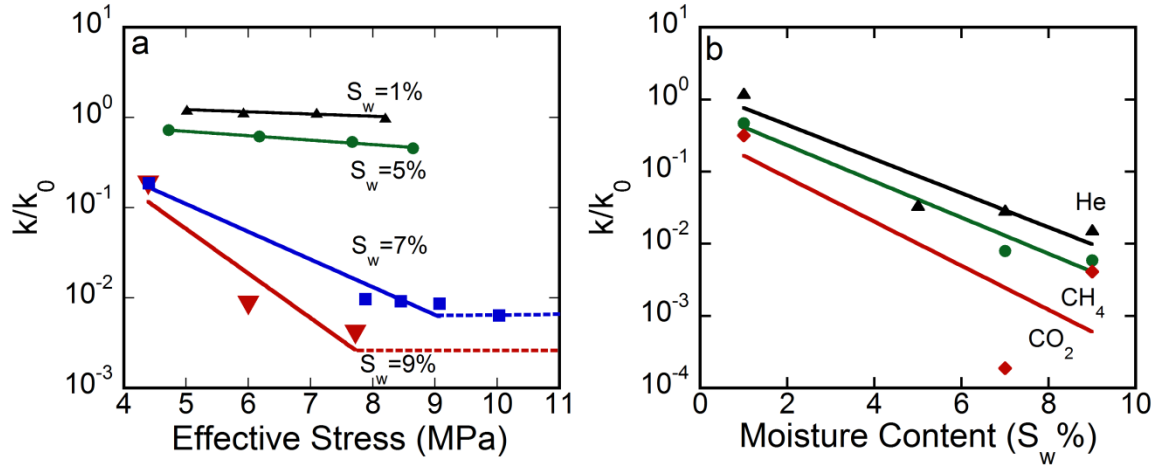
Figure 1.5: Analytical fits to the measured permeability evolution. a. Evolution in permeability with effective stress equation (10) for Helium permeability and b. Evolution of permeability with moisture content equation (11) in coal. R^2 fit for all curves are 99% except CO_2.

3.5 Parameter Optimization

The prior observations and characterizations were used to describe a phenomenological model for the combined response to stress, gas pressure and moisture content. The evolution of permeability may be represented by the superposition of individual processes as,

$$\frac{k}{k_0} = f\left(\sigma', p_g, S_w\right) \tag{12}$$

where effective stress σ' and moisture content S_w are as previously defined and p_g is the pore pressure of gas (CH_4, CO_2, He). The change in aperture of the fracture largely results from a change in effective stress and sorption induced swelling as shown in Figure 1.6. The term $e^{-\delta S_w}$ represents the occluding effect of moisture is a pre-factor for both effective stress and gas pressure and its presence can either enhance or depress the magnitude of the two above mentioned processes. Therefore, the cumulative effect can be represented as the sum of sorptive-swelling and stress-dilatational effects and the product of these two concurrent influences with the influence of moisture content (Figure 1.6). This is further explained in Figure 1.6. When stress is applied to the coal (Figure 1.6a) the aperture of the fracture reduces (Figure 1.6b). For a sorptive gas injected into the fracture under constant confining stress condition, the aperture is further reduced by inducing swelling (Figure 1.6c). The increase in moisture content further magnifies the reduction in permeability which may be due to the occlusion of the pores and the change in Young's modulus of the matrix. Mathematically, this can be represented as,

$$\frac{k}{k_0} \propto (\text{Effective stress} + \text{Sorption induced swelling}) * \text{Moisture occluding effect}$$

$$\frac{k}{k_0} = \left\{\left(1 + \frac{C.p}{p+P_L}\right)^3 + e^{-\beta\sigma'}\right\} * e^{-\delta S_w} \tag{13}$$

MATLAB® curve fit toolbox was used to optimize the values of the parameters (C, P_L, β and δ). This function utilizes the lsqcurvefit algorithm to find the best possible set of values under prescribed constraints (MATLAB Curvefit Toolbox, 2009).
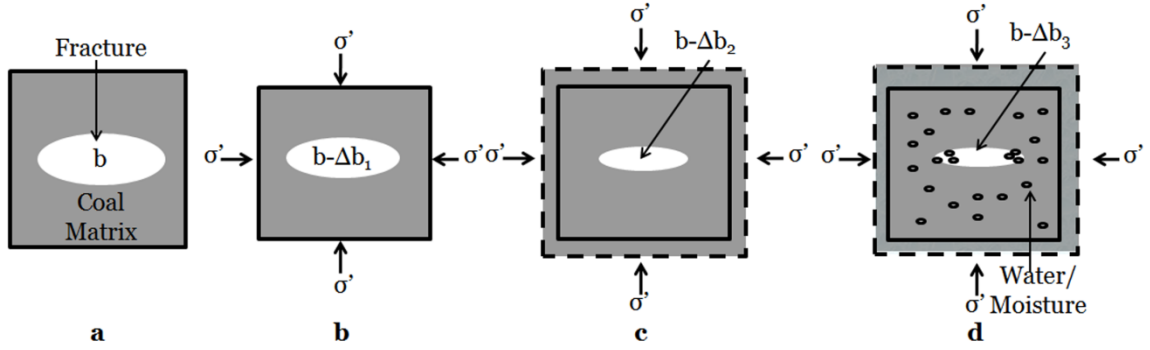
Figure 1.6: Representation of mechanistic processes interplaying simultaneously in ECBM. a) A unit of coal-fracture system. b) Reduction in aperture 'b' by 'Δb1' on application of stress. c) Reduction in aperture by 'Δb2' due to sorption induced swelling in stress-constrained unit. d) Reduction in aperture by 'Δb3' due to moisture infiltration. Here Δb1<Δb2<Δb3<Δb4.

Permeability reduces as the coal swells reducing fracture aperture with increasing gas pressure of the sorbing gas. As the peak Langmuir strain is approached, the reduction in permeability halts and permeability increases linearly with gas pressure (Figure 1.7). The reduction in permeability ranges from 5 to 10 folds depending on the gas injected (Figure 1.7). A regain in permeability was observed at sufficiently high gas pressures. For

instance, the CH_4 permeability in the 7% moisture saturated coal decreases by ~200% as gas pressure increases from ~1.5 MPa to ~4.1 MPa. The coal regains its original permeability as gas pressure is further increased to ~6.2 MPa. The reduction in permeability is 40 folds for CH_4 and 60 folds for CO_2 in moist coal (7% moisture content) with respect to dry coal (Figure 1.7). The rate of permeability loss is controlled by crack geometry (Izadi et al., 2011), the Langmuir swelling strain ε_L and the void "stiffness" β. However, the rate of permeability increase is controlled by crack geometry and void "stiffness" alone. The permeability evolution may be approximated by a single non-dimensional variable incorporating fracture spacing, fracture-length, Langmuir strain, and initial permeability. Here Langmuir strain is defined as the swelling induced strain in coal at certain gas pressure. The swelling increases and the permeability decreases with an increase in gas pressure of the sorbing gas (Figure 1.7a-b, Region I). We eliminate the possibility of the Klinkenberg effect as the size of cleats (~0.5mm) is significantly higher than the mean free path of the gas used (~0.3nm). Therefore, the decrease in permeability in Region I can only be attributed to sorption induced swelling. However, permeability increases as the pressures of the infiltrating gas becomes approximately equal to the pressure at which maximum adsorption occurs.

This model represents the principal features of permeability evolution in swelling media and is a mechanistically consistent and plausible model for behavior. The proposed model tracks the role of gas pressure, effective stress and moisture content on the evolution of permeability in coal. To the best of our knowledge, no current permeability model accounts for the presence of moisture despite experimental evidence for the same.
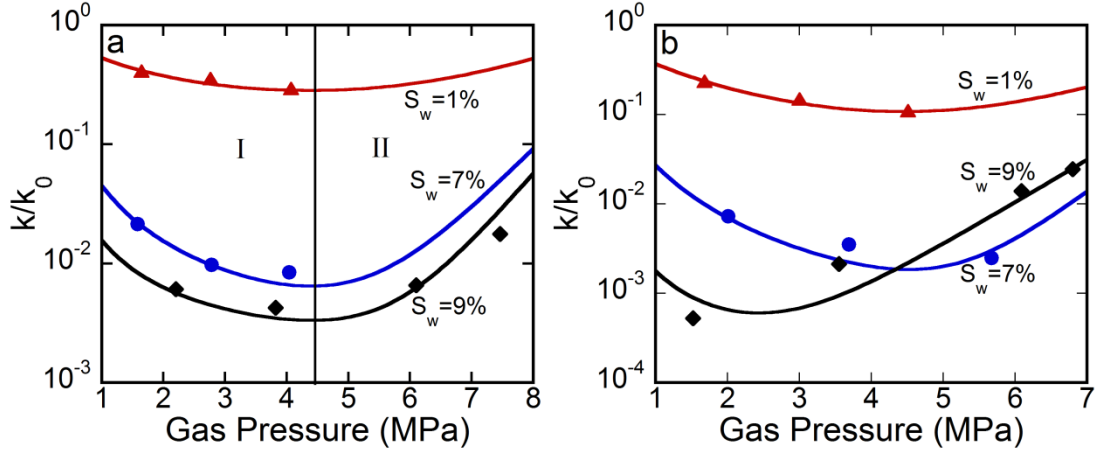
Figure 1.7: Analytical fits to the equation (13) for the observations of permeability evolution with a. CH_4 b. CO_2 at various moisture-content of coals. Region I is swelling dominant and Region II effective stress dominant.

3.6 Congruence of fit pattern with physical phenomenon

The fitting parameters for C, P_L, β and δ recovered as described previously are summarized in Table 1.2. These parameters may be described in terms of the physical processes they represent. In this section, we explore the appropriateness of these parameters relative to measured parametric magnitudes reported in the literature.

1. **Parameter C**: After rearranging equation 8, the Langmuir strain may be expressed as $\varepsilon_L = \left(\frac{Cab_0}{s^2}\right)$. Typical values of cleat spacing s=5 mm, cleat width a=~5 mm, cleat aperture $b_0 = \left(\frac{1}{2}\right)$ mm were obtained from the dry coal used in this work. The range of values for parameter C was obtained from Table 1.2. Equation 8 yields the values of ε_L using typical values of s, a, b_0 and C. The Langmuir strain ε_L varies in the range of

(0.05-0.1) similar to magnitudes previously recorded (Day et al., 2011; Reucroft and Patel, 1986).

2. **Parameter P_L**: Langmuir pressures P_L vary in the range (2.0-0.1) MPa (Table 1.2). We observe that minimum permeabilities occur at ~4.1 MPa (Figure 1.7). Minimum permeability occurs at a pressure after which no additional sorption take place. A shift of ~1.8MPa is observed in the case of CO_2 at 9% moisture content.

3. **Parameter β**: The parameter β, increases from 0.5 to 1.4 for moisture contents ranging from 1% to 9%. Dry coals are stiffer than the moist coals and as a result their permeabilities are less affected by changes ineffective stresses. These findings are consistent with the observations of others (White and Mazurkiewicz, 1989).

4. **Parameter δ**: The moisture induced offset δ of permeability is higher for CO_2 (1.88) than for CH_4 (1.1). This indicates that CO_2 has a higher impact on swelling even in the presence of moisture and retains molecular access those sites which remain inaccessible to moisture (Prinz and Littke, 2005). A plausible argument is that the transport of CO_2 to adsorption sites is easier because of the smaller kinetic diameter of the CO_2 molecule.

Table 1.2: Typical value of the fit parameters in equation 13. See text for the definition of fir parameters.

Gas, S_w%	Fit Parameters			
	C	P_L	β	
1. CH_4, 1	0.56	1.9	0.5	
2. CH_4, 7	0.9	0.4	1.2	.1
3. CH_4, 9	0.89	0.2	1.4	
4. CO_2, 1	0.84	2	0.6	
5. CO_2, 7	0.96	0.4	1.4	.9
6. CO_2, 9	0.96	0.1	1.1	

3.7 Model Validation

The mechanistic model proposed in this paper has been validated using the CH_4 and CO_2 permeability evolution data reported on a water saturated Pennsylvanian Anthracite coal (Wang et al., 2011) and CO_2 permeability evolution data reported on a European high volatile bituminous coal (Pini et al., 2009a).

The permeability evolution observed for CH_4 and CO_2 on naturally fractured coal samples from Northumberland basin in Pennsylvania (Wang et al., 2011)(Figure 1.8a), shows the normalized permeability evolution data for CH_4 and CO_2 under 6 MPa of constant confining stress. The normalizing factor used was the helium permeability of dry coal under no confining stress i.e. k_0 (2.37×10^{-17} m^2). The goodness of fit for both CH_4

and CO_2 is greater than 99.8% i.e. the trend predicted by the proposed model is in excellent agreement with the published data. The values of the fitting parameters are shown in Figure 1.8a. The absence of adsorption and strain measurement data on Pennsylvanian Anthracite coal restricts us from any direct parametric comparison. However, we have compared our model fitting parameter values with those of coals of similar rank from other basins in the world. It is important to note that the literature values for Langmuir pressure (P_L) and Langmuir strain (ε_L) are reported for pulverized coal while our model derives these values based upon the permeability evolution data on cores. The Langmuir pressure P_L for CH_4 (~0.6 MPa) is of the same order of magnitude as those (~1 MPa) reported for powdered Chinese anthracite coal (Li et al., 2010). The model-driven Langmuir strain (ε_L) for CO_2 is 0.011 which is close to the reported value (0.028) for powdered anthracite coal (Walker Jr et al., 1988). The different values for P_L and ε_L would yield different production characteristics. It may be noted here that the majority of the experimental data (Wang et al., 2011) fall in Region II, the region dominated by effective stress. However our permeability evolution data covers both Regions I and II although the majority is in Region I. The acceptable fits on experimental data in both regions using our proposed model suggest a broad, and perhaps a universal, applicability. Intuitively, when gas pressure approaches, zero (gauge pressure), then, for a given confining stress, the permeability to sorbing gases (CH_4 and CO_2) should be equivalent to that for the non-sorbing gases (He) as the null swelling and effective stress effects are all equivalent. This is expected because at zero pressure (vacuum), the effect of sorption (water, CH_4 and CO_2) on permeability is negligible. Although, the region below 0.5 MPa is not of practical interest for ECBM application, our initial extrapolation

to zero pressure suggests a convergence in permeability of He in dry coal with the permeability of CH_4 and CO_2 in water saturated coal (Figure 1.8).

The model has also been validated against permeability evolution data on CO_2 for a bituminous coal sample in both region I as well region II (Figure 1.8b) (Pini et al., 2009a). The model explains the data with a goodness of fit 98%. Also, we observe that the model-driven Langmuir pressure value P_L (0.7MPa) agrees very well with the reported experimental value (0.8 MPa) for this coal. Additionally, both data sets from (Wang et al., 2011) and (Pini et al., 2009a) though made on different samples, show a similar trend in convergence of He permeability with those of CH_4 and CO_2. These validations indicate the robustness of the proposed model despite variations in coal properties.
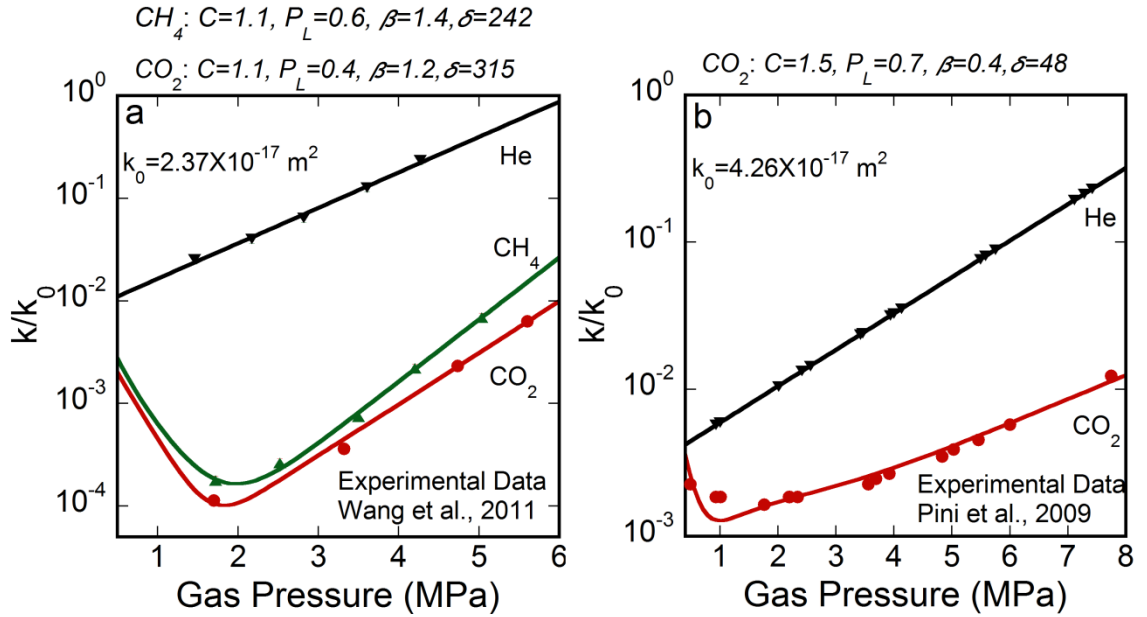
Figure 1.8: Analytical fits to the equation (13) for the observations of permeability evolution with a. CH_4 b. CO_2 at various moisture-content of coals. Region I is swelling dominant and Region II effective stress dominant.

4 Lumped Parameter Model for ECBM Optimization

Enhanced coalbed methane recovery with CO_2 injection operates by the preferential sorption of CO_2 in the coal matrix; CH_4 residing within the matrix desorbs as CO_2 is sorbed. We follow the evolution of the permeability of the coal with gas pressure of CH_4 and CO_2 as CO_2 is injected and CH_4 is recovered at upstream and downstream sites, respectively. The CH_4-permeability is higher than the CO_2-permeability in the dry to medium-moist coals for practical ranges of reservoir pressures (Figure 1.9a). We plot the permeability evolution versus gas pressure curves using our mechanistic model presented in equation 13. Specifically, we explore the conditions required to ensure that permeability remains higher during CO_2 assisted ECBM than the initial permeability to CH_4. The conditions that ensure that both injection (CO_2) and recovery (CH_4) permeabilities remain higher than the initial reservoir (CH_4) permeability may be schematically represented as in Figure 1.9a. Initial reservoir permeability at pressure P_r (assuming 100% CH_4) can be equal to the CO_2-permeability (assuming 100% CO_2 at the end of ECBM) at another pressure P_i (Figure 1.9a).

$$k_{P_r}^{CH_4} = k_{P_i}^{CO_2} \tag{14}$$

where initial reservoir permeability, $k_{P_r}^{CH_4}$ and permeability at the end of ECBM recovery, $k_{P_i}^{CO_2}$ describe the response. Pressures P_r and P_i may be solved-for numerically using equation (14). We use the permeability fitting parameters (Table 1.2) to explore

34

two scenarios of initial reservoir pressures either below (under-) or above (over-) saturation pressures; though oversaturated reservoirs are the most common (Pashin, 2010; Pashin and McIntyre, 2003). Here, the pressure range below the pressure point at which the adsorption isotherm plateaus has been referred to as undersaturation region and the one above this pressure point as oversaturation region. It should be noted that the pressure point separating the under- and over- saturation regions itself is always greater than the Langmuir pressure p_L.

Undersaturated Reservoir: If the initial reservoir pressure is lower than the pressure at which maximum adsorption occurs, then the reservoir should be initially depressurized to pressure P_i by withdrawing CH_4 (Figure 1.9a). We calculate withdrawal/injection pressure P_i for an initial reservoir pressure P_r using equation (14). This scenario is represented as the 'withdrawal' region in Figure 1.9. For an undersaturated reservoir, recovery of CH_4 will always increase the permeability at the recovery well and CO_2 injection can only retain the original permeability or better if the injection pressure rises above the critical pressure and an additional amount defined by the nested CH_4-CO_2 permeability curves (Figure 1.9a). This condition may be avoided if initial injection of a non-sorbing gas, for example N_2, is used as a substitute for CO_2.

This optimized injection schedule ensures that there is no reduction in permeability during ECBM recovery. Figure 1.9b, shows the necessary extent of initial depressurization (P_r-P_i) for any initial reservoir pressure for a variety of initial moisture contents in coal.

Oversaturated Reservoir: If the initial reservoir pressure is greater than the pressure at which maximum adsorption occurs, then elevating reservoir pressure without the injection of sorbing gas is first required. This can be accomplished with the injection of non-adsorbing gas (e.g. N_2) would result in a higher permeability by moving up the CH_4 permeability curve (Schepers et al., 2010) (Figure 1.9a). The injection of CO_2 should only follow when the reservoir gas pressure is above the required pressure obtained from equation 14. More CO_2 is adsorbed in the coal as the injection proceeds and at time t=∞ (end of ECBM) maximum swelling would occur resulting in a minimum permeability value. The permeability at the end of this cycle is then guaranteed to be at least equal to that at the beginning of the ECBM process (Figure 1.9a). The discontinuity in the pressure-permeability relations (Figure 1.9b) at a pressure equal to the saturation pressure shows a demarcation line between the injection and withdrawal region.

For reservoirs initially at pressures above the saturation pressure (over-) then withdrawal pressures will reduce permeability unless the pressure change is sufficiently large to carry the reservoir through the critical pressure, identified as the permeability minimum at about the pressure where maximum adsorption occurs. For CO_2 injection the permeability at the injection well may be retained above the initial reservoir permeability if injection pressures are typically of the order of one to a few MPa above the critical reservoir pressure.

Both scenarios discussed above provide the basis to define the appropriate production pressures and their scheduling to optimally recover CH_4 using the injection of CO_2, but do not guarantee that breakthrough of CO_2 to the production well will not occur. This case requires a more involved analysis.
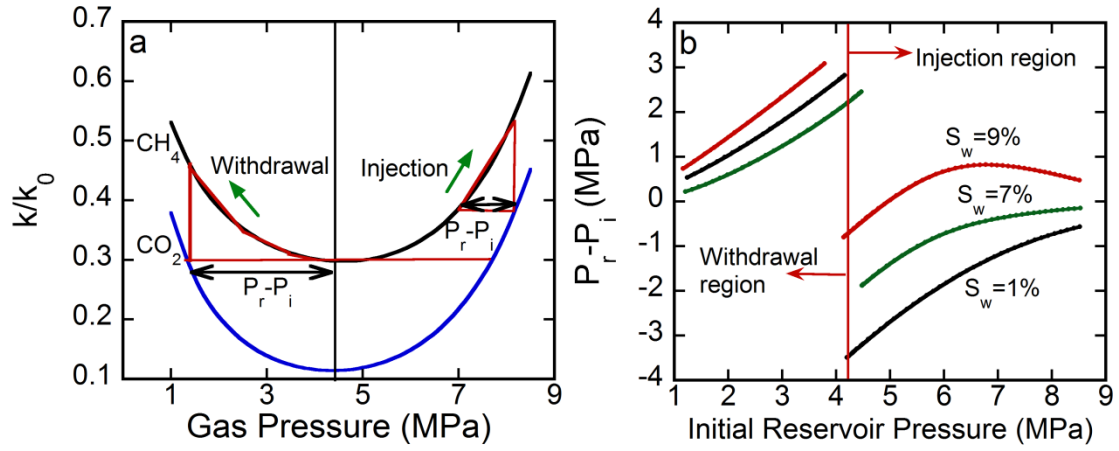
Figure 1.9: Analytical fits to the equation (13) for the observations of permeability evolution with a. CH_4 b. CO_2 at various moisture-content of coals. Region I is swelling dominant and Region II effective stress dominant.

5 Conclusions

The permeability evolution in bituminous coal with injection of both sorptive and non-sorptive gases under mechanically constrained condition was investigated. Also, the effect of critical processes involved in ECBM recovery from coalbed reservoirs related to the evolution of permeability in bituminous coal were quantified. The following conclusions can be drawn from this study.

1. Measurement of permeability of a bituminous coal from the Uinta Basin showed that the permeability decreases with increasing pressure of the sorbing gas. This decrease may be as high as an order of magnitude for this coal. The reduction in permeability halts at a critical pressure corresponding to the point at which maximum

adsorption is achieved and then increases as a consequence of diminishing effective stresses.

2. We confirm permeability to be dependent primarily on three processes: sorption-induced swelling, stress-induced cleat closure and pore occlusion due to the presence of moisture in coal. Further, the effect of each process on permeability evolution was quantified.

3. We confirm that the presence of moisture lowers net permeability folds compared to dry coal. The decrease in He permeability may be as high as ~100 folds if the moisture content is increased from 1% to 9%. This behavior is overprinted on the sorptive decrease in permeability, which are greater for $CO_2 > CH_4 > He$.

4. A mechanistic model was proposed which represents the permeability evolution under mechanically constrained conditions as effective stress, gas pressure and moisture content modulate behavior in the coal. Also, we showcase this model to explain the permeability evolution data published in the literature.

5. Two ECBM optimization scenarios representing both "undersaturated" and "oversaturated" reservoirs were indentified based on the initial reservoir pressure. Additionally, we identify two ECBM optimization strategies which could prevent permeability loss during this process.

7 References

ASTM, 2007. D1412 - 07 Standard test method for equilibrium moisture of coal at 96 to 97 percent relative humidity and 30°C.

ASTM, International, 2010. D3302/D3302M - 10, Standard test method for total moisture in coal.

ASTM D388, 2005. Standard classification of coals by rank. IHS, Pennsylvania, United States.

ASTM D7582, 2010. Standard test methods for proximate analysis of coal and coke by macro thermogravimetric analysis.

Bai, M., Elsworth, D., Roegiers, J.C., 1993. Modeling of naturally fractured reservoirs using deformation dependent flow mechanism. International Journal of Rock Mechanics and Mining Sciences & Geomechanics Abstracts 30, 1185-1191.

Bai, M., Roegiers, J.-C., Elsworth, D., 1995. Poromechanical response of fractured-porous rock masses. Journal of Petroleum Science and Engineering 13, 155-168.

Brace, W.F., Walsh, J.B., Frangos, W.T., 1968. Permeability of Granite under high pressure. J. Geophys. Res. 73, 2225-2236.

Busch, A., Gensterblum, Y., 2011. CBM and CO2-ECBM related sorption processes in coal: A review. International Journal of Coal Geology 87, 49-71.

Bustin, R.M., Cui, X., Chikatamarla, L., 2008. Impacts of volumetric strain on CO2 sequestration in coals and enhanced CH4 recovery. AAPG Bulletin 92, 15-29.

Chikatamarla, L., Bustin, R.M., Cui, X., 2009. CO2 sequestration into coalbeds: Insights from laboratory experiments and numerical modeling. AAPG Studies in Geology 59, 457-474.

Chikatamarla, L., Cui, X., Bustin, R.M., 2004a. Implications of volumetric swelling/shrinkage of coal in sequestration of acid gases, International Coalbed Methane Symposium Proceedings, Tuscaloosa, AL.

Chikatamarla, L., Cui, X., Bustin, R.M., 2004b. Implications of volumetric swelling/shrinkage of coal in sequestration of acid gases, The Intenrational Coalbed Methane Symposium, Tuscaloosa, Alabama.

Clarkson, C.R., Pan, Z., Palmer, I., Harpalani, S., 2010. Predicting sorption-induced strain and permeability increase with depletion for coalbed-methane reservoirs. SPE Journal 15, 152-159.

Cui, X., Bustin, R.M., Chikatamarla, L., 2007. Adsorption-induced coal swelling and stress: Implications for methane production and acid gas sequestration into coal seams. J. Geophys. Res. 112, B10202.

Czerw, K., 2011. Methane and carbon dioxide sorption/desorption on bituminous coal—Experiments on cubicoid sample cut from the primal coal lump. International Journal of Coal Geology 85, 72-77.

Day, S., Fry, R., Sakurovs, R., 2011. Swelling of moist coal in carbon dioxide and methane. International Journal of Coal Geology 86, 197-283.

Day, S., Fry, R., Sakurovs, R., Weir, S., 2010. Swelling of coals by supercritical gases and its relationship to sorption. Energy & Fuels 24, 2777-2783.

Day, S., Sakurovs, R., Weir, S., 2008. Supercritical gas sorption on moist coals. International Journal of Coal Geology 74, 203-214.

Durie, R.A., 1991. The Science of Victorian brown coal: structure, properties, and consequences for utilization. Butterworth-Heinemann.

Durucan, S., Edwards, J.S., 1986. The effects of stress and fracturing on permeability of coal. Mining Science and Technology 3, 205-216.

Durucan, S., Shi, J.-Q., 2009. Improving the CO_2 well injectivity and enhanced coalbed methane production performance in coal seams. International Journal of Coal Geology 77, 214-221.

EPA, 2004. Evaluation of impacts to underground sources of drinking water by hydraulic fracturing of coalbed methane reservoirs- final report, p. 424.

Fry, R., Day, S., Sakurovs, R., 2009. Moisture-induced swelling of coal. International Journal of Coal Preparation and Utilization 29, 298 - 316.

Gash, B.W., Volz, R.F., Potter, G., Corgan, J.M., 1993. In The effect of cleat orientation and confining pressure on cleat porosity, permeability and relative permeability in coal, International Coalbed Methane Conference, University of Alabama, Tuscaloosa, Alabama, pp. 247-255.

Glick, D.C., Mitchell, G.D., Davis, A., 2005. Coal sample preservation in foil multilaminate bags. International Journal of Coal Geology 63, 178-189.

Gu, F., Chalaturnyk, R.J., 2005. Analysis of coalbed methane production by reservoir and geomechanical coupling simulation. Journal of Canadian Petroleum Technology 44, 33-42.

Gu, F., Chalaturnyk, R.J., 2006. Numerical simulation of stress and strain due to gas sorption/desorption and their effects on in situ permeability of coalbeds. Journal of Canadian Petroleum Technology 45.

Han, F., Busch, A., van Wageningen, N., Yang, J., Liu, Z., Krooss, B.M., 2010. Experimental study of gas and water transport processes in the inter-cleat (matrix) system of coal: Anthracite from Qinshui Basin, China. International Journal of Coal Geology 81, 128-138.

Harpalani, S., Chen, G., 1995. Estimation of changes in fracture porosity of coal with gas emission. Fuel 74, 1491-1498.

Izadi, G., Wang, S., Elsworth, D., Liu, J., Wu, Y., Pone, D., 2011. Permeability evolution of fluid-infiltrated coal containing discrete fractures. International Journal of Coal Geology 85, 202-211.

Jasinge, D., Ranjith, P.G., Choi, S.K., 2011. Effects of effective stress changes on permeability of Latrobe valley brown coal. Fuel 90, 1292-1300.

Joubert, J.I., Grein, C.T., Bienstock, D., 1973. Sorption of methane in moist coal. Fuel 52, 181-185.

Joubert, J.I., Grein, C.T., Bienstock, D., 1974. Effect of moisture on the methane capacity of American coals. Fuel 53, 186-191.

Kelemen, S.R., Kwiatek, L.M., Lee, A.G.K., 2006. Swelling and sorption response of selected Argonne Premium bituminous coals to CO2, CH4, and N2, International Coalbed Methane Symposium, Tuscaloosa, AL, U.S.A.

Kelemen, S.R., Kwiatek, L.M., Siskin, M., Lee, A.G.K., 2005. Structural Response of Coal to Drying and Pentane Sorption. Energy & Fuels 20, 205-213.

Kiyama, T., Nishimoto, S., Fujioka, M., Xue, Z., Ishijima, Y., Pan, Z., Connell, L.D., 2011. Coal swelling strain and permeability change with injecting liquid/supercritical CO2 and N2 at stress-constrained conditions. International Journal of Coal Geology 85, 56-64.

Levine, J.R., 1991. The impact of oil formed during coalification on generation and storage of natural gas in coal bed reservoir system, 3rd Coalbed Methane Symposium Proceedings, Tuscaloosa, AL.

Levine, J.R., 1996. Model study of the influence of matrix shrinkage on absolute permeability of coal bed reservoirs. Geological Society, London, Special Publications 109, 197-212.

Levy, J.H., Day, S.J., Killingley, J.S., 1997. Methane capacities of Bowen Basin coals related to coal properties. Fuel 76, 813-819.

Li, D., Liu, Q., Weniger, P., Gensterblum, Y., Busch, A., Krooss, B.M., 2010. High-pressure sorption isotherms and sorption kinetics of CH4 and CO2 on coals. Fuel 89, 569-580.

Liu, H.-H., Rutqvist, J., 2010. A New Coal-Permeability Model: Internal Swelling Stress and Fracture–Matrix Interaction. Transport in Porous Media 82, 157-171.

Liu, J., Chen, Z., Elsworth, D., Miao, X., Mao, X., 2010a. Evaluation of stress-controlled coal swelling processes. International Journal of Coal Geology 83, 446-455.

Liu, J., Chen, Z., Elsworth, D., Miao, X., Mao, X., 2010b. Linking gas-sorption induced changes in coal permeability to directional strains through a modulus reduction ratio. International Journal of Coal Geology 83, 21-30.

Liu, J., Elsworth, D., Brady, B.H., 1997. Analytical evaluation of post-excavation hydraulic conductivity field around a tunnel. International Journal of Rock Mechanics and Mining Sciences 34, 181.e181-181.e187.

Liu, J., Wang, J., Chen, Z., Wang, S., Elsworth, D., Jiang, Y., 2011. Impact of transition from local swelling to macro swelling on the evolution of coal permeability. International Journal of Coal Geology 88, 31-40.

Mathews, J.P., Pone, J.D.N., Mitchell, G.D., Halleck, P., 2011. High-resolution X-ray computed tomography observations of the thermal drying of lump-sized subbituminous coal. Fuel Processing Technology 92, 58-64.

Mazumder, S., Farajzadeh, F., 2010. An alternative mechanistic model for permeability changes of coalbeds during primary recovery of methane, SPE Asia Pacific Oil and Gas Conference and Exhibition. SPE, Brisbane, Queensland.

Menon, V.C., Leon, C.A.L.Y., Kyotani, T., Radovic, L.R., 1991. The effect of moisture on the sorption of gases by coal, Prepr. Pap. - Am. Chem. Soc., Div. Fuel Chem., American Chemical Society, New York, NY, pp. 20-IEC.

Min, K.-B., Rutqvist, J., Elsworth, D., 2009. Chemically and mechanically mediated influences on the transport and mechanical characteristics of rock fractures. International Journal of Rock Mechanics and Mining Sciences 46, 80-89.

Norinaga, K., Kumagai, H., Hayashi, J.-I., Chiba, T., Sasaki, M., 1997. Type of water associated with coal, Argonne National Lab, San Francisco.

Ouyang, Z., Elsworth, D., 1993. Evaluation of groundwater flow into mined panels. International Journal of Rock Mechanics and Mining Sciences & Geomechanics Abstracts 30, 71-79.

Palmer, I., 2009. Permeability changes in coal: Analytical modeling. International Journal of Coal Geology 77, 119-126.

Palmer, I., Mansoori, J., 1998. How permeability depends on stress and pore pressure in coalbeds: a new model, SPE Annual Technical Conference and Exhibition. Society of Petroleum Engineers, Denver, Colorado.

Pan, Z., Connell, L.D., 2007. A theoretical model for gas adsorption-induced coal swelling. International Journal of Coal Geology 69, 243-252.

Pan, Z., Connell, L.D., 2012. Modelling permeability for coal reservoirs: A review of analytical models and testing data. International Journal of Coal Geology 92, 1-44.

Pan, Z., Connell, L.D., Camilleri, M., Connelly, L., 2010. Effects of matrix moisture on gas diffusion and flow in coal. Fuel 89, 3207-3217.

Pashin, J.C., 2010. Variable gas saturation in coalbed methane reservoirs of the Black Warrior Basin: Implications for exploration and production. International Journal of Coal Geology 82, 135-146.

Pashin, J.C., McIntyre, M.R., 2003. Temperature-pressure conditions in coalbed methane reservoirs of the Black Warrior basin: implications for carbon sequestration and enhanced coalbed methane recovery. International Journal of Coal Geology 54, 167-183.

Pini, R., Ottiger, S., Burlini, L., Storti, G., Mazzotti, M., 2009. Role of adsorption and swelling on the dynamics of gas injection in coal. J. Geophys. Res. 114, B04203.

Pone, J.D.N., Halleck, P.M., Mathews, J.P., 2010. 3D characterization of coal strains induced by compression, carbon dioxide sorption, and desorption at in-situ stress conditions. International Journal of Coal Geology 82, 262-268.

Prinz, D., Littke, R., 2005. Development of the micro- and ultramicroporous structure of coals with rank as deduced from the accessibility to water. Fuel 84, 1645-1652.

Radliński, A.P., Busbridge, T.L., Gray, E.M., Blach, T.P., Cheng, G., Melnichenko, Y.B., Cookson, D.J., Mastalerz, M., Esterle, J., 2009. Dynamic Micromapping of CO2 Sorption in Coal. Langmuir 25, 2385-2389.

Reeves, S., 2003. Geologic sequestration of CO2 in deep, unmineable coalbeds: An integrated research and commercial-scale field demonstration project. Department of Energy, Houstan.

Reucroft, P.J., Patel, H., 1986. Gas-induced swelling in coal. Fuel 65, 816-820.

Robertson, E.P., 2005. Measurement and modeling of sorption-induced strain and permeability changes in coal. Idaho National Laboratory, Idaho.

Robertson, E.P., Christiansen, R.L., 2007. Modeling laboratory permeability in coal using sorption-induced-strain data. SPE Reservoir Evaluation & Engineering 10.

Rogers, R.E., 1994. Coalbed Methane: Principles and Practice. PTR Prentice Hall, Englewood Cliffs, N.J.

Schepers, K.C., Oudinot, A.Y., Ripepi, N., 2010. Enhanced gas recovery and CO2 storage in coalbed-methane reservoirs: optimized injected-gas composition for mature basins of various coal rank, SPE International Conference on CO2 Capture, Storage, and Utilization, New Orleans, Louisiana, USA.

Seidle, J.P., Jeansonne, M.W., Erickson, D.J., 1992. Application of matchstick geometry to stress dependent permeability in coals, SPE Rocky Mountain Regional Meeting. SPE, Casper, Wyoming.

Seidle, J.R., Huitt, L.G., 1995. Experimental measurement of coal matrix shrinkage due to gas desorption and implications for cleat permeability increases, International Meeting on Petroleum Engineering. Society of Petroleum Engineer.

Shi, J.-Q., Durucan, S., 2005. A model for changes in coalbed permeability during primary and enhanced methane recovery. SPE Reservoir Evaluation & Engineering 8.

Shi, J.-Q., Durucan, S., 2008. Modelling of mixed-gas adsorption and diffusion in coalbed reservoirs, SPE Unconventional Reservoirs Conference, Keystone, Colorado, USA.

Siemons, N., Busch, A., 2007. Measurement and interpretation of supercritical CO_2 sorption on various coals. International Journal of Coal Geology 69, 229-242.

Siriwardane, H.J., Gondle, R.K., Smith, D.H., 2009. Shrinkage and swelling of coal induced by desorption and sorption of fluids: Theoretical model and interpretation of a field project. International Journal of Coal Geology 77, 188-202.

Soeder, D.J., 1991. The effects of overburden stress on coalbed methane production. TechBooks, Sponsored by American Association of Petroleum Geologists, Energy Minerals Division, Fairfax, VA.

Somerton, W.H., Söylemezoglu, I.M., Dudley, R.C., 1975. Effect of stress on permeability of coal. International Journal of Rock Mechanics and Mining Sciences & Geomechanics Abstracts 12, 129-145.

Unsworth, J.F., Fowler, C.S., Heard, N.A., Weldon, V.L., McBrierty, V.J., 1988. Moisture in coal: 1. Differentiation between forms of moisture by n.m.r. and microwave attenuation techniques. Fuel 67, 1111-1119.

US-DOE, 2004. Coalbed methane premier: New source of natural gas–environmental implication, Background and development in the Rocky Mountain West. National Petroluem Technology Office, p. 77.

van Bergen, F., Krzystolik, P., van Wageningen, N., Pagnier, H., Jura, B., Skiba, J., Winthaegen, P., Kobiela, Z., 2009. Production of gas from coal seams in the Upper Silesian Coal Basin in Poland in the post-injection period of an ECBM pilot site. International Journal of Coal Geology 77, 175-187.

van Bergen, F., Pagnier, H., Krzystolik, P., 2006. Field experiment of enhanced coalbed methane-CO2 in the upper Silesian basin of Poland. Environmental Geosciences 13, 201-224.

Walker Jr, P.L., Verma, S.K., Rivera-Utrilla, J., Khan, M.R., 1988. A direct measurement of expansion in coals and macerais induced by carbon dioxide and methanol. Fuel 67, 719-726.

Wang, S., Elsworth, D., Liu, J., 2011. Permeability evolution in fractured coal: the roles of fracture geometry and water content. International Journal of Coal Geology 87, 13-25.

Wang, S., Elsworth, D., Liu, J., 2012. A mechanistic model for permeability evolution in fractured sorbing media. Journal of Geophysical Research in press.

White, J.M., Mazurkiewicz, M., 1989. Effect of moisture content on mechanical properties of Nemo coal, Moberly, Missouri U.S.A. Mining Science and Technology 9, 181-185.

Wolfram Mathematica 7.2, 2009. Uncertainty analysis tool.

Wu, Y., Liu, J., Chen, Z., Elsworth, D., Pone, D., 2010a. A dual poroelastic model for CO2-enhanced coalbed methane recovery. International Journal of Coal Geology 86, 177-189.

Wu, Y., Liu, J., Elsworth, D., Chen, Z., Connell, L., Pan, Z., 2010b. Dual poroelastic response of a coal seam to CO2 injection. International Journal of Greenhouse Gas Control 4, 668-678.

Wu, Y., Liu, J., Elsworth, D., Miao, X., Mao, X., 2010c. Development of anisotropic permeability during coalbed methane production. Journal of Natural Gas Science and Engineering 2, 197-210.

Chapter 2 : Effect of CO2 Injection on Homogeneously and Heterogeneously Permeable Coalbed Reservoirs

Abstract

Enhanced coalbed methane (ECBM) can be recovered by injecting a gas such as carbon dioxide into the reservoir to displace methane. The contrast between density, viscosity, and permeability of the resident and displacing fluids affects the efficiency of ECBM recovery. The prediction of earlier breakthrough becomes complex as the permeability may vary by orders of magnitude during gas injection and methane recovery. Predominantly, the reservoir permeability is modulated by the pore pressure of the sorptive gas (CH_4 and CO_2) and effective stresses. Here we explore the possibility of early breakthrough and its implications for managing coalbed reservoirs during CO_2 assisted ECBM. A coupled finite element (FE) model of binary gas flow, diffusion, competitive sorption and permeability change is used to explore the effect of CO_2 injection on net recovery, permeability evolution and injectivity in uniform and homogeneously permeable reservoirs. This effect is evaluated in terms of dimensionless pressure (p_D), permeability (k_D) and fracture spacing (x_D) on the recovery of methane and permeability evolution for ECBM and non-ECBM scenarios. We have considered two scenarios (4MPa and 8 MPa) of constant pressure injection of CO_2 for ECBM. The increase in production rate of CH_4 is proportional to k_D but inversely proportional to x_D.

Further, a reservoir with initial permeability heterogeneity was considered to explore the effect of CO_2 injection on the evolution of permeability heterogeneity – whether heterogeneity increases or decreases. The evolution of permeability

49

heterogeneity is investigated for the same two CO_2 injection scenarios. For the specific

parameters selected, the model results demonstrate that: (1) The injection of CO_2 in

coalbed reservoirs increases the production nearly 10 fold. (2) At higher injection

pressures the recovery is rapid and the production increases dramatically - the production

increases 2 fold on increasing the CO_2 injection pressure from 4 MPa to 8 MPa (3)

However, CO_2 breakthrough occurs earlier at higher injection pressures. (4) The

permeability heterogeneity in the reservoir is reduces after a threshold time (~500 days)

although the overall heterogeneity is increased relative to the initial condition is overall

increased for both non-CO_2 and CO_2 injection scenarios. This indicates that the

homogenizing influence of CO_2-sorption-swelling is outpaced by CH_4-desorption-

shrinkage and effective stress influences. This leaves the reservoir open to short-

circuiting and earlier breakthrough of CO_2 rather than having this effect damped-out by

the homogenizing influence of swelling. (5) The cumulative volume of CO_2 produced

and stored in the reservoir is proportional to the injection pressure.

1 Introduction

Enhanced coalbed methane (ECBM) recovery may be promoted by the injection of carbon dioxide as CO_2-ECBM. The lower physisorption affinity of CH_4 in coal promotes its desorption on injection of CO_2 in coal seams (Karacan, 2003; Larsen, 2004). The enhanced recovery of CH_4 with injection of CO_2 can be as high as 90% as compared to conventional pressure depletion methods (50%) (IPCC, 2005). There is potential for CO_2 sequestration in deep unminable coal seams ranging from 6 to 20% of the total sequestration capacity worldwide (IPCC, 2005).

Coalbed reservoirs are self-sourcing with the majority of the CH_4 stored in the adsorbed state in thecoal matrix (Rogers, 1994). Some laboratory investigations for pure gas adsorption on pulverized coal indicated that the adsorption of CO_2 on a molar basis may be approximately two times that of CH_4 in American bituminous coals (White et al., 2005). The volumetric adsorption capacity ratio of CO_2/CH_4 on coal ranges from one on anthracite coal to ten for low-rank coals (IPCC, 2005). This ratio may be larger at higher pressures for all ranks coal (Hall et al., 1994; Krooss et al., 2002). The permeability of coalbed reservoirs is principally determined by the fracture network (cleats) while the coal matrix is considered relatively impermeable (Harpalani and Chen, 1995). The cleat permeability is controlled by the dynamic effective stress regime and by the adsorption/desorption induced swelling/shrinkage of the matrix during continued production (Harpalani and Chen, 1997; Harpalani and Schraufnagel, 1990; Kumar et al.,

51

2012). Gas adsorption and related swelling is influenced by sorption capacity, coal rank, maceral composition and the composition of the permeating gas (Chikatamarla et al., 2004; Kumar et al., 2012; Levine, 1996; Pone et al., 2010). The dynamics of swelling/shrinkage becomes more complex if the coalbed methane production is assisted by CO_2 injection. The presence of sorptive gases (CH_4 and CO_2) swells the matrix resulting in reduction of cleat aperture while desorption promotes cleat dilation for constrained coals under in situ conditions. CO_2-injection for ECBM often results in net swelling of the coal matrix (Chikatamarla et al., 2004; Harpalani and Chen, 1997; Levine, 1996; Pekot and Reeves, 2002) and the additional matrix strain will reduce the fracture aperture leading to porosity and permeability loss (Fokker and van der Meer, 2004; Shi and Durucan, 2004). The competitive adsorption, sorption capacity, matrix shrinkage/swelling and permeability transformations are among the important factors affecting CO_2 assisted ECBM. The sorption/desorption induced swelling/shrinkage and the resultant volumetric strain affecting permeability has been studied in detail (Harpalani and Chen, 1999; Karacan, 2003, 2007). With continuous production of methane from a bituminous coal, the permeability increases one-hundred fold and the rate of increase accelerates (Mitra et al., 2012). The displacement of CH_4 with CO_2 injection in laboratory experiments causes significant changes in the stress/strain fields (Wang et al., 2010) and decreases the permeability which is partly attributed to swelling. The adsorption of CO_2 is thought to be responsible for the microfractures observed along the maceral-maceral interface for a high-volatile bituminous coal under unconfined condition (Hol et al., 2012). However, microfracturing may also occur upon depressurization as the contributions of different lithotype permeability and gas capacities cause strains within

the coal (Clarkson and Bustin, 1997; Karacan, 2003; Pone et al., 2009). The resulting

porosity enhancement may help in the transport of CO_2 in the coal seam. There have been

many experimental studies exploring the effect of coal rank (Day et al., 2008; Shen et al.,

2011), maceral composition (Day et al., 2008), moisture content (Wang, 2012), sorption

(Viete and Ranjith, 2006) and in situ stress on the strain dilation (Chen et al., 2010;

Harpalani and Chen, 1997; Pone et al., 2010), stiffness (Masoudian-Saadabad et al.,

2011), porosity loss (Harpalani and Chen, 1995), permeability transformations (Kumar et

al., 2012; Wang, 2012), sorption capacity (Hol et al., 2011; Wang et al., 2010; Weniger et

al., 2012) and transport characteristics.

There are multiple demonstration sites around the world exploring both CBM and

ECBM. The Allison unit in the San Juan basin (US), for example explored CO_2-ECBM.

The CH_4 production data on CO_2 injection in coal seams indicated various phenomena

e.g. matrix shrinkage/swelling leading to permeability enhancement/loss (Reeves, 2003).

Up to a one-hundred fold increase in permeability was observed in some wells (Clarkson

et al., 2008; Reeves, 2003; Shi and Durucan, 2010).

Reservoir simulation studies for production forecast and history matching have

been conducted for various CBM and ECBM fields (Durucan and Shi, 2009; Shi and

Durucan, 2010; Wu et al., 2010a). The recovery of methane with CO_2 injection causes a

series of coal-gas interactions which include injection/depletion induced volumetric

swelling/shrinkage, dynamic changes in stress patterns and the coal characteristics.

Various models have been proposed to predict these permeability transformations (Bai et

al., 1993; Clarkson et al., 2010; Durucan and Shi, 2009; Gu and Chalaturnyk, 2006;

Harpalani and Chen, 1995; Levine, 1996; Liu et al., 2010a, b; Liu et al., 1997; Ouyang

and Elsworth, 1993; Palmer, 2009; Palmer and Mansoori, 1998; Pan et al., 2010; Shi and Durucan, 2005; Shi and Durucan, 2008; Wang et al., 2012). They may be categorized as strain-based, stress-based and purely empirical (Palmer, 2009). An existing single well for CO_2-ECBM micro-pilot test in anthracite coals of South Qinshui basin, Shanxi Province, China was successfully simulated for the production of CH_4 (Wu et al., 2011). ECBM recovery and CO_2 storage in Appalachian thin seams was simulated for horizontal wells and it was recommended that the mixture of flue gas and CO_2 would yield better recovery than the pure CO_2 injection (Durucan and Shi, 2009). The observations from a CO_2-ECBM test project in a 6m thick coal seam at Yubari, Northern Japan were found to be consistent with CO_2 sorption induced swelling in coal (Fujioka et al., 2010).

These observations from experimental, pilot plant, and simulation studies may be exploited for optimizing CO_2-ECBM recovery. The model implemented here includes the dynamics of gas flow, diffusion, competitive sorption and permeability change to explore the effect of CO_2 injection on net recovery, permeability evolution, and injectivity in a homogeneous reservoir. The cleats in the coal have a wide range of apertures therefore the permeability of the fractures may vary over a similarly wide range. To explore and quantify permeability evolution under such practical constraints we extended our FE model to examine the impact of permeability heterogeneity.

2 This Study

In CO_2-ECBM recovery the relatively high viscosity fluid CO_2 displaces a less viscous fluid, CH_4, present in the reservoir. A dual porosity FE model for binary gases (CH_4 and CO_2) is assembled where coal matrix and fractures are represented by dual continua. This model may be used for explicitly quantifying the interactions between the binary gases and sorbing solid media during CO_2 assisted ECBM recovery. We have implemented a general porosity model for matrix and fractures together with a general permeability model for the matrix. A new model for fracture permeability, under conditions of in situ stress and constrained displacement has been implemented (Kumar et al., 2012). The FE model implemented here presents insights into the non-linear response of CH_4 depletion, CO_2 injection, porosity transformation, permeability evolution for the matrix and fracture system during continued production of CH_4 with concomitant injection of CO_2. A logical sequence of this model extends to a model which has initial fracture permeability heterogeneity in the coalbed reservoir. This FE model assumes a Gaussian normal distribution of permeability at the beginning of the production and predicts the change in permeability during the life span of the reservoir. The behavior of the CO_2-ECBM system is governed by a set of field equations consisting of coal deformation, multi-gas adsorption, and gas transport. These equations are coupled with porosity and permeability transformations in both matrix and fractures within an FE solver. We have made some assumptions to allow the solving of these highly non-linear constitutive and field equations simultaneously.

2.1 Assumptions

The coal is conceptualized as solid blocks (coal matrix) attached together with spring (fractures) as shown in Figure 2.1. Here fracture spacing and fracture aperture are referred as *a* and *b* respectively. More details may be found in our previous publications (Bai et al., 1993; Kumar et al., 2012; Tao et al., 2012; Wu et al., 2010a; Wu et al., 2010b).

The following assumptions were implemented for the development of FE simulator.

1) The CBM reservoir consist of dual elastic continuum namely matrix and fracture. They are homogeneous, isotropic and isothermal.

2) The water in the reservoir is an immobile phase and the gas flow obeys Darcy Law for single phase flow.

3) The gas present in the pores of the reservoir is ideal and its viscosity is a function of temperature but not pressure.

4) Zero strain condition exists in the reservoir.
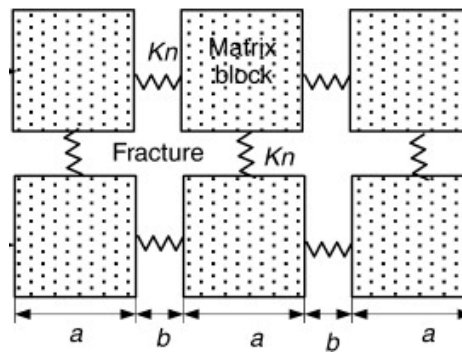
Figure 2.1: Schematic representation of coal-fracture dual continuum system (Wu et al., 2010a).

2.2 Field Equations

2.2.1 Binary Gas Adsorption

A coalbed methane reservoir often contains more than 80% CH_4 and a mixture of other higher hydrocarbons and CO_2 (Rice, 1993). This study assumes that the CBM reservoir contains only CH_4 (85%) and CO_2 (15%). This gas mixture governs the reservoir characteristics. The remaining gas components are ignored. The equation of state for an ideal gas holds the following relation between pressure, volume and temperature in both matrix and fractures (equation 1)

$$pV = nRT \tag{1}$$

If the concentration C is represented as the number of moles per unit volume, $C = \frac{n}{V}$ then equation (1) can be rewritten as equation (2),

$$p = CRT \tag{2}$$

where p [Pa] is pressure, V [m^3] is volume, R [m^3.Pa/K/mol] is gas constant, n is number of moles, T [K] is temperature.

The gas adsorbed in the coal matrix follows a Langmuir sorption relation and the gas volume adsorbed per unit of coal mass can be calculated using the Langmuir equation (Langmuir, 1916) as given in equation (3)

$$V = \frac{V_L p_m}{p_m + p_L} \qquad (3)$$

where V_L is the adsorbed volume per unit of coal at infinite pressure, p_m is the equilibrium pressure of gas in the matrix, p_L is the Langmuir pressure and V is the volume adsorbed per unit of coal mass at pressure p_m.

The adsorption of two (binary) or more than two gases in an adsorbent may be expressed by the extended Langmuir isotherm (ELI) as follows (equation 4):

$$V_k = \frac{V_{k0} C_k b'_k}{1 + \sum_{j=1}^{N} C_j b'_j} \qquad (4)$$

where V_{k0} is the adsorbed volume of pure species per unit of coal at infinite pressure, C_k is the equilibrium concentration of gas in the matrix, b'_k is $1/(p_L.R.T)$ and V is the volume adsorbed per unit of coal mass at concentration c_m for species k. Similarly, the contribution of an individual species in a n-species mixture towards sorption-induced volumetric strain may be expressed as (Wu et al., 2010a) as

$$\varepsilon_k = \varepsilon_{Lk} \frac{C_k b'_k}{1 + \sum_{j=1}^{n} C_j b'_j}. \qquad (5)$$

The total sorption induced strain can be calculated by summing the strain caused by each species as, (Wu et al., 2010a)

$$\varepsilon_s = \sum_{k=1}^{n} \varepsilon_k = \sum_{k=1}^{n} \varepsilon_{Lk} \frac{C_k b'_k}{1 + \sum_{j=1}^{n} C_j b'_j} \qquad (6)$$

where ε_{Lk} is the strain developed by a pure species at infinite pressure, ε_k is the strain developed at concentration of gas C_k in the matrix for species k and ε_s is the total strain

developed by all species in the coal. Note that *k=1* and 2 are for CH_4 and CO_2 respectively.

2.2.2 Binary Gas Transport

Typically a CBM reservoir is partially dewatered first to produce gas. The onset of water removal occurs when the seam pore pressure is below a critical pressure usually corresponding to saturation pressure (Kumar et al., 2012). The pressure depletion in the reservoir triggers various transport process on different length scales.

1) In the primary porosity system (*i.e.* coal matrix) the permeability is negligible and the diffusion (primarily Fickian) is the dominant mode of flow. 2) In the secondary porosity system (i.e. face or butt cleat system (fractures)) the flow is laminar and obeys Darcy law. 3) Transfer of mass between matrix and fractures where either medium may act as source or sink depending upon the sense of the pressure differential.

A detailed analysis may be found in previous publications (Wu et al., 2010a; Wu et al., 2010b). The mass balance equation incorporating the previously mentioned convective, diffusive and transfer fluxes may be expressed as,

$$\frac{\partial m_k}{\partial t} + \nabla.\left(\vec{v}.\rho_{gk}\right) + \nabla.\left(-D_k.\nabla m_{kf}\right) = Q_{sk} \tag{7}$$

where the gas content of a component gas k is m_k which includes both free-phase and adsorbed gas. The mass of each component of gas present in a unit of coal-matrix and fracture system can be written as,

For fracture: $m_{fk} = \varphi_f.C_{fk}.M_{fk}$ $\tag{8}$

For matrix: $m_{mk} = \varphi_m . C_{mk} . M_{mk} + (1 - \varphi_{m0}) . \rho_c . \rho_{sg} . \frac{V_{Lk} b\prime_k C_{mk}}{1 + C_{m1} b\prime_1 + C_{m2} b\prime_2}$ (9)

The convective velocity $\vec{v}$ is determined by the concentration gradient in the

fracture or matrix and can be expressed as,

$$\vec{v}_f = -\frac{k_f RT}{\mu} \nabla C_{fk}$$ (10)

$$\vec{v}_m = -\frac{k_m RT}{\mu} \nabla C_{mk}$$ (11)

where ρ_{gk} is the gas density, ρ_{sg} is the gas density at standard conditions, ρ_c is the coal

density, M_k is the molar mass of component k, Q_{sk} is the gas source or sink, and D_k is the

hydrodynamic dispersion coefficient defined as,

$$D_{fk} = \beta_c . \vec{v}_f + D_{fk0}$$ (12)

$$D_{mk} = \beta_c . \vec{v}_m + D_{mk0}$$ (13)

where, D_{k0} is the coefficient of molecular diffusion of component k and β_c is the

dynamic dispersivity.

The transfer flux ω_k between matrix and fracture for a component of gas k may

be written as (Mora and Wattenbarger, 2009)

$$\omega_k = -\frac{3\Pi^2}{a^2}$$ (14)

where a is the fracture spacing in a cube block model (Warren and Root, 1963).

2.3 Constitutive Equations

2.3.1 Porosity Model for Matrix and Fracture

The porosity for the coal matrix can be defined (Liu et al., 2010a, b; Liu et al., 2011; Wu et al., 2010a; Wu et al., 2011) as a function of single gas adsorption,

$$\varphi_m = \varphi_{m0} - \frac{\alpha}{K} \frac{1}{\frac{b_0}{aK_f}+\frac{1}{K}} \left(\frac{\varepsilon_L P_m}{P_L+P_m} - \varepsilon_v \right) \tag{15}$$

where φ_{m0} is the initial matrix porosity, α is the Biot coefficient for the coal matrix, K is the matrix bulk modulus, K_f is the modified fracture stiffness, $K_n = K_f/b_0$ is the fracture stiffness, b_0 is the initial fracture aperture and φ_m is the matrix porosity.

If the sorption is caused by a binary mixture of gases then the volumetric strain term in equation (15) can be replaced by equation (6) and the matrix porosity equation yields,

$$\varphi_m = \varphi_{m0} - \frac{\alpha}{K} \frac{1}{\frac{b_0}{aK_f}+\frac{1}{K}} \left(\sum_{k=1}^{2} \varepsilon_{Lk} \frac{C_{mk}b\prime_k}{1+\sum_{j=1}^{n} C_{mj}b\prime_j} - \varepsilon_v \right) \tag{16}$$

Similarly, the porosity of the fracture system can be expressed as (Wu et al., 2010a)

$$\frac{\varphi_f}{\varphi_{f0}} = 1 + \frac{\Delta b}{b_0} = 1 - \frac{3}{\varphi_{f0}+\frac{3K_f}{K}} \left(\sum_{k=1}^{2} \varepsilon_{Lk} \frac{C_{mk}b\prime_k}{1+\sum_{j=1}^{n} C_{mj}b\prime_j} - \varepsilon_v \right) \tag{17}$$

where φ_{f0} is the initial fracture porosity, Δb is the differential change in aperture and φ_f is the fracture porosity. The subscripts *f* and *m* are for fracture and matrix respectively in each parameter.

2.3.2 Permeability Model for Matrix and Fracture

The permeability of the matrix can be expressed as (Wu et al., 2010a),

$$\frac{k_m}{k_{m0}} = \left(1 - \frac{\alpha}{\varphi_{m0}K} \frac{1}{\frac{b_0}{aK_f} + \frac{1}{K}} \left(\sum_{k=1}^{2} \varepsilon_{Lk} \frac{C_{mk}b'_k}{1 + \sum_{j=1}^{n} C_{mj}b'_j} - \varepsilon_v\right)\right)^3 \tag{18}$$

where, k_{m0} is the initial matrix permeability and k_m is the evolving permeability of the matrix.

Based on our previous work (Kumar et al., 2012) the permeability of the fracture network in coal may be expressed as,

$$\frac{k_{fk}}{k_{f0k}} = \left\{\left(1 + \frac{C_k p_{mk}}{p_{mk} + p_{Lk}}\right)^3 + e^{-\beta_k \sigma'}\right\} * e^{-\delta_k S_w} \tag{19}$$

where k_{f0} is the initial permeability of the fracture system, p_m is the gas pressure in the matrix, p_L is the Langmuir pressure constant, σ' is effective stress, S_w is the moisture content of the coal and k_f is the permeability of the fracture system. The fitting parameters are C, β and δ. Note that subscript k=1 or 2 is for CH_4 and CO_2 respectively.

3 Analysis of Permeability

3.1 Flow Instability in CO_2 sweep

In the context of ECBM recovery, a high viscosity fluid (CO_2) displaces a low viscosity fluid i.e. interstitial CH_4. The high viscosity fluid CO_2 exhibits lower permeability than CH_4 at the same pore pressure under similar confining conditions (Kumar et al., 2012). The possible flow instability is investigated using Saffman-Taylor

instability criterion (Saffman and Taylor, 1958). The velocity of the displacing and displaced fluid is assumed to be the same on either side of the sweeping front. The perturbations grow with time in an unstable front. This can be formulated as follows after ignoring the gravitational effects.

$$\left(\frac{\left(\frac{\mu_1 \varphi_1}{k_1} - \frac{\mu_2 \varphi_2}{k_2} \right) U}{\left(\frac{\mu_1 \varphi_1}{k_1} + \frac{\mu_2 \varphi_2}{k_2} \right)} \right) \geq 0 \tag{20}$$

Here μ_1 and μ_2 are viscosities, ϕ_1, ϕ_2 are porosities and k_1, k_2 are permeability for CH_4 and CO_2 respectively. The velocity of the displacing front is represented by U.

If the porosity is assumed to be equal on both side of the displacing front then equation (20) may be rewritten as,

$$\frac{k_1}{k_2} \leq \frac{\mu_1}{\mu_2} \tag{21}$$

The maximum viscosity ratio for CH_4 to CO_2 is ~3/4. However the permeability ratio on the left hand side of equation (26) is more than 1 at a given pore pressure for both gases. This indicates that the displacing front is inherently and unconditionally stable and the amplitude of any perturbation would dampen for the case of a homogeneous medium but with a step change in permeability across the front. However, this analysis does not necessarily hold for heterogeneous permeabilities, but may be an indication of expected response.

3.2 Dimensionless Analysis

In a unit volume of fracture, the mass of the species and its rate of change is the net result of advection of the species into the volume which is governed by Darcy flow

$\nabla . \left(-\frac{k_f}{\mu} p_f \nabla . p_f \right)$ and addition or removal of the species from the volume due to

exchange with the matrix $\pm \frac{3\Pi^2}{a^2} \frac{k_m}{\mu} p_f (p_f - p_m)$. The mass balance of the unit volume is

governed by,

$$[\varphi_f] \frac{\partial p_f}{\partial t} + \nabla . \left(-\frac{k_f}{\mu} p_f \nabla . p_f \right) = -\frac{3\Pi^2}{a^2} \frac{k_m}{\mu} p_f (p_f - p_m) \tag{22}$$

Equation (22) can be rearranged as

$$\frac{1}{p_f} [\varphi_f] \frac{\partial p_f}{\partial t} + \nabla . \left(-\frac{k_f}{\mu} \nabla . p_f \right) = -\frac{3\Pi^2}{a^2} \frac{k_m}{\mu} (p_f - p_m) \tag{23}$$

Dividing equation (23) by $p_m, k_m/\mu$ and $1/a^2$ the resulting form may be

expressed as

$$\frac{\mu a^2}{k_m p_f p_m} [\varphi_f] \frac{\partial p_f}{\partial t} - a^2 \frac{k_f}{k_m} \nabla . \left(\nabla . \frac{p_f}{p_m} \right) = 3\pi^2 \left(1 - \frac{p_f}{p_m} \right) \tag{24}$$

For the sake of simplicity the one dimensional form may be written as

$$\frac{\mu a^2}{k_m p_f} [\varphi_f] \frac{\partial (p_f/p_m)}{\partial t} - \frac{k_f}{k_m} \frac{\partial}{\partial (x/a)^2} \left(\frac{p_f}{p_m} \right) = 3\pi^2 \left(1 - \frac{p_f}{p_m} \right) \tag{25}$$

The dimensionless variables in equation (25) are pressure p_D, permeability k_D,

characteristics length x_D and time t_D. They can be expressed as

$$p_D = \left(\frac{p_f}{p_m} \right); \; k_D = \left(\frac{k_f}{k_m} \right); \; x_D = \left(\frac{x}{a} \right); \; t_D = \left(\frac{t}{\frac{\mu a^2}{k_m p_f}} \right)$$

The dimensionless form of the mass conservation relation can be written as

$$\varphi_f \frac{\partial p_D}{\partial t_D} - k_D \frac{\partial p_D}{\partial x_D{}^2} = 3\pi^2 (1 - p_D) \tag{26}$$

Equation (26) indicates that the dimensionless pressure, permeability and

characteristic length may play an important role in the production. This has been

investigated by varying p_D, k_D and x_D parameters in the later sections.

4 Model Implementation

The physics implemented in this study simulates the results of CO_2 assisted ECBM. The model simulates a five well pattern where an injection well (IW) lies at the center of a square array of four production wells (PW) Figure 2.2. All the wells are assumed to be vertical and pierce the horizontal seam through its entire height.

We have utilized conservation of mass for each gas together with flux transfer between matrix and fracture depending on the pressure difference. The exchange of gases (CH_4 and CO_2) under the phenomenon of adsorption/desorption, governed by the extended Langmuir isotherm, triggers transformations in porosity and permeability in the matrix-fracture system. The transformations in porosity and permeability affect the flow of fluid in the fracture network which is governed by Darcy's law. Darcy and diffusion driven flow are implemented in the matrix however, diffusion is the dominant transport mode. The CH_4 residing in the matrix is released as the gas pressure reduces and results in matrix-shrinkage. The fracture network receives the released CH_4. With the continued production of CH_4 and injection of CO_2, the permeability changes with time due to matrix shrinkage/swelling effects. Presumably, a higher rate of CO_2 injection would staunch the reservoir permeability quickly and the permeability drop-rate would be higher.

Also, permeability heterogeneities are employed in the model with mean permeability defining behavior indexed to that of the homogeneous system. The range of the permeability varies from very low (same as that of matrix) to very high (equal to one

Darcy). This allows us to investigate the effect of CO_2 injection on the evolving

heterogeneity of the reservoir.
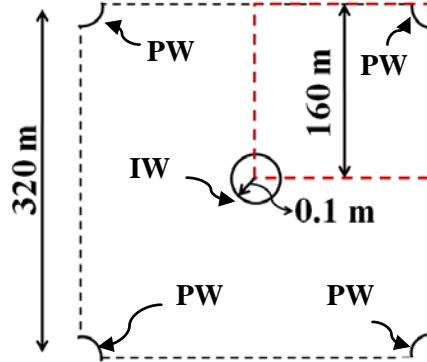
Figure 2.2: A typical five well patterns with four production wells (PW) and one injection

well (IW) at the center.

4.1 Model Description

For the sake of simplicity only a one-quarter section, as outlined with the red

dotted line in Figure 2.2, is simulated. This one-quarter section of the reservoir is

represented by a two dimensional block of sides 160 m x 160 m (Figure 2.3). The lower

left corner has a one-quarter section of the CO_2 injection well (IW) and the upper right

corner of the geometry has a one-quarter section of a CH_4 production well (PW), (Figure

2.3). The diameter of the wells is assumed to be 0.1 m. The model has no flow conditions

for all the boundaries except the well boundaries where a constant pressure condition has

been assumed at the well boundaries. It was also assumed that the production well

produces at 0.1 MPa or 1 atm bottom-hole pressure. We have considered three scenarios

of CO_2 injection: namely no injection, and injection at pressures of 4 MPa and 8 MPa,

respectively. The initial pore pressures of CH_4 and CO_2 in the reservoir have been

assumed as 3.0 MPa and 0.5 MPa, respectively. All boundaries of the simulated area are

fixed. The values of the properties used in this model are given in Table 2.1 (Wu et al.,

2010a). The total simulation time was for 30 years ($\sim 10^9$ seconds). The model has been

implemented in an adaptive mesh mode for fluid dynamics. All the results obtained in

this study are independent of mesh size and time step.
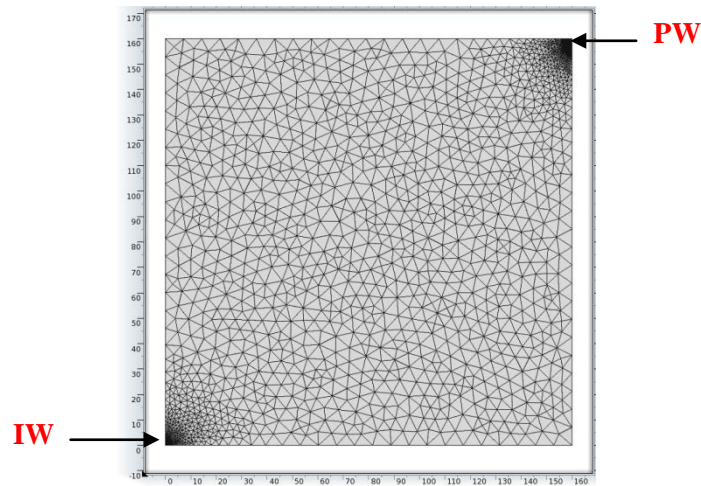
Figure 2.3: Schematic of a one-quarter section (shown with red dotted boundary in figure

2.2) of a five-well pattern. The grid has been laid over the geometry using COMSOL

Multiphysics

Table 2.1: Modeling parameters used in simulations (NIST; Wu et al., 2010a).

Symbol	Parameter	Value	Unit
E	Young's modulus of coal	2.71	GPa
E_S	Young's modulus of coal grain	8.13	GPa
N	Poisson's ratio of coal	0.34	-
ρ_c	Density of coal	1.25×10^3	kg/m^3
μ_{CH_4}	CH$_4$ dynamic viscosity	1.15×10^{-5}	Pa.s
μ_{CO_2}	CO$_2$ dynamic viscosity	1.60×10^{-5}	Pa.s
P_{L,CH_4}	CH$_4$ Langmuir pressure constant	2.07	MPa
P_{L,CO_2}	CO$_2$ Langmuir pressure constant	1.38	MPa
V_{L,CH_4}	CH$_4$ Langmuir volume constant	0.0256	m^3/kg
V_{L,CO_2}	CO$_2$ Langmuir volume constant	0.0477	m^3/kg
ε_{L,CH_4}	CH$_4$ Langmuir volumetric strain constant	0.0128	-
ε_{L,CO_2}	CO$_2$ Langmuir volumetric strain constant	0.0237	-
ϕ_{m0}	Initial porosity of matrix	0.0423	-
ϕ_{f0}	Initial porosity of fracture	0.001	-
k_{m0}	Initial permeability of matrix	3.0×10^{-17}	m^2
k_{f0}	Initial permeability of fracture	3.0×10^{-15}	m^2
a	Fracture spacing	0.01	m
b	Average aperture of the fracture	1×10^{-3}	m

4.2 Homogeneous system

The initial permeability of the fracture network is assumed homogeneous i.e. all the mesh elements in the reservoir have the same permeability at time zero. As the CBM reservoir starts producing with or without the injection of CO$_2$ the permeability of the

reservoir changes. The total production, the transformation of concentration ratio (CH_4/CO_2) and the rate of production are investigated for varying injection pressures, fracture-matrix permeability ratios, and fracture spacing under three scenarios of CO_2 injection. These injection scenarios are those of no injection, and injection at 4 MPa and 8 MPa discussed earlier.

4.2.1   *Effect of Injection Pressure*

The total cumulative production from the CBM reservoir in 30 years is shown in figure 2.4a under three scenarios. It is clear from figures 2.4a & 2.4b that the injection of CO_2 at 8 MPa yields the highest cumulative production (2×10^5 m^3) with the maximum rate of recovery (peak rate 300 m^3/day) in ~30 years. Also, a spectacular increase in the rate of production is observed in the case of CO_2 injection as compared to no injection. The rate of production decreases almost exponentially with injection pressure. The highest production rate occurs with 8 MPa injection while no injection yields the minimum production rate (Figure 2.4b). It is important to note that the "no-injection" scenario yields significantly less production in ~30 years than that of the 8 MPa injection case (~$1/10^{th}$). It indicates that the injection of CO_2 increases the net CH_4 production. These simulations results are in agreement with previous findings for homogeneous reservoirs (Durucan and Shi, 2009; Wu et al., 2010a). The injection of CO_2 however is expected to reduce the permeability and therefore the injectivity. Figure 2.5, shows the permeability evolution in the matrix and fractures for the three scenarios considered. The injection of CO_2 at 8 MPa and the no-injection scenarios exhibit the highest and lowest

69

fracture permeability respectively in a period of ~30 years. If the observation from CH_4

production and permeability evolution are combined it is apparent that injection at 8 MPa

yields the highest production with a maximum permeability, while injection at 4 MPa

yields three fold less production as compared to the 8 MPa injection but two fold more

that no injection. The permeability in the 4 MPa injection case was between that for the 8

MPa and no injection cases during the life of the reservoir. These observations indicate

that the reservoir yields the lowest production with minimum injectivity in the no

injection case, therefore the CO_2-ECBM approach is useful for this reservoir.

The surface map of methane mole fraction in the matrix (Figure 2.6) indicates that

the CH_4 content decreases faster with CO_2 injection than with no injection. However, the

velocity of the sweeping front is approximately twice faster in the 8 MPa injection than

for the 4 MPa injection. For instance, at the end of 100 days, the CO_2 front reaches only

20 m from the injection well bore for the 4 MPa injection case but 40 m when injection

was carried out at 8 MPa (Figure 2.6). Thus, higher injection pressures yield a greater

swept area in a given time. The ratio of average concentration ratio of the two gases CH_4

and CO_2 in the reservoir may also indicate the efficiency and rate of sweep. The

concentration ratio of CH_4:CO_2 decreases faster in both matrix and fracture for 8 MPa

versus 4MPa and is faster for 4 MPa than for the no-injection scenario (8 MPa> 4MPa>

no-injection; Figure 2.7) indicating faster and more effective recovery of methane from

the reservoir for the higher the pressure.
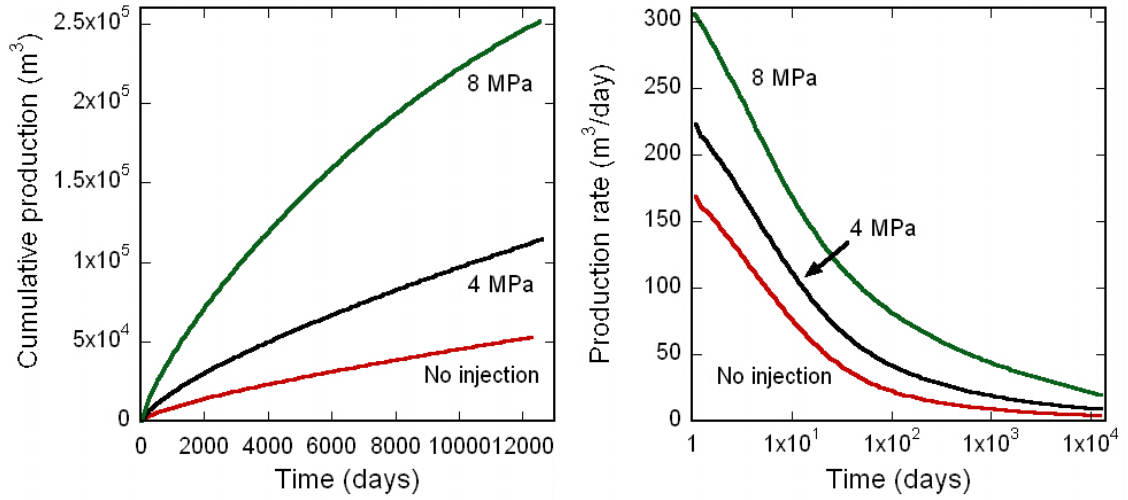
Figure 2.4: a) Total cumulative production of CH_4 for constant pressure CO_2 injection (4 MPa and 8 MPa) and no CO_2 injection scenarios b) Rate of production of CH_4 for two CO_2 injection (8 MPa and 4 MPa) and no CO_2 injection scenarios.
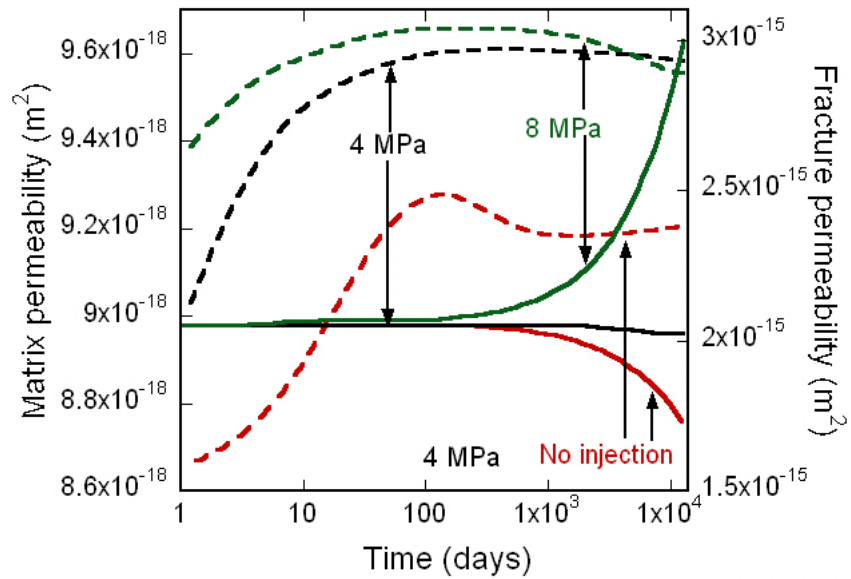
Figure 2.5: The average permeability of the matrix and fracture for no injection, 4 MPa injection and 8 MPa injection scenarios. The solid and dashed lines represent matrix and fracture permeability respectively.

71
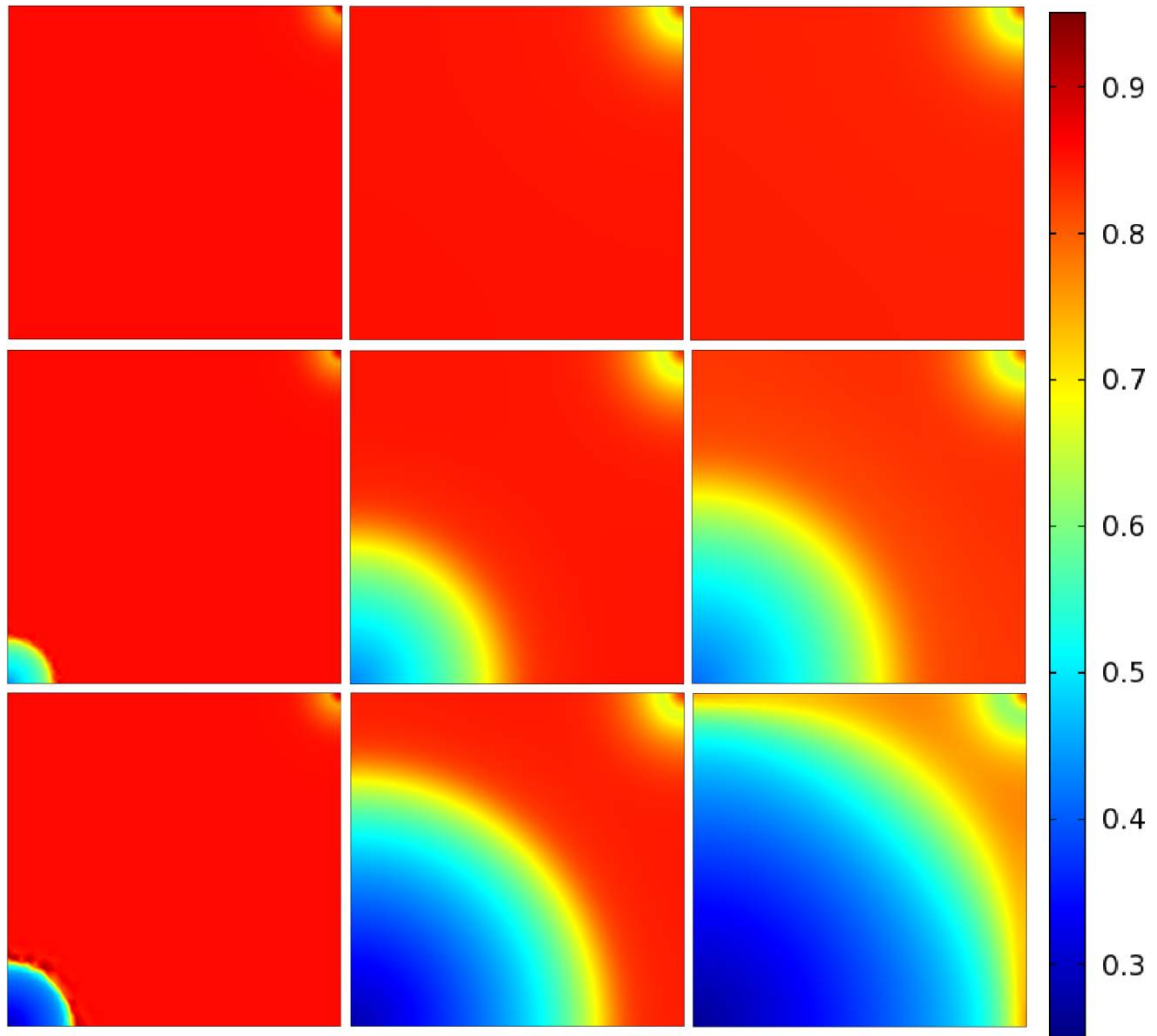
Figure 2.6: The distribution of methane mole fraction for no injection, 4 MPa injection and 8 MPa injection scenarios (from top to bottom) at various times 100, 3000 and 7000 days (from right to left). The low and high color represents the value of 0.25 and 0.95 respectively.
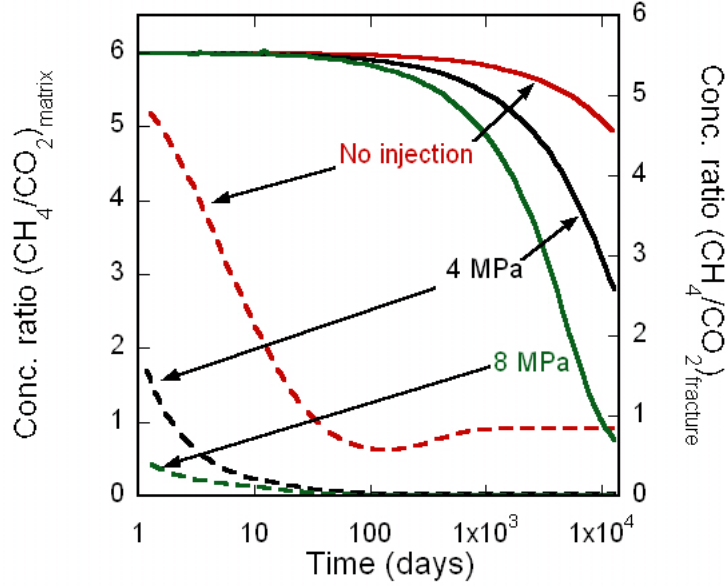
Figure 2.7: The evolution of ratio of average concentration of CH_4 and CO_2 in the matrix (solid lines) and fracture (dashed lines) for no injection, 4 MPa injection and 8 MPa injection scenarios at various time steps.

4.2.2 Effect of Fracture Matrix Permeability Ratio

Based on the dimensionless analysis it is clear that the dimensionless permeability $k_d = k_f/k_m$ may have a significant effect on the total gas production and rate of production. The dimensionless permeability is varied by varying the ratio k_{f0}/k_{m0} to the values of 1, 10, 100 for no injection, 4 MPa and 8 MPa injection. The evolution of dimensionless permeability (k_d) is shown in Figure 2.8. The dimensionless permeability remains almost constant for 10-100 days depending upon the initial value. The rise in k_d occurs earlier for higher values of k_d compared to lower values. The dashed lines in Figure 2.8 shows the evolution of k_d at the center of the block mid-way between wells

73

(point *A:* (80,80)). The evolution of k_d at point A approximately represents the k_d for the entire reservoir. At later times (1000-10000 days), k_d becomes almost constant indicating that the relative change in the permeability of matrix and fracture is close to steady state. It is interesting to note that the permeability evolution in these three cases have different characteristics with gradual changes until ~30 years.
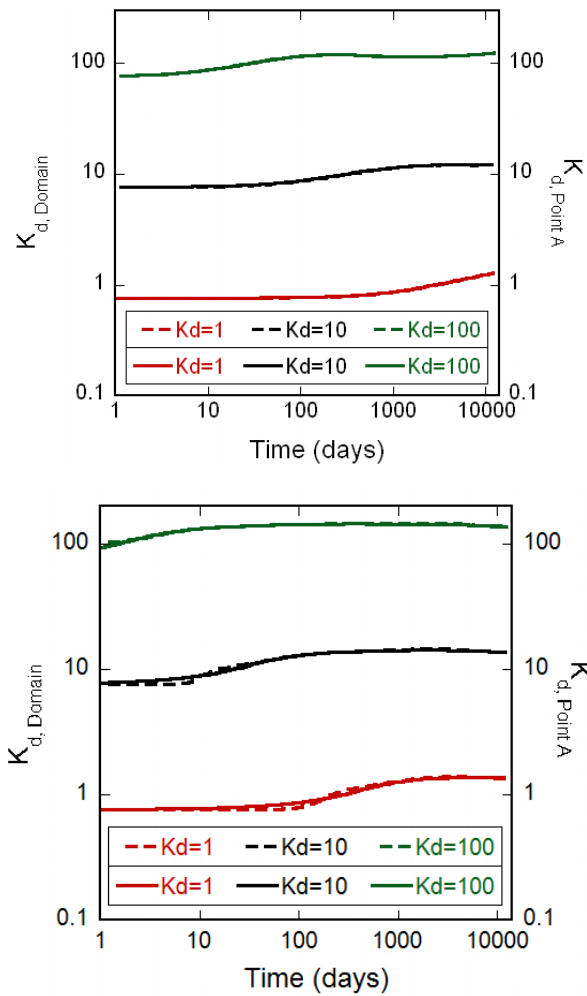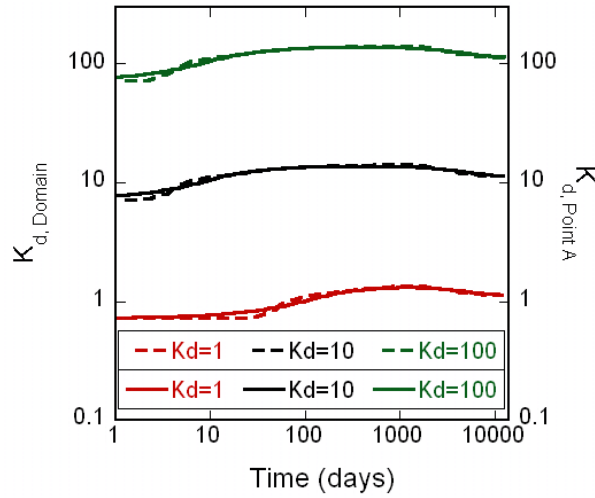
Figure 2.8: The evolution of dimensionless permeability (k_d) with time for a) No injection, b) 4 MPa injection and c) 8 MPA injection (top to bottom). The solid lines represent the mean value of (k_d) for the entire reservoir and dashed lines show the value for a point A (80, 80).

Figure 2.9 (a & b), shows the evolution of permeability of matrix and fracture for two scenarios of CO_2 injection (4 MPa and 8 MPa) along the cut section (IW) for various times. The matrix permeability decreases from injection well to production well in the 4 MPa and 8 MPa injection cases. As the matrix exchanges CH_4 with the injected CO_2 the permeability of the matrix increases (Figure 2.9a & b). The permeability of the matrix is higher near the injection well as compared to the area near the production well. Permeability is reduced at the production well due to matrix shrinkage accompanying CH_4 and CO_2 desorption in the vicinity of the production wellbore. The rate of change of permeability change in the matrix is faster for 8 MPa injection compared to the 4 MPa injection case. The permeability change front moved only 100 m away from the injection

well in ~10 years in the case of 4 MPa injection while it has travelled 150 m for injection at 8 MPa.

The fracture permeability evolution was more dramatic than the permeability transformations in the matrix. The change in matrix permeability is as high as ~10% while the change in fracture permeability may vary by ~200%. The fracture permeability is principally governed by the concentration of sorptive gases, their mole fractions and effective stresses (Kumar et al., 2012). To a large extent, the fracture permeability increases away from the injection wellbore and achieves a maximum value and then decreases on approaching the production wellbore. However the fracture permeability observations are slightly different for each scenario of CO_2 injection considered for this study. For instance, the permeability decreases away from the injection wellbore until ~10 m and then increases reaching a limiting value followed by a drop towards the production well bore in the case of 8 MPa injection. The CO_2 affected permeability zone travels from 50 m (100 days) to 150 m (>10 years) in the case of 4 MPa injection while it reaches to 200 m in the same time frame if the CO_2 is injected at 8 MPa. As the matrix adsorbs more gas it expands and the porosity of the matrix increases and therefore the permeability is enhanced but the matrix swelling decreases the fracture permeability by occupying the fracture space reducing the fracture permeability. However, the fracture permeability evolution is influenced by additional parameters too.

Figure 2.9(c), shows the permeability evolution in matrix and fracture at point *A* (80, 80), which is equidistant from injection and production wells, for 4 MPa and 8 MPa injection scenarios. The matrix permeability remains unaffected for ~100 days and then decreases for 10 years. The permeability of matrix was regained as the matrix adsorbs

injected CO_2. The permeability of the matrix at the end of 30 years is higher than its

initial value in the case of 8 MPa injection however the gain in permeability with CO_2

injection at 4 MPa was less as it just recovered to its initial value. The fracture

permeability at point A (equidistant from the injection and production wells) increases

with time, reaching a plateau in ~3 years and then decreases until ~30 years. This

behavior is attributed to shrinkage caused by production at earlier times followed by

swelling due to enhanced sorption of CO_2 occurring later. It is important to note that the

matrix and fracture permeability evolve in opposite directions but by different

multipliers. If the matrix permeability increases at a point then the fracture permeability

competitively decreases and vice versa.
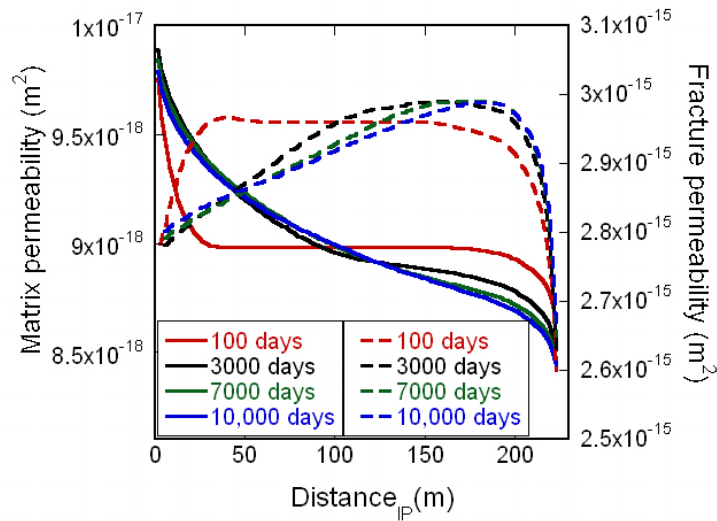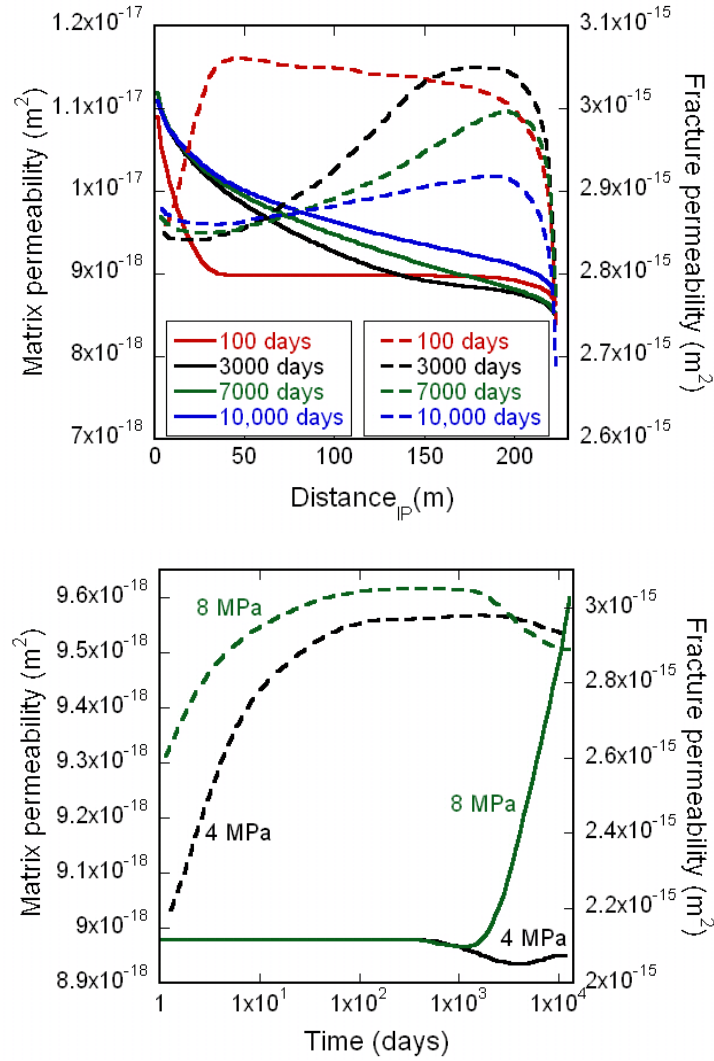
Figure 2.9: The matrix and fracture permeability along a cut section (IW) for injection at a) 4 MPa b) 8 MPa c) Evolution of matrix and fracture permeability at point *A* (80, 80) for 4 MPa and 8 MPa injection at various time steps. The solid lines show the matrix permeability and the dashed line represent matrix permeability at various times.

4.2.3 Effect of Fracture Spacing

The dimensionless analysis of equation (26) indicates that the dimensionless length $x_D = a/L$ is another parameter which may play a significant role on production. The value of the parameter L was fixed for the five well pattern configurations. Three scenarios of dimensionless length were simulated corresponding to fracture spacing a as 0.01, 0.02 and 0.04 m for CO_2 injection at 4 MPa. The injection of CO_2 at 4 MPa may allow slow removal of CH_4 as it is only 0.5 MPa higher than the initial reservoir pressure. The evolution of permeability has been investigated under mild pressure CO_2 injection i.e. 4 MPa. The production rate was higher in the case of the smallest fracture spacing (Figure 2.10) which could be attributed to the reduced diffusive length for sorption/desorption. Relatively small diffusive lengths allow more gas to flow into the fractures and the flow in the fracture is faster than the diffusive flow in matrix. Therefore, the diffusive length acts as a rate determining parameter for the production. The cumulative production also increases marginally with decreasing fracture spacing (not shown). The ratio of concentrations of CH_4 to CO_2 decays faster with smaller values of fracture spacing (Figure 2.11a). As the diffusive lengths are small the exchange of CO_2 with CH_4 was faster allowing a quicker CH_4 recovery. The concentration ratio drops rapidly within fractures as compared to matrix. The CH_4 present in the fracture is recovered almost instantaneously (~10 days) at the start of CO_2 injection. More gas is removed from the matrix due to an increased concentration gradient after removal of free CH_4 from the fractures and this process accelerates when the coal matrix exchanged CH_4 with injected CO_2. The evolution of dimensionless permeability with fracture spacing

was investigated for the 4 MPa injection case (Figure 2.11b). The change in dimensionless permeability k_d increases by 40-60% of its initial values in ~30 years depending on the initial fracture spacing (Figure 2.11b). The change in the values of dimensionless permeability indicates that the fractures achieve significantly higher values of permeability in comparison to matrix as the depletion proceeds. The highest change observed (~60%) for k_d was for the longest fracture spacing (a=0.04 m) as the highest volume shrinkage occurs for the longest fracture spacing. The volume shrinkage assists the fracture to accommodate more fluid to flow in the Darcy regime.
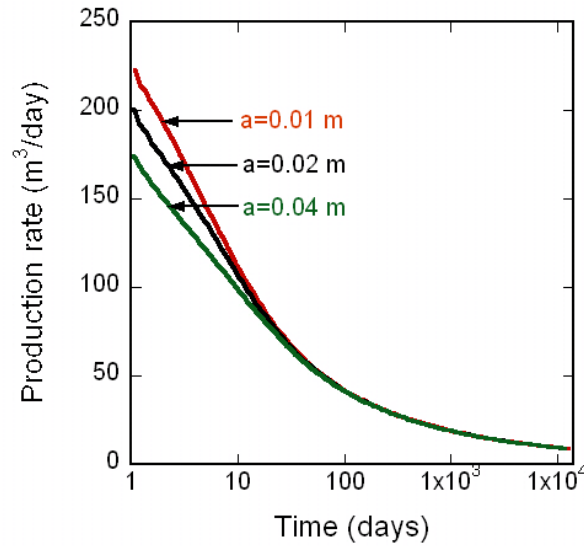
Figure 2.10: The rate of production with varying fracture spacing on constant pressure injection of CO_2 at 4 MPa.
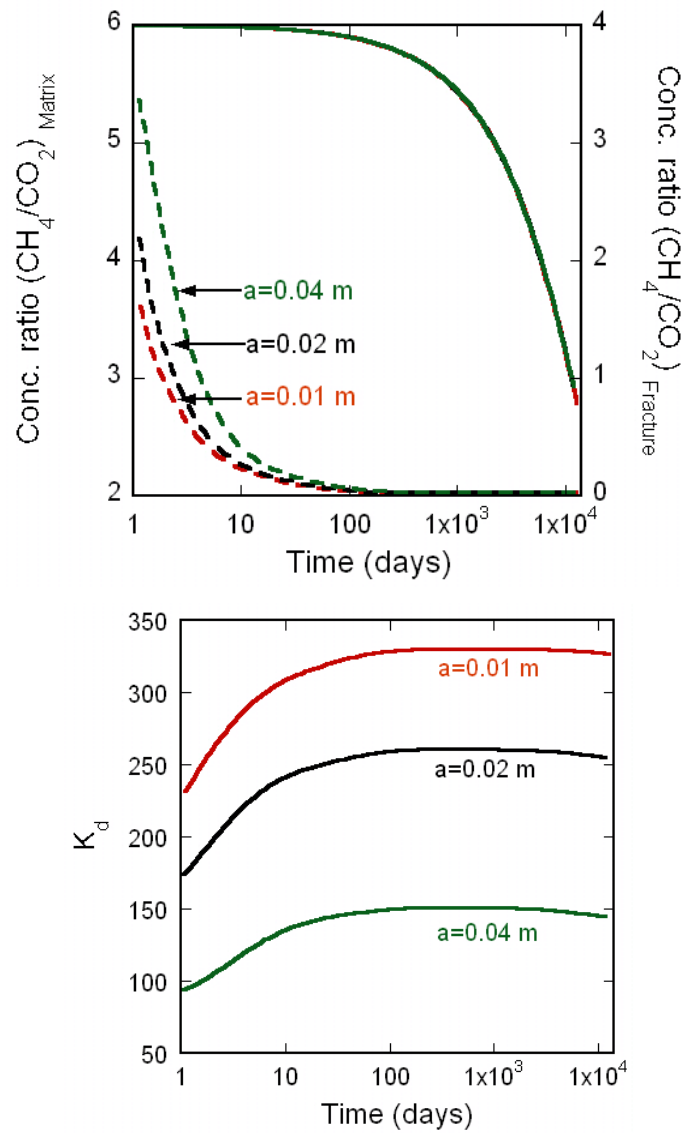
Figure 2.11: a) The ratio of average concentration of CH_4 and CO_2 in the matrix at various time steps. The solid lines show the concentration ratio in matrix and the dashed lines represent the concentration ratio in fractures. b) The evolution of average dimensionless permeability with time.

4.3 Heterogeneous System

The natural fracture network of a coalbed reservoir offers a wide range of spatial variation in permeability due to the variation in the fracture apertures from one location to another. This spatial distribution of permeability is referred as permeability heterogeneity. To the best of our knowledge, previous models developed for CO_2-ECBM did not include consideration of this heterogeneity in permeability. This methodology allows a more realistic representation of coalbed reservoirs produced under CO_2-ECBM. To achieve this the permeability is distributed in the geometry as a Gaussian normal distribution such that the average permeability remains identical to that of a homogeneous configuration and the permeability values range from a maximum (10^{-13} m^2) to a minimum (10^{-18} m^2). This heterogeneity in permeability is shown in Figure 2.12 and is accommodated by coupling with binary gas adsorption, binary gas transport, porosity transformations and permeability evolution in the matrix and fracture as a dual continuum present in the reservoir. The reservoir was simulated to investigate the effect of CO_2 injection on the reinforcing or ameliorating of heterogeneity, permeability evolution of the matrix and fractures, earlier breakthrough and CO_2 storage under various scenarios of CO_2 injection.
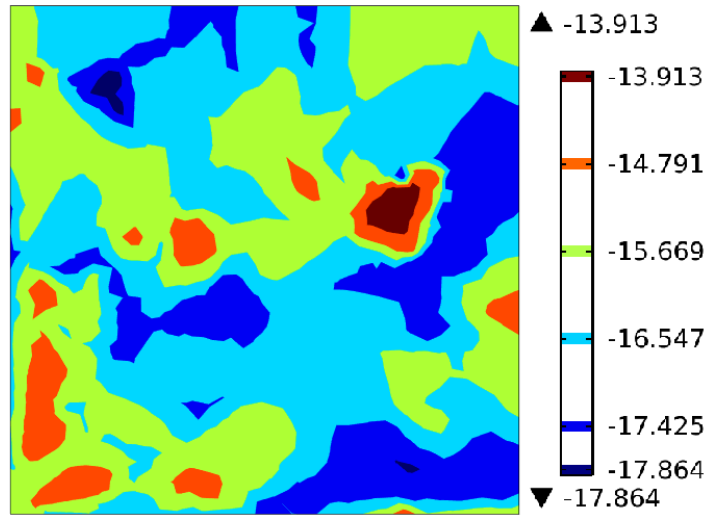
Figure 2.12: The fracture permeability in the reservoir varies from 10^{-13} to 10^{-18} m^2. The variation assumes Gaussian normal distribution with mean as 10^{-15} m^2.

4.3.1 Effect on Heterogeneity

The initial permeability heterogeneity may increase or decrease with various CO_2 injection scenarios. This was explored using a heterogeneous permeability configuration with specified mean and standard deviation. If the standard deviation of the total observations is small then the observations are closely spaced. The standard deviation of sparsely spaced observations is high. For example, if the standard deviation of permeability decreases then the reservoir attains more uniform permeability configuration. Figure 2.13, shows the evolution of average fracture permeability and standard deviation of the permeability for various scenarios of CO_2 injection. The production of methane induces matrix shrinkage in the reservoir and the average fracture permeability increases for a year and then decreases (~5 years) followed by a permeability plateau after 20 years. For Case I (Figure 2.13). The drop in permeability for

83

1-5 years was due to increased mole fraction of CO_2 due to pressure driven depletion. The permeability for ECBM scenarios (4 MPa and 8 MPa) increases for the earlier times achieving a maximum in ~100 days then decreases as the concentration of CO_2 increased in the reservoir. The decrease in permeability at later times (>20 years) was due to exchange of CH_4 with more sorptive CO_2.

The evolution of the standard deviation of the permeability for the no injection scenario suggests that the reservoir shifts towards a more heterogeneous permeability configuration with continued production (Figure 2.13). The matrix surrounded by high permeability fractures desorbs faster compared to the matrix surrounded by low permeability fractures. The CH_4 desorption results in matrix shrinkage and fracture aperture enhancements. Which further accelerates the preferential desorption from high permeability areas. In this process, the larger aperture fractures tend to increase in aperture at a faster rate than smaller aperture fractures, resulting in more heterogeneous distribution of permeability. There is an increase in standard deviation of permeability followed by reduction in its values for the 4 MPa and 8 MPa CO_2 injection cases. The increase in standard deviation may be attributed to matrix shrinkage at earlier times followed by matrix swelling due to enhanced sorption of injected CO_2. The decrease in standard deviation indicates that the permeability heterogeneity reduces with time and the reservoir achieves a more homogenous configuration under ECBM approaches. A practical implication is that the CO_2 flows through the largest aperture fractures first inducing swelling in the nearby matrix which results in reduction of the fracture apertures. The reduction in permeability of the larger aperture fractures diverts the fluid through the other higher permeability fractures. We expect a selective flow mechanism

84

where CO_2 flow finds a path of least resistance (higher permeability) in the reservoir and when the resistance increases with time it diverts the fluid to the lower resistance path. This process helps the reservoir to achieve more homogeneous permeability configuration as indicated by changes in the standard deviation of permeability (Figure 2.13).
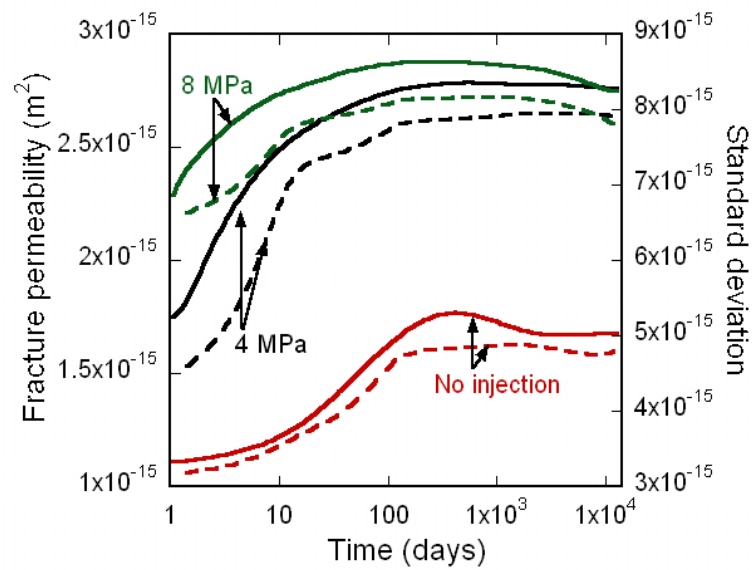
Figure 2.13: The mean and standard deviation of permeability in the reservoir at various times. The injection of CO_2 has been considered for 4 MPa and 8 MPa pressure. The no-injection scenario is also shown. The solid and dashed lines indicate fracture permeability and standard deviation respectively.
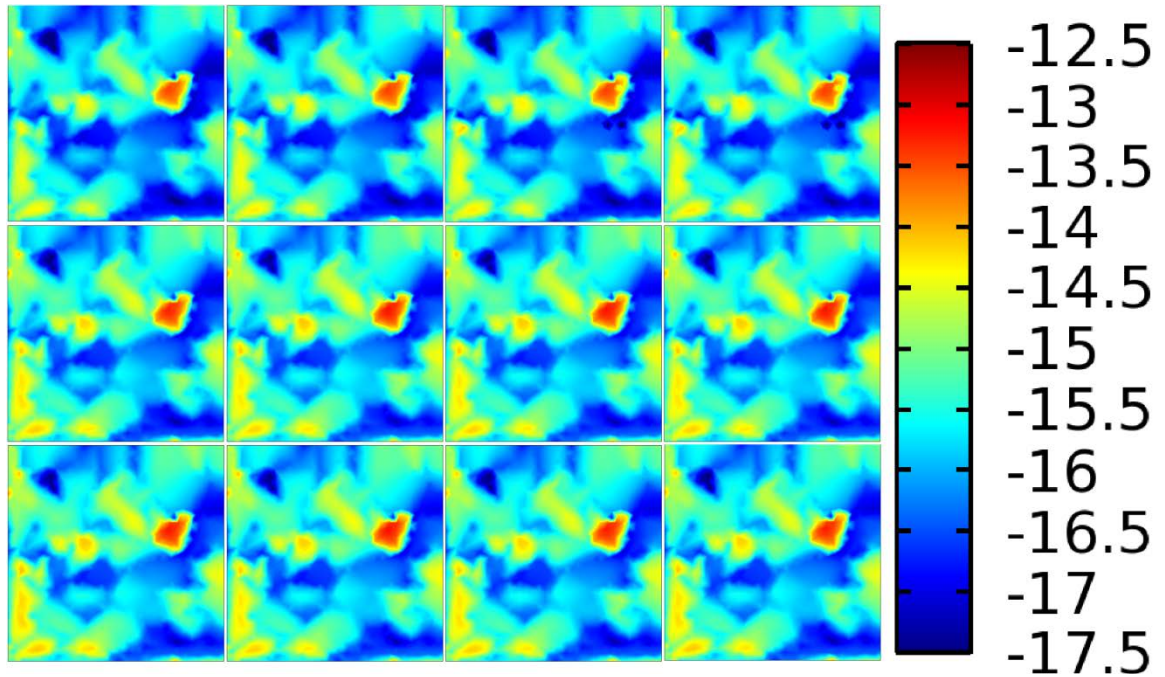
Figure 2.14: The surface map of fracture permeability at various time steps (100, 3000, 7000 and 10,000 days) for no injection, 4 MPa and 8 MPa CO_2 injection scenarios. The dark color shows less permeable areas in the reservoir.

4.3.2 Effect on Fracture and Matrix Permeability

The evolution of permeability in matrix and fracture was investigated for the reservoir with initial permeability heterogeneity. Figure 2.15, shows the evolution of average matrix and fracture permeability for no injection, 4 MPa and 8 MPa injection scenarios. The permeability evolution show similar trend as observed before in homogeneous permeability configuration (Figure 2.15). The permeability of the fracture increased for all scenarios in the beginning and then dropped as the sorption of injected CO_2 occurs. The concentration of CO_2 and CH_4 in the matrix is plotted across the diagonal section linking IW to PW for the reservoir for the three cases considered for the

86

study for various times (Figure 2.16). The concentration profile in all three cases was smooth despite the initial heterogeneity in fracture permeability. This indicated the innate stability of the sweeping CO_2 front even within a reservoir containing permeability heterogeneity. Pockets of high concentration were observed at earlier times in areas (fracture only) with initial low permeability (not shown). However, the concentration in these pockets reduces with time. The reduction of CH_4 concentration and increase of CO_2 concentration increased with injection pressure (Figure 2.16 b & Figure 2.16c). As time proceeds, the concentration of CO_2 increases in the reservoir and the concentration profile along the cut section becomes steeper with time (Figure 2.16).
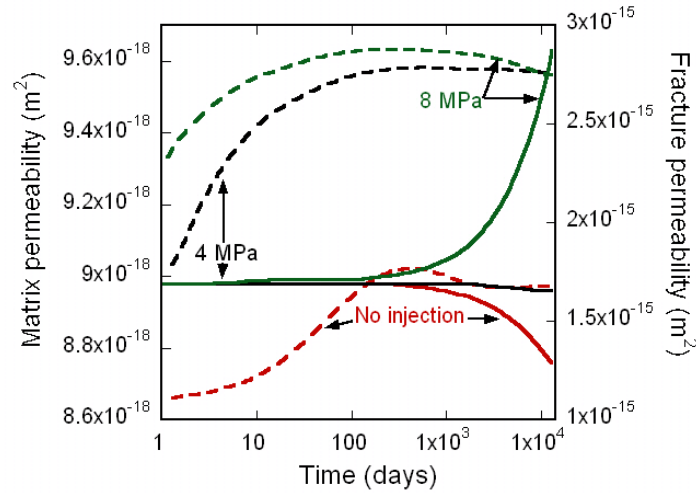
Figure 2.15: The evolution of permeability in matrix and fracture in the domain. The permeability value represents the average for the entire reservoir. The solid and dashed lines indicate matrix permeability and fracture permeability respectively.
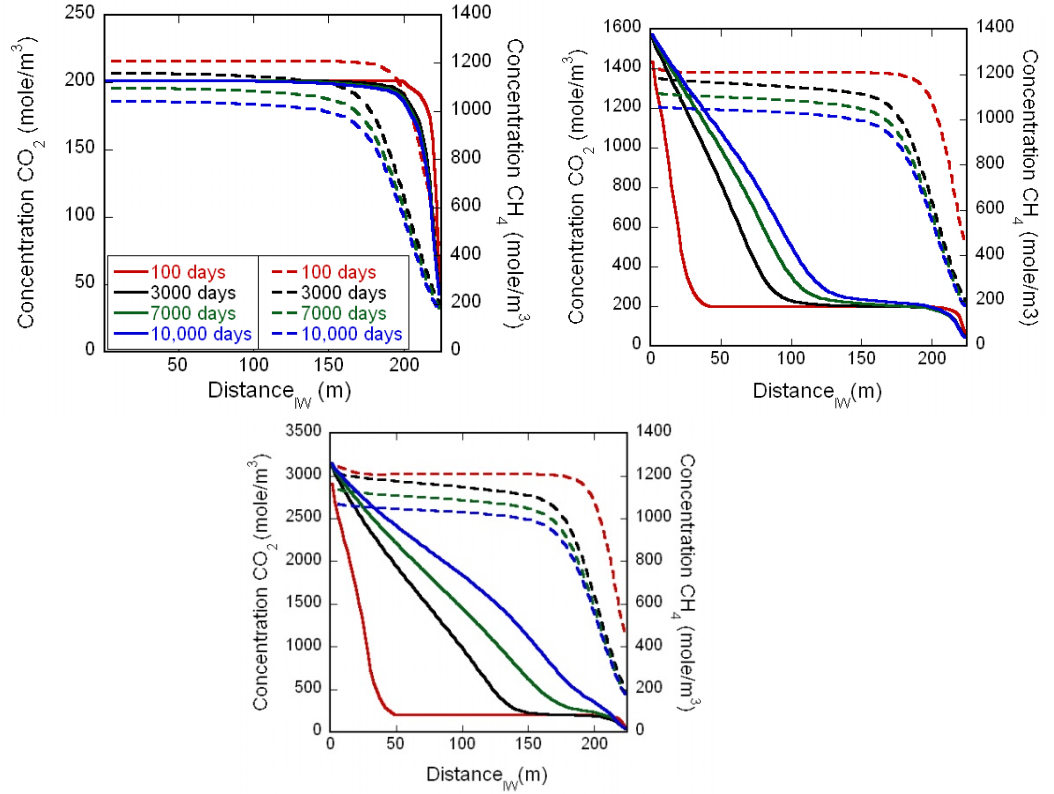
Figure 2.16: The variation in concentration of CH_4 and CO_2 along the diagonal (IW-PW) at various time steps. a) no injection (top left) b) 4 MPa injection (top right) and c) 8 MPa injection (bottom). The time legends are shown in Figure 2.16(a). The solid and dashed lines indicate CO_2 and CH_4 concentrations respectively.

4.3.3 Effect on Breakthrough

Enhanced production for CBM reservoirs is observed with CO_2 injection. However a significant fraction of injecting fluid (CO_2) will also be recovered in the production wells before recovering the majority of the interstitial fluid (CH_4) referred. This is known as 'breakthrough'. We investigate the breakthrough for the heterogeneous

distribution of permeability under no injection and two CO_2 injection scenarios. The evolution of average concentration ratio (CH_4/CO_2) in the fracture and matrix is shown in Figure 2.17. The concentration ratio drops rapidly in the fractures (~10-100 days) compared to the matrix where this process might take ~25 years. The injection pressure affects both the fracture permeability and therefore the quantity of injected CO_2 volume in the reservoir. Therefore, injection pressure affects the rate of the concentration reduction in the fractures (Figure 2.17). Among the three cases, the fracture permeability is highest with 8 MPa CO_2 injection (Figure 2.15) hence the movement of injecting fluid (CO_2) is faster in this case which promotes the faster removal of residing fluid (CH_4) in the fracture. This fast removal of CH_4 from the system results in the sharp decline of concentration ratio (Figure 2.17). Presumably, faster removal of CH_4 triggers the matrix to release more gas into the fracture network to equilibrate the concentration in fracture. The released CH_4 is removed by CO_2 and the system keeps removing increasingly more and more CH_4 with the help of injected CO_2 The injection of CO_2 at higher pressure (8 MPa) increases the total recovery (Figure 2.18 a) and the rate of production but it also increases the CO_2 production (Figure 2.18a). It is important to note that the CH_4 and CO_2 may be separated at the well-head and the CO_2 may be re-injected. The relative expense of separation of the CO_2 is relevant to the overall economic viability of ECBM production.

The mole fraction of production on a volume basis is shown in Figure 2.18 (b). Here, breakthrough is defined as the time when the production stream contains a majority of injected fluid. This happens when the mole fraction of CO_2 is 0.5 or the ratio of their produced volumes is 1. Figure 2.18, indicates that the 8 MPa injection scenario

approaches the earlier breakthrough faster as compared to 4 MPa and no-injection scenario. The volumetric ratio of CO_2 and CH_4 in the production stream is highest when CO_2 is injected at 8 MPa, indicating that the production stream contains a significant amount of CO_2 in comparison to the 4 MPa or no-injection scenarios. The observations from total production of CH_4 and CO_2 and their volumetric ratio do not rationalize the preference of one scenario over the others. However, it is clear that the maximum production of CH_4 could be achieved only with 8 MPa injection though it would also yield higher CO_2 production leading to higher separation costs.
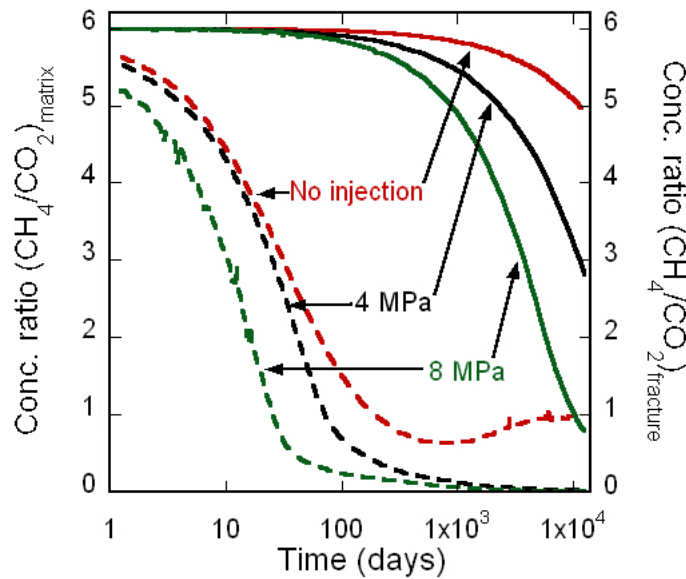
Figure 2.17: Evolution of the average of concentration ratio (CH_4 and CO_2) in the reservoir with time. A sharp decline from one value to another shows displacement without mixing flow. The solid and dashed lines indicate the concentration ratio (CH_4: CO_2) in the matrix and fracture respectively.
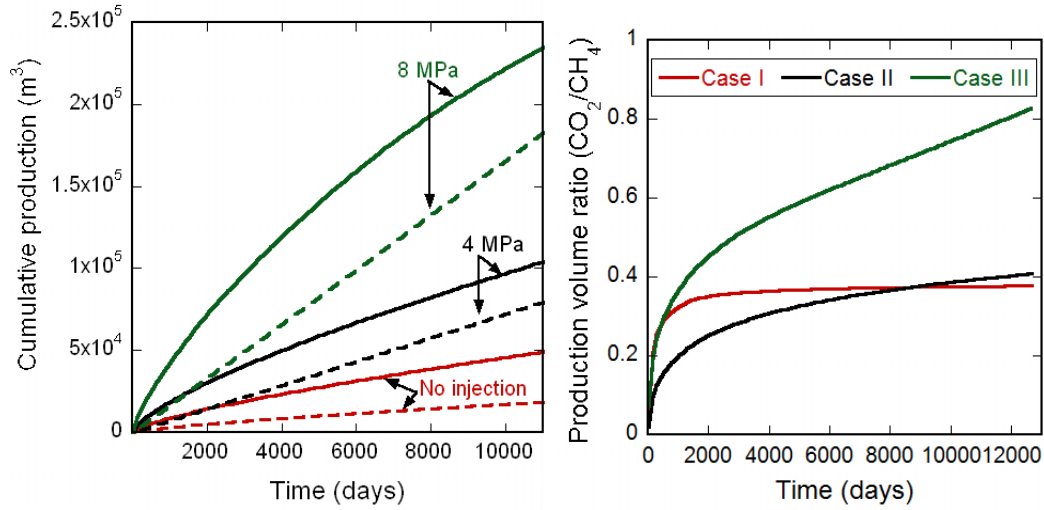
Figure 2.18: a) The cumulative production of CH_4 and CO_2 over time b) The volume ratio of CO_2/CH_4 in the production well for no-injection, 4 MPa and 8 MPa injections. The solid and dashed lines indicate cumulative production of CH_4 and CO_2 respectively in Figure 2.18(a).

4.3.4 Effect on CO_2 Storage

The CO_2 assisted ECBM may also be utilized for CO_2 sequestration. The injected CO_2 is partly stored in the reservoir and a fraction of it is recovered with the CH_4 production. Figure 2.19, shows the cumulative CO_2 stored in the reservoir in ~30 years. The net CO_2 stored in the reservoir increases with time for both 4 MPa and 8 MPa CO_2 injections. The volume of CO_2 stored in the reservoir at 8 MPa injection is double that stored for injection at 4 MPa.

The majority of CO_2 in the coalbed reservoirs are in the adsorbed state in the coal-matrix. The stored CO_2 increases with injection pressure (Figure 2.19). Congruent with

the Langmuir isotherm (equation (4)) the adsorbed gas in the matrix increases with gas

pressure leading to enhanced storage of CO_2 in the coalbed at higher injection pressures.
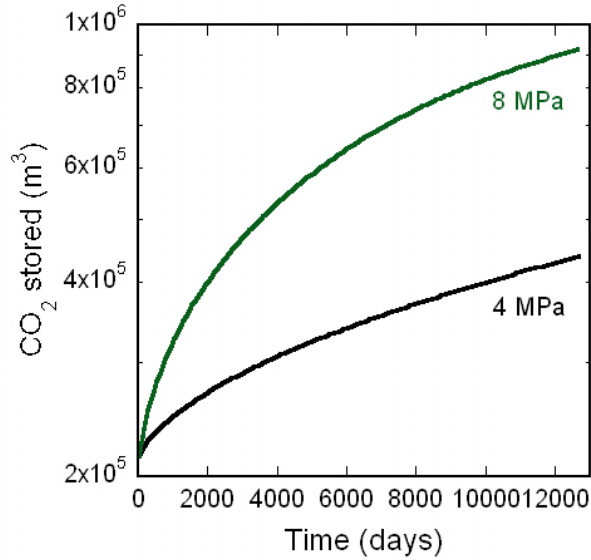
Figure 2.19: The cumulative volume of CO_2 sequestered by injection of CO_2 at 4 MPa

and 8 MPa over ~30 years.

5 Conclusions

In this work, the interactions between binary gas mixtures (CO_2 and CH_4) and

dual solid media (coal matrix and fracture) are simulated using a commercially available

finite element (FE) solver. The FE solver is utilized to implement various models into a

coupled simulator. The implemented model includes binary gas flow, diffusion,

competitive sorption and permeability change to explore the effect of CO_2 injection on

net recovery, permeability evolution and injectivity in uniform or homogeneous

permeability reservoirs. The dimensionless parameters (pressure p_D, permeability k_D and

spacings x_D) are derived and their effect on permeability evolution is explored for CBM

(no CO_2-injection) and CO_2-ECBM (4 MPa and 8 MPa) injection scenarios. Further, a reservoir with initial permeability heterogeneity is considered to explore the effect of CO_2 injection on the evolution of permeability heterogeneity – whether heterogeneity increases or decreases. The results indicate the complexity of the interaction of coal matrix-fracture systems with dual sorptive gases CH_4 and CO_2. However, some general observations and conclusions of this study are:

(1) The injection of CO_2 in coalbed reservoirs increases the production of CH_4 nearly 10 fold.

(2) At higher injection pressures the recovery is rapid and the production increases dramatically - the production increases 2 fold on increasing the CO_2 injection pressure from 4 MPa to 8 MPa

(3) However, CO_2 breakthrough occurs earlier at higher injection pressures.

(4) The permeability heterogeneity in the reservoir is reduced after a threshold time (~500 days) although the overall heterogeneity is increased relative to the initial condition is overall increased for both non-CO_2 and CO_2 injection scenarios. This indicates that the homogenizing influence of CO_2-sorption-swelling is outpaced by CH_4-desorption-shrinkage and effective stress influences. This leaves the reservoir open to short-circuiting and earlier breakthrough of CO_2 rather than having this effect damped-out by the homogenizing influence of swelling.

(5) The cumulative volume of CO_2 produced and stored in the reservoir is proportional to the injection pressure.

6 References

Bai, M., Elsworth, D., Roegiers, J.C., 1993. Modeling of naturally fractured reservoirs using deformation dependent flow mechanism. International Journal of Rock Mechanics and Mining Sciences & Geomechanics Abstracts 30, 1185-1191.

Chen, Z., Liu, J., Elsworth, D., Connell, L.D., Pan, Z., 2010. Impact of CO_2 injection and differential deformation on CO_2 injectivity under in-situ stress conditions. International Journal of Coal Geology 81, 97-108.

Chikatamarla, L., Cui, X., Bustin, R.M., 2004. Implications of volumetric swelling/shrinkage of coal in sequestration of acid gases, International Coalbed Methane Symposium Proceedings, Tuscaloosa, AL.

Clarkson, C.R., Bustin, R.M., 1997. Variation in permeability with lithotype and maceral composition of Cretaceous coals of the Canadian Cordillera. International Journal of Coal Geology 33, 135-151.

Clarkson, C.R., Jordan, C.L., Gierhart, R.R., Seidle, J.P., 2008. Production Data Analysis of Coalbed-Methane Wells. SPE Reservoir Evaluation & Engineering 11, 311-325.

Clarkson, C.R., Pan, Z., Palmer, I., Harpalani, S., 2010. Predicting sorption-induced strain and permeability increase with depletion for coalbed-methane reservoirs. SPE Journal 15, 152-159.

Day, S., Duffy, G., Sakurovs, R., Weir, S., 2008. Effect of coal properties on CO_2 sorption capacity under supercritical conditions. International Journal of Greenhouse Gas Control 2, 342-352.

Durucan, S., Shi, J.-Q., 2009. Improving the CO2 well injectivity and enhanced coalbed methane production performance in coal seams. International Journal of Coal Geology 77, 214-221.

Fokker, P.A., van der Meer, L.G.H., 2004. The injectivity of coalbed CO2 injection wells. Energy 29, 1423-1429.

Fujioka, M., Yamaguchi, S., Nako, M., 2010. CO2-ECBM field tests in the Ishikari Coal Basin of Japan. International Journal of Coal Geology 82, 287-298.

Gu, F., Chalaturnyk, R.J., 2006. Numerical simulation of stress and strain due to gas sorption/desorption and their effects on in situ permeability of coalbeds. Journal of Canadian Petroleum Technology 45, 52-62.

Hall, F.E., Zhou, C., Gasem, K.A.M., Jr., R.L.R., Yee, D., 1994. Adsorption of Pure Methane, Nitrogen, and Carbon Dioxide and Their Binary Mixtures on Wet Fruitland Coal, SPE Eastern Regional Meeting. Copyright 1994, Society of Petroleum Engineers Inc., Charleston, West Virginia.

Harpalani, S., Chen, G., 1995. Estimation of changes in fracture porosity of coal with gas emission. Fuel 74, 1491-1498.

Harpalani, S., Chen, G., 1997. Influence of gas production induced volumetric strain on permeability of coal. Geotechnical and Geological Engineering 15, 303-325.

Harpalani, S., Chen, G., 1999. Positive impact of gas production induced stress and strain on coal permeability, 9th ISRM Congress. A.A. Balkema. Permission to Distribute - International Society for Rock Mechanics., Paris, France.

Harpalani, S., Schraufnagel, R.A., 1990. Shrinkage of coal matrix with release of gas and its impact on permeability of coal. Fuel 69, 551-556.

Hol, S., Peach, C.J., Spiers, C.J., 2011. Applied stress reduces the CO2 sorption capacity of coal. International Journal of Coal Geology 85, 128-142.

Hol, S., Spiers, C.J., Peach, C.J., 2012. Microfracturing of coal due to interaction with CO2 under unconfined conditions. Fuel 97, 569-584.

IPCC, 2005. Special report in carbon dioxide capture and storage, Cambridge.

Karacan, C.Ö., 2003. Heterogeneous Sorption and Swelling in a Confined and Stressed Coal during CO2 Injection. Energy & Fuels 17, 1595-1608.

Karacan, C.Ö., 2007. Swelling-induced volumetric strains internal to a stressed coal associated with CO2 sorption. International Journal of Coal Geology 72, 209-220.

Krooss, B.M., van Bergen, F., Gensterblum, Y., Siemons, N., Pagnier, H.J.M., David, P., 2002. High-pressure methane and carbon dioxide adsorption on dry and moisture-equilibrated Pennsylvanian coals. International Journal of Coal Geology 51, 69-92.

Kumar, H., Elsworth, D., Liu, J., Pone, D., Mathews, J.P., 2012. Optimizing enhanced coalbed methane recovery for unhindered production and CO2 injectivity. International Journal of Greenhouse Gas Control 11, 86-97.

Langmuir, I., 1916. The constitution and fundamental properties of solids and liquids Part I Solids. Journal of the American Chemical Society 38, 2221-2295.

Larsen, J.W., 2004. The effects of dissolved CO2 on coal structure and properties. International Journal of Coal Geology 57, 63-70.

Levine, J.R., 1996. Model study of the influence of matrix shrinkage on absolute permeability of coal bed reservoirs. Geological Society, London, Special Publications 109, 197-212.

Liu, J., Chen, Z., Elsworth, D., Miao, X., Mao, X., 2010a. Evaluation of stress-controlled coal swelling processes. International Journal of Coal Geology 83, 446-455.

Liu, J., Chen, Z., Elsworth, D., Miao, X., Mao, X., 2010b. Linking gas-sorption induced changes in coal permeability to directional strains through a modulus reduction ratio. International Journal of Coal Geology 83, 21-30.

Liu, J., Elsworth, D., Brady, B.H., 1997. Analytical evaluation of post-excavation hydraulic conductivity field around a tunnel. International Journal of Rock Mechanics and Mining Sciences 34, 181.e181-181.e187.

Liu, J., Wang, J., Chen, Z., Wang, S., Elsworth, D., Jiang, Y., 2011. Impact of transition from local swelling to macro swelling on the evolution of coal permeability. International Journal of Coal Geology 88, 31-40.

Masoudian-Saadabad, M., Airey, D., Gainey, A., Morris, T., Berger, J., 2011. The mechanical properties of CO2-saturated coal specimens, Harmonising Rock Engineering and the Environment. CRC Press.

Mitra, A., Harpalani, S., Liu, S., 2012. Laboratory measurement and modeling of coal permeability with continued methane production: Part 1 – Laboratory results. Fuel 94, 110-116.

Mora, C.A., Wattenbarger, R.A., 2009. Analysis and verification of dual porosity and CBM shape factor. Journal of Canadian Petroleum Technology 48.

NIST, Thermophysical properties of fluid systems. http://webbook.nist.gov/chemistry/fluid/.

Ouyang, Z., Elsworth, D., 1993. Evaluation of groundwater flow into mined panels. International Journal of Rock Mechanics and Mining Sciences & Geomechanics Abstracts 30, 71-79.

Palmer, I., 2009. Permeability changes in coal: Analytical modeling. International Journal of Coal Geology 77, 119-126.

Palmer, I., Mansoori, J., 1998. How permeability depends on stress and pore pressure in coalbeds: a new model, SPE Annual Technical Conference and Exhibition. Society of Petroleum Engineers, Denver, Colorado.

Pan, Z., Connell, L.D., Camilleri, M., Connelly, L., 2010. Effects of matrix moisture on gas diffusion and flow in coal. Fuel 89, 3207-3217.

Pekot, L.J., Reeves, S.R., 2002. Modeling the effects of matrix shrinkage and differential swelling on coalbed methane recovery and carbon sequestration. Department of Energy.

Pone, J.D.N., Halleck, P.M., Mathews, J.P., 2010. 3D characterization of coal strains induced by compression, carbon dioxide sorption, and desorption at in-situ stress conditions. International Journal of Coal Geology 82, 262-268.

Pone, J.D.N., Hile, M., Halleck, P.M., Mathews, J.P., 2009. Three-dimensional carbon dioxide-induced strain distribution within a confined bituminous coal. International Journal of Coal Geology 77, 103-108.

Reeves, S.R., 2003. Enhanced CBM recovery, coalbed CO2 sequestration assessed. Oil & Gas Journal 101, 49.

Rice, D.D., 1993. Composition and origins of coalbed gas.

Rogers, R.E., 1994. Coalbed Methane: Principles and Practice. PTR Prentice Hall, Englewood Cliffs, N.J.

Saffman, P.G., Taylor, G., 1958. The Penetration of a Fluid into a Porous Medium or Hele-Shaw Cell Containing a More Viscous Liquid. Proceedings of the Royal Society of London. Series A, Mathematical and Physical Sciences 245, 312-329.

Shen, J., Qin, Y., Wang, G.X., Fu, X., Wei, C., Lei, B., 2011. Relative permeabilities of gas and water for different rank coals. International Journal of Coal Geology 86, 266-275.

Shi, J.-Q., Durucan, S., 2005. A model for changes in coalbed permeability during primary and enhanced methane recovery. SPE Reservoir Evaluation & Engineering 8, 291-299.

Shi, J.-Q., Durucan, S., 2008. Modelling of mixed-gas adsorption and diffusion in coalbed reservoirs, SPE Unconventional Reservoirs Conference, Keystone, Colorado, USA.

Shi, J.-Q., Durucan, S., 2010. Exponential Growth in San Juan Basin Fruitland Coalbed Permeability With Reservoir Drawdown: Model Match and New Insights. SPE Reservoir Evaluation & Engineering 13, pp. 914-925.

Shi, J.Q., Durucan, S., 2004. A numerical simulation study of the Allison unit CO2-ECBM pilot: the impact of matrix shrinkage and swelling on ECBM production and CO2 injectivity, in: Rubin, E.S., Keith, D.W., Gilboy, C.F., Wilson, M., Morris, T., Gale, J., Thambimuthu, K. (Eds.), 7th International Conference on Greenhouse Gas Control Technologies.

Tao, S., Wang, Y., Tang, D., Xu, H., Lv, Y., He, W., Li, Y., 2012. Dynamic variation effects of coal permeability during the coalbed methane development process in the Qinshui Basin, China. International Journal of Coal Geology 93, 16-22.

Viete, D.R., Ranjith, P.G., 2006. The effect of CO2 on the geomechanical and permeability behaviour of brown coal: Implications for coal seam CO2 sequestration. International Journal of Coal Geology 66, 204-216.

Wang, G.X., Wei, X.R., Wang, K., Massarotto, P., Rudolph, V., 2010. Sorption-induced swelling/shrinkage and permeability of coal under stressed adsorption/desorption conditions. International Journal of Coal Geology 83, 46-54.

Wang, S., 2012. Gas transport, sorption, and mechanical response of fractured coal, Energy and Mineral Engineering. The Pennsylvania State University, University Park.

Warren, J.E., Root, P.J., 1963. The Behavior of Naturally Fractured Reservoirs. SPE Journal 3, 245-255.

Weniger, P., Francǔ, J., Hemza, P., Krooss, B.M., 2012. Investigations on the methane and carbon dioxide sorption capacity of coals from the SW Upper Silesian Coal Basin, Czech Republic. International Journal of Coal Geology 93, 23-39.

White, C.M., Smith, D.H., Jones, K.L., Goodman, A.L., Jikich, S.A., LaCount, R.B., DuBose, S.B., Ozdemir, E., Morsi, B.I., Schroeder, K.T., 2005. Sequestration of Carbon Dioxide in Coal with Enhanced Coalbed Methane RecoveryA Reviewâ€Energy & Fuels 19, 659-724.

Wu, Y., Liu, J., Chen, Z., Elsworth, D., Pone, D., 2010a. A dual poroelastic model for CO2-enhanced coalbed methane recovery. International Journal of Coal Geology 86, 177-189.

Wu, Y., Liu, J., Elsworth, D., Chen, Z., Connell, L., Pan, Z., 2010b. Dual poroelastic response of a coal seam to CO2 injection. International Journal of Greenhouse Gas Control 4, 668-678.

Wu, Y., Liu, J., Elsworth, D., Siriwardane, H., Miao, X., 2011. Evolution of coal permeability: Contribution of heterogeneous swelling processes. International Journal of Coal Geology 88, 152-162.

Chapter 3 : Permeability Evolution of Propped Artificial Fractures in Coal

Abstract

Proppants are often utilized during hydraulic fracturing to aid the retention of the fracture aperture. However, for coal the permeability enhancement may be mitigated due to proppant-coal embedment within the natural/artificial fractures of coalbed methane reservoirs that are subject to CO_2 enhanced recovery. The reduction in effective fracture aperture occurs under stress conditions either when CO_2-induced coal softening causes proppant penetration into the coal fracture surface or coal swelling encroaches into the propped facture. Coal swelling is a well-established phenomenon, however there are limited investigations into coal softening under stressed conditions. Here permeability transformations at simulated in situ conditions were evaluated through a suite of laboratory experiments conducted on split-cores of high-rank coals and granite (as non-swelling control). A single smooth-surface saw-cut fracture was created and the permeability evolution measured for both non-sorbing (He) and sorbing (CO_2) gases at constant applied confining stress of 10 MPa. Permeability was also measured for the idealized case of a uniform monolayer of #70-140 mesh quartz sand proppant sand introduced within the saw-cut fracture for coal and for the granite control. The increase in He permeability was as high as ~10 fold over the unpropped fracture for a monolayer of proppant sandwiched within the coal or granite fractures. A similar increase in permeability with the addition of proppant was observed in the case of sorptive gas (CO_2) for coal. For He there was an exponential increase in permeability with increasing gas

pressure (p=1-6 MPa) for both coal and granite without proppant, as expected, as the effective stress on the core was reduced. However, with CO_2 the permeability decreased in the 1-4 MPa pressure range due to either coal swelling or softening or their combination but increased above 4 MPa due to reduced effective stress. Optical profilometry pre- and post-exposure was used to quantify any surface deformation due to proppant embedment. Comparison of the fracture surface before and after showed only infrequent new isolated pits, similar to the size of the proppant grains. Thus for these coals under these conditions there was no significant contribution of coal softening towards permeability reduction. Thus, the permeability reduction was attributed to coal swelling alone. The slight increase in surface roughness following exposure to CO_2 was presumed due to irreversible rearrangement of the coal structure due to CO_2 uptake then loss. A mechanistic model explains the evolution of permeability in a propped artificial fracture due to interaction with a sorbing gas (CO_2). Permeability evolves with a characteristic 'U-shaped' trend with increasing gas pressure at constant confining stress – permeability reduces to a minimum at approximately double the Langmuir pressure flanked by elevated permeabilities at either low sorptive states (low p) or at low effective stress (high p). An excellent fit is recovered between model and experimental observations.

1 Introduction

Low permeability coalbed reservoirs are often artificially fractured with a proppant-slurry to retain the enhanced permeability (Davidson et al., 1995; Holditch et al., 1988) that is created by hydraulic fracturing. This process is also used extensively for tight shale and sand reservoirs to enhance production. However, the dynamics of effective stresses in coalbed methane reservoirs and potential coal softening on exposure to carbon dioxide (CO_2, or other gases) may result in proppant embedment in the fracture walls that may result in loss of aperture and related permeability loss. Prior experimental (Piggott and Elsworth, 1993; Walsh, 1981) and analytical evaluations (Bai and Elsworth, 1994; Elsworth and Yasuhara, 2010; Yasuhara and Elsworth, 2008; Yasuhara et al., 2006) of fractured rocks indicate that permeability is strongly influenced by the variation in mechanical, chemical, thermal, and hydraulic processes.

Recently, proppant embedment and fracture closure have received additional attention for hard rock as optimization of proppant effectiveness is necessary to prevent fracture closure as effective stresses increases with methane depletion (Cooke, 1977). Mechanisms of fracture conductivity impairment have been explored including the roles of fines migration (Pope et al., 2009), proppant diagenesis (LaFollette and Carman, 2010; Lee et al., 2010), proppant crushing (Terracina et al., 2010), and reduction in fracture aperture due to the embedment of proppant grains into the surface of the hydraulic fracture (Freeman et al., 2009; Lacy et al., 1997). Proppant embedment studies on 20/40 and 40/60 mesh Ottawa sand and sintered bauxite indicate that the embedment is primarily modulated by closure stress, proppant size and fluid viscosity (Lacy et al.,

104

1997). The reduction in fracture conductivity at higher effective stresses occurs due to generation of proppant-fines in hard rocks (such as granite) and due to coal swelling (with gas exposure) or embedment of proppant. The reduction in conductivity may be up to 60% in rock (Lacy et al., 1997) and perhaps higher for coal. With higher temperatures, extended duration of stress loading, and pressurized fluid saturation levels may accelerate the fines generation or proppant embedment (Freeman et al., 2009). An increase in temperature decreases the fracture conductivity due to the thermal expansion of asperities under mechanical constraints (Stoddard et al., 2011). The time dependent tensile strength, proppant hardness, and fatigue failure of proppant under reservoir conditions are known to affect proppant efficacy (LaFollette and Carman, 2010;Freeman et al., 2009). The fracture treatment may also be impacted by proppant-diagenesis, which evolves as a result of mineral dissolution, transport and re-precipitation in the particle interstices. Thus various mechanisms may be responsible for porosity and permeability loss in proppant packs within hard rocks (Lee et al., 2010) if the proppant layer is sufficiently thick so that the surface asperities do not play a significant role (Stoddard et al., 2011).

Although the behavior of propped artificial fractures in granite and carbonates has been well explored, the response of proppant packs in soft sorbing media (coal) is poorly understood due to the complex range of behaviors. It is well known that coal can soften upon exposure to "good" solvents becoming ductile or plastic and easily deformable (Brenner, 1984, 1985). It is also known that CO_2 (used to enhance coalbed methane extraction or for sequestration) can act as a modifier for select polymer systems to increase their flexibility by lowering the glass transition point (Neyertz et al., 2010;

Tomasko et al., 2003). Above the glass transition temperature this allows for coal deformation and also a more rapid diffusion for small molecules. Thus it is necessary to explore response of coals to CO_2 (Larsen, 2004) to ensure due diligence in protecting public safety. Thus both coal-CO_2 *swelling* and coal *softening* could both contribute to a permeability reduction for thin-but-propped coal fractures. Both causes would result in effective aperture reduction either to coal penetrating the proppant pack void spaces (via coal swelling), or the proppant penetrating the coal (via coal softening). Coals will differ from hard rock as they are typically: (1) stiffer than the proppant grain (2) exhibits swelling or shrinking and (3) weaken upon interaction with sorptive gases (CO_2 or CH_4) developing dynamic strains (Perera and Ranjith, 2012; Viete and Ranjith, 2006), and (4) perhaps soften. These processes are expected to result in permeability transformations.

Here the permeability evolution of an artificial saw–cut "fracture" in bituminous and anthracite cores both with and without proppant was explored for both inert helium (He) and sorbing carbon dioxide (CO_2) as permeating gases. Permeability evolution was determined using the pulse-transient technique at constant applied confining stress (10 MPa) for non-propped and propped fractures at different (saturated) pore pressures. The evolution of surface morphology was evaluated using optical profilometry to aid in establishing the role, if any, of coal softening on permeability evolution. We also used these observations to constrain mechanistic models of permeability evolution of propped fractures in sorbing media.

2 Experimental Methods

Cylindrical cores of bituminous and anthracite rank coals and a westerly granite were longitudinally-split to produce a single diametral artificial fracture. Fluid (gas) injection experiments were performed on the fracture in these cores in both non-propped and propped mode with samples stressed to in situ conditions but under ambient laboratory temperature (20C). The gases He and CO_2 were used as permeants to investigate the role of swelling/softening and effective stress on the dynamic evolution of permeability.

2.1 Samples

Two contrasting coal lithotypes were used in the experiments: bituminous coal from the Uinta Basin, Colorado and anthracite from Pennsylvania. The coal block samples were cored horizontally (parallel to bedding) to produce the core plugs. The calorific value of sampled bituminous and anthracite coals were 12000 and 14286 BTU/lb (ASTM International D388, 2005) on a dry basis, respectively. The fixed carbon, volatile material and ash yield on a dry basis are 57%, 38%, 5% for bituminous and 86%, 7%, 4% for anthracite coals (ASTM International D7582, 2010). The moisture content of the coals are 5% and 2% respectively (ASTM International D3302/D3302M-10, 2010).

Six cylindrical cores of 2.5 cm diameter and 5 cm length were obtained and their ends cut to obtain flat surfaces. Cores were cut in to two halves (horizontally lengthwise) using a thin diamond coated blade to produce smooth opposing surfaces forming an idealized fracture. The cut-surfaces of the coal were polished to remove the minor saw indents. Fine sand paper (#400) to very fine cotton cloth with alumina powders from 0.3 μm to 0.05 μm were used to polish the coal surface (ASTM International D5671, 2011). Surface roughness was quantified by optical profilometry (Kumar et al., 2009; Rousseau et al., 2010). The split-cores were re-mated either without or with a uniform monolayer of 70-140 mesh proppant sand. The cores were then wrapped in aluminum foil (to prevent diffusive loss of CO_2) and sheathed in a latex jacket before being enclosed in a pressurized core holder for the permeability experiments. The granite core was similarly prepared.

2.2 Apparatus

An apparatus in simple triaxial configuration was used for the injection of gases under predefined effective stress paths and capable of concurrent measurement of permeability (Figure 3.1). All experiments were completed under a constant applied total stress with axial and confining stresses equivalent. The apparatus comprised a tri-axial cell to confine the sample at prescribed stresses, an axial strain gauge to monitor the shrinkage or swelling in the axial direction, ISCO syringe pumps to apply stresses and to measure volume strains (axial and confining), pressure transducers to monitor the upstream and downstream reservoir pressures and a data acquisition system. Additional

details of the equipment are described elsewhere (Kumar et al., 2012). A transient pulse

test method (described in section 2.4) was used to determine the sample permeability.

Permeability was evaluated from the rate of pressure decay/gain in the

upstream/downstream reservoirs (Brace et al., 1968) assuming no sorption during the

short duration (<10 min) experiments.

Both pre- and post-experiment an optical profilometer (Zygo NewView^{TM} 7300)

was used to quantify the surface indentation caused by stressing of the sample and by gas

composition. In the interferometer a light beam is split into two paths. One path of light

impinges on the specimen surface and is reflected. The other is reflected from a reference

mirror. Reflections from these surfaces are recombined and projected onto an array

detector to determine path differences by interference. This enables surface topography to

be resolved to fractions of the wavelength of light. Resolution in the plane and vertical to

the plane is 2 μm and 0.1 μm respectively. A 10X objective was used with 0.5X zoom

length. The surface topology of a region 7mm× 8mm was obtained by stitching-together

~30 micrographs at high resolution with the field of view overlapping by ~20%.
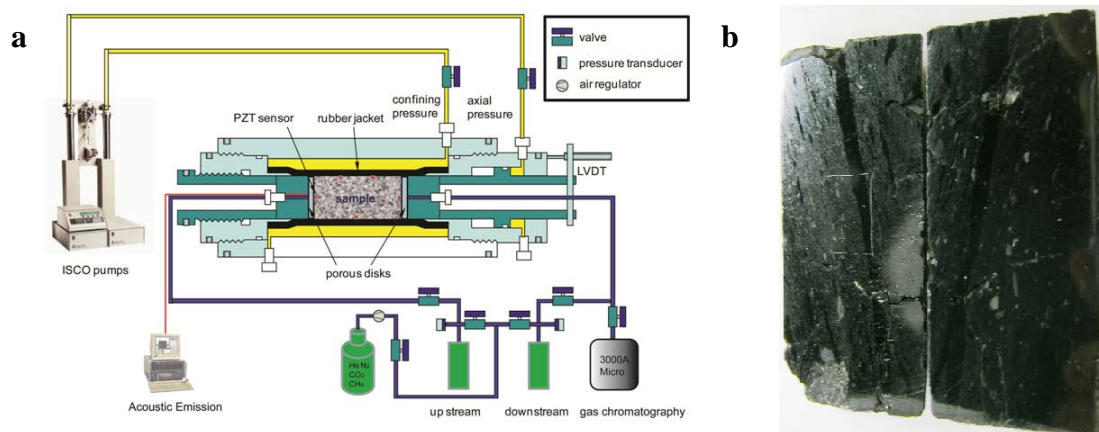
Figure 3.1: a) Schematic of transient pulse test permeability set-up b) a polished fracture surface.

2.3 Procedures

The cores (granite or coal) were held within the triaxial core holder and stresses applied. The experiments were conducted at constant confining stress of 10 MPa (equivalent to an effective stress at ~1000 m or ~3300 feet depth). The permeability experiments included injection of He and CO_2 in both non-propped and propped coal fractures. The suite of experiments were conducted on coal cores of differing composition (bituminous and anthracite) to explore the evolution permeability of an artificial fracture as a result of injection of either inert (He) or sorbing (CO_2) gas. Also, He was used as permeant in the non-propped and propped fracture in a split-core of Westerly granite as a control sample to explore the effect of stress alone on permeability absent the influence of coal swelling or proppant embedment. Table 1, provides the ranges of experimental variables.

Table 3.1: Suite of variables and prescribed ranges utilized in the experiments, for gas pressure P_p, permeability k, axial stress σ_1, confining stress σ_3, and axial strain ε_a.

Experimental Variables	Experimental Range
Temperature (T)	Constant
Gas pressure (Pp, MPa)	1-6 (coal), 1-6 (granite)
Axial stress (σ_1, MPa)	10 (coal), 17 (granite)
Confining stress (σ_3, MPa)	10 (coal), 17 (granite)
Gas type	He, CO_2

The experimental protocol sequence was performed under constant isotropic stress with incremental gas pressures. The suite of experiments included:

1. *Non-propped fracture - He permeability*: Helium (considered to be a non-adsorbing fluid) was circulated in the non-propped coal sample.

2. *Non-propped fracture - CO_2 permeability*: The sample is at equilibrium with CO_2 and permeability measured by transient pulse test at different saturated conditions (gas pressures 1-6 MPa).

3. *Propped fracture - He permeability*: The artificial fracture in the sample was propped open with a monolayer of proppant. Helium was injected in the sample at different gas pressures and the permeability determined.

4. *Propped fracture - CO_2 permeability*: The sample was vented overnight to the atmosphere and permeated using CO_2. The permeability was measured on the saturated sample.

Surface micrographs were captured using optical interferometry and contain information on the surface roughness including the height/depth of the surface features. The surface micrographs were obtained for the surface both before and after (<30 min) the experimental suite for a single sample. To allow comparison, same sample is used for entire experimental suite for a given coal.

2.4 Data Processing Methods

The transient pulse test method is utilized to evaluate the coal permeability (Brace et al., 1968). In a typical run, a coal core is packed and placed under axial and radial stress in the triaxial apparatus as shown in Figure 3.1. A mild vacuum is applied to evacuate the air from the sample reservoir system. The core is saturated with gas (He or CO_2) to an equilibrium pressure before applying a pressure pulse. A pressure pulse is allowed to flow through the core from the upstream reservoir to the downstream reservoir until the pressure reaches equilibrium i.e. upstream and downstream pressures are approximately equal. This equilibrium pressure has been referred to as gas pressure. The pressure pulse is significantly smaller (<10%) than the initial gas pressure in the system. As the Langmuir pressures for lumped coals are in the range of mega Pascal, we assumed that there is insignificant additional adsorption with less than 10% increment in gas pressure. The pressure loss in the upstream reservoir and pressure gain in the downstream reservoir are recorded with time. This process is repeated until the predetermined value of gas pressure is achieved. The pressure-time profile from the experiment was used to obtain permeability, k (Brace et al., 1968), as in equation 1.

$$k = \frac{\gamma \cdot \mu \cdot L \cdot V_{up} V_{down}}{P_{eq} \cdot A \cdot (V_{up} + V_{down})} \quad (3)$$

Where permeability $k(m^2)$ is calculated from the decay parameter $\gamma(s^{-1})$ for a known gas

viscosity μ(Pa.s), sample length L(m), equilibrium pressure at the end of the experiment

P_{eq}(N/m^2) and cross sectional area of the specimen A(m^2) relative to

upstream/downstream reservoir volumes $V_{up/down}$(m^3), measured initial pressure

$p_{up/down0}$(N/m^2) and transient upstream/downstream reservoir pressures

$p_{up/down}$(N/m$^{2.}$), as in equation 2.

$$\gamma = \frac{\log\left(\frac{d(p_{up} - p_{down})}{(p_{up0} - p_{down0})}\right)_t}{dt} \quad (4)$$

The value of γ is the slope of the line obtained from a $\log\left(\frac{d(p_{up} - p_{down})}{(p_{up0} - p_{down0})}\right)$ versus time

straight line plot. This method yields a single value of permeability for a single pulse.

Pressure-decay in the upstream reservoir and complementary pressure-gain in the

downstream reservoir for a typical pulse test in moist coal with non-adsorbing (He) gas is

shown in Figure 3.2. Pulse-decay data are reduced for $dP_o = p_{up0} - p_{down0}$, $dP_t = p_{up} - p_{down}$ and P_{eq}. A typical set of observations is used for the calculation of

uncertainty in the permeability. More details of the analysis and error propagation may be

found elsewhere (Kumar et al., 2012). In addition to the permeability data, the evolution

of roughness of the fracture surfaces was recovered from micrographs obtained by optical

profilometry and reduced using MetroPro. The surface roughness and the indentation into

the surface were quantified.

3 Results and Discussions

The permeability experiments for He and CO_2 were conducted at constant total stress of 10 MPa for coal and at 17 MPa for granite while pore pressures were varied within the range given in Table 3.1. The permeability of the artificial fracture in granite is modulated by the effect of diminishing effective stress, alone, while those for core are influence by the combined effects of effective stress and swelling/softening. This enables the evolution of permeability to be determined in coal as a function of both gas pressure (swelling/softening) and effective stress whereas for the granite control the influence of swelling/softening is sensibly absent.

3.1 Permeability evolution of a fracture in granite

Helium was injected into the split-core of granite at effective stresses ranging from 10 MPa to 17 MPa and in incremental steps to explore the evolution of permeability. The effective stresses were incremented/decremented by decrementing/incrementing the pore pressure under constant confining stress. The permeability of the core decreases with an increase in effective stress in both non-propped and propped fractures as shown in Figure 3.2. The permeability of the propped fracture is ~10-fold that of the non-propped fracture due to the increase in effective aperture. Furthermore, the permeability of the propped fracture decreases at a faster rate

114

with a unit increase in effective stress relative to the non-propped fracture (Figure 3.2), presumably as a result of proppant stiffness, repacking or crushing, or a combination of all three. The permeability follows an exponentially decreasing trend with increasing effective stress in both propped and non-propped cases (Figure 3.2).
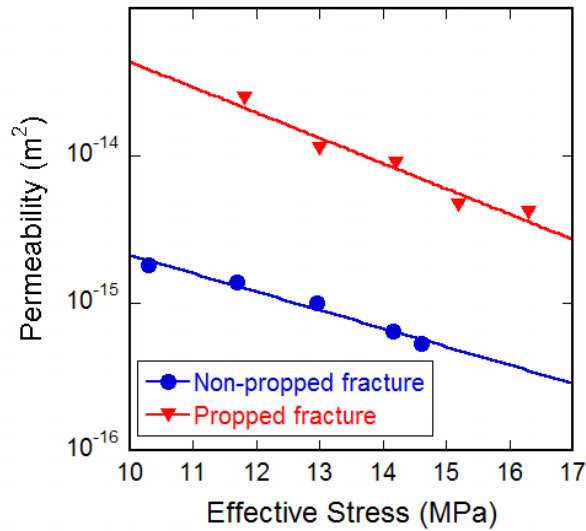
Figure 3.2: The permeability evolution in an artificial fracture in Westerly granite core on injection of helium under non-propped and propped conditions.

When the stress increases from 17 MPa to 25 MPa, the proppant can be significantly crushed into fines in the granite fracture. These fines may move to the cavities in fracture-contact surface accumulating within the fracture and inhibiting gas flow in open pathways. Evidence for accumulation of fines in specific locations within fractures was visible on the surface (Figure 3.3). These observations are in agreement with past discussions on proppant crushing (Lacy et al., 1997).
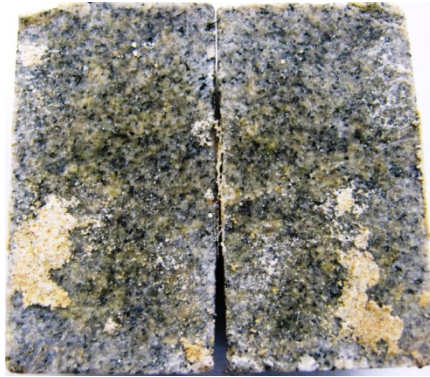
Figure 3.3: The fines are generated and reshuffled in the artificial fracture during the permeability test. The deposition of the fines in the pathways will inhibit flow therefore decreased permeability.

3.2 Permeability evolution of a fracture in coal

Smooth artificial fracture surfaces were prepared in split-core-plugs of bituminous and anthracite coals. The permeability evolution was followed for both non-propped and propped fractures with varying gas pressures (proxy for effective stresses) and compositions (He and CO_2) as shown in Figures 3.4a and 3.4b. The He permeability of the propped fracture is ~10-fold that of the non-propped fracture (Figure 3.4a and 3.4b). Similar to the case for the rigid fracture (granite) the permeability of the artificial fracture also increases exponentially with decreasing effective stress, both non-propped and propped. In the non-propped fracture, the permeability increases three-fold while it increases only twofold in propped fracture when the gas pressure is increased from 2 MPa to 4 MPa indicating that the rate of increase in the permeability being faster in non-propped fracture relative to that in propped fracture (Figure 3.4a). This observation for

coal may be attributed to its lower stiffness, which causes surface-deformation instead of proppant crushing (as observed in the granite core) thus possibly allowing proppant embedment. Notably, coal swelling is not likely to cause on He injection. Therefore, surface deformation may play a major role in permeability evolution in coal. Experiments were however performed at lower applied confining stress (10 MPa) than the granite as coalbed reservoirs are typically not as deep. Thus, proppant crushing is unlikely under these conditions given the relative strengths of sand and coal.

The CO_2 permeability evolution in non-propped and propped artificial fractures for bituminous coal is shown in Figures 3.4a and b. The CO_2 permeability of non-propped fracture increases with gas pressure (Figure 3.4a). The increase in pore pressure of sorptive gas under constant confining stress in intact coal induces swelling resulting in permeability decrease (Kumar et al., 2012). But, at a gas pressure greater than the saturation pressure, the decrease in permeability halts and the permeability starts increasing due to the effect of diminishing effective stresses (Kumar et al., 2012). Non-propped fractures do not demonstrate this behavior (Wang et al., 2011) instead they follow the trend in oversaturated region as observed by Kumar et al., 2012. Our observations are consistent with previous results on fractured coal (Wang et al., 2011) (Figure 3.4a). The CO_2 permeability of propped fracture in bituminous coal is as high as 10 to 100 fold that of non-propped fracture depending upon the conditions. Interestingly, the permeability evolution in propped fractures exhibit behavior similar to the intact coal (Kumar et al., 2012). The increase in gas pressure decreases the permeability which halts at certain threshold pressure referred to as saturation pressure and then increases at a pressure greater than the saturation pressure. The permeability evolution curve with pore

pressure shows a point of inflection (Figure 3.4a). The magnitude of change in permeability for the propped fracture was higher than that for the non-propped fracture. Intuitively, these observations may be explained by either swelling of the coal or by proppant embedding in the increasingly softer coal due to the presence of sorbing gas, or a combination of the two phenomena. It is important to note that these experiments are extreme case of fracture embedment as only monolayer of proppant was sandwiched in the fracture. The effect on permeability due to proppant embedment may be significantly small in larger aperture fractures as multiple proppant layers are expected. The multilayer of proppant would register the permeability equivalent to a sand-bed until the fracture is near closing. The permeability evolution in non-propped and propped fracture in anthracite coal is shown in Figure 3.4b. Similar to the bituminous coal, the He permeability increases with gas pressure for anthracite coal also but the magnitude of change is smaller. The CO_2 permeability evolution trends are also similar in both coals, the key difference being the magnitude of permeability change which is smaller in anthracite coal due to reduced sorptive capacity/strain and possibly inhibited softening. The quantification of surface indentation is explored in later sections of the paper.
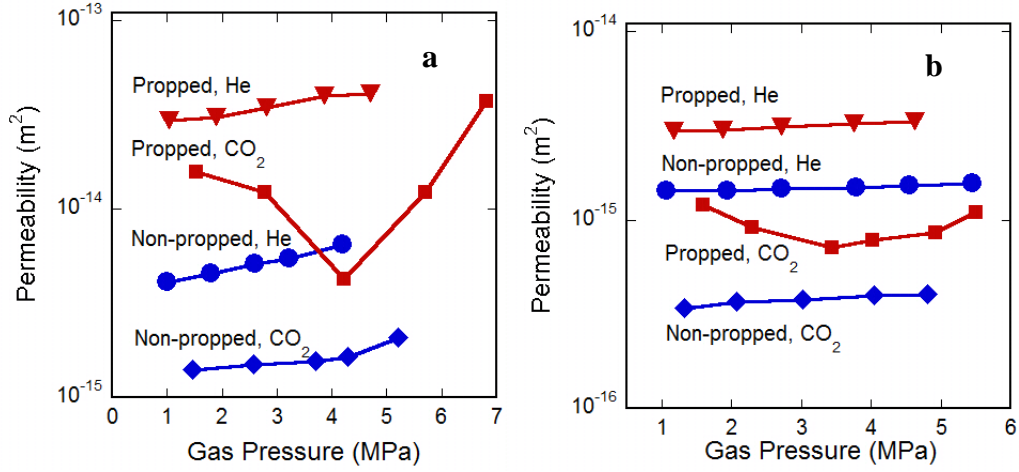
Figure 3.4: The permeability evolution of non-propped and propped fracture on injection of He and CO_2 a) bituminous coal b) anthracite coal. The observations are reported at 10 MPa of constant confining stress.

4 Analysis

In the following section, a mechanistic model was developed which includes important processes occurring in propped artificial fracture during CO_2 injection. Further, the experimental observations of permeability evolution are utilized to constrain the model. The quantification of the proppant indentation was quantified using an optical profilometer.

4.1 Mechanistic Model

A mechanistic model for permeability evolution was developed based on observations in an artificial fracture under non-propped and propped condition in stress-constrained coal. The permeability of an artificial fracture under non-propped and propped condition has been assumed much higher than the coal matrix. In the proposed model, proppant grains are assumed to be acting as rock-bridges embedded into the coal matrix. The permeability evolution of the 'matrix embedded rock-bridge' system depends on the processes namely sorption/desorption resulting in swelling/shrinkage of matrix and the change in effective stress leading to proppant embedment/proppant retreat (Figure 3.5). These processes directly modulate the cleat permeability by changing the cleat aperture (Izadi et al., 2011; Tao et al., 2012).

An idealized fracture consisting of two parallel surfaces isolated with sandwiched proppant grains (Figure 3.5) has been assumed for the development of permeability model. The void volume available for flow (CO_2) changes with overburden stress and swelling in turn affecting the permeability. An exaggerated schematic of a proppant filled an artificial fracture is shown (Figure 3.5). A monolayer of proppant is sandwiched in the fracture. The proppant grain might embed into the fracture wall as the normal stress increases or the coal softens on exposure to sorptive gas (e.g. CO_2). Further, CO_2 may swell the coal leading to blocking of flow pathways for the fluid.
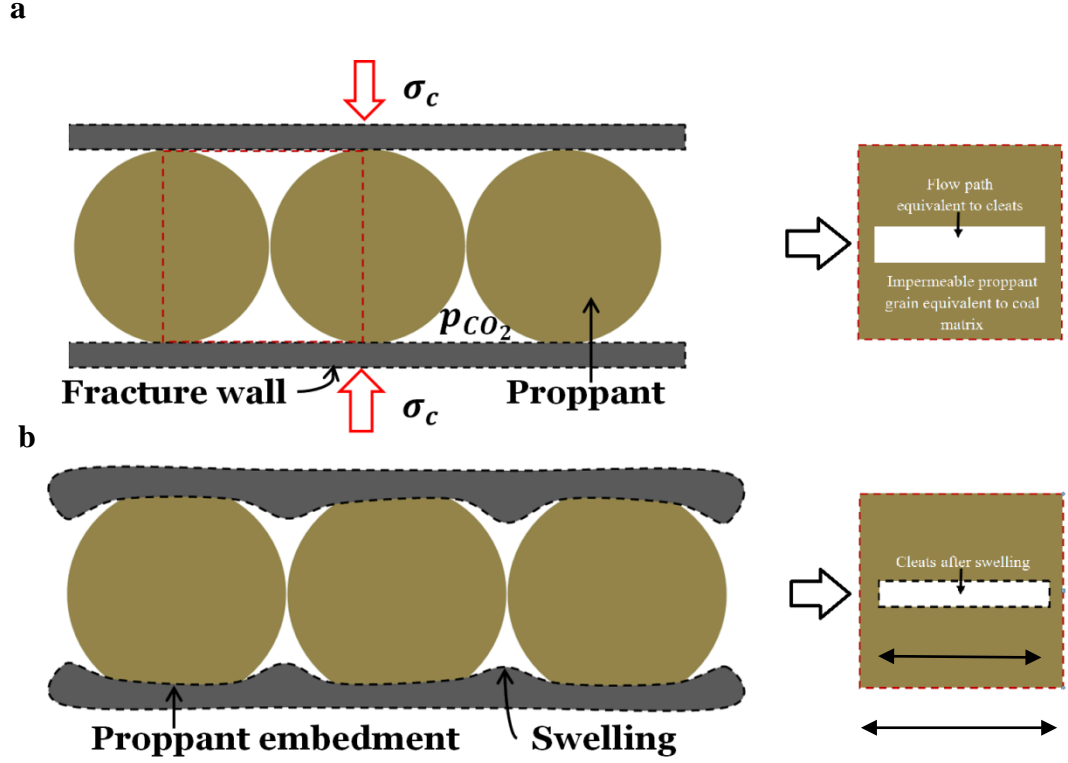
Figure 3.5: The sorption induced swelling and normal stress driven embedment is shown. A single unit is shown in red dashed lines which are similar to the model proposed Izadi et al., 2010 for matrix-fracture system a) Before the application of normal stress and sorptive gas pressure b) After proppant embedment and swelling.

The mechanistic model developed here assumes that the permeability modulates as a function of proppant embedment and sorption induced swelling. The mathematical formulation is presented below.

The embedded radius of a hard sphere (proppant) pressed against a flat surface (coal fracture surface) can be represented,

$$r_1 = R\sqrt{\frac{\sigma'}{\pi c}} \qquad (1)$$

Here r_1 is the radius of the portion (circular) embedded into the surface, R is the radius of proppant grain, σ' is the effective stress and c is the cohesive strength of coal. The embedded height (h_1) of sandwiched proppant grain,

$$h_1 = R\left(1 - \sqrt{1 - \frac{\sigma'}{\pi c}}\right)$$
(2)

The total volume V_1 of proppant grain embedded into the two fracture surfaces can be calculated as,

$$V_1 = 2\frac{1}{3}\pi h_1^2 \left(3R - h_1\right)$$
(3)

Consider a cubical unit of coal of side $2R$ containing a proppant grain. The volumetric strain developed in this unit due to sorption-induced swelling may be written as,

$$\Delta V = \alpha\varepsilon_L\left(\frac{P}{P + P_L}\right)(2R)^3$$
(4)

Here ΔV is the volumetric strain developed through swelling, α is a arbitrary shape factor, P is the pore pressure of gas and P_L is the Langmuir pressure.

If h_2 is the resultant new embedded height due to stress and swelling then the change in embedded volume can be represented as,

$$2\frac{1}{3}\pi h_2^2 \left(3R - h_2^2\right) = V_1 + \Delta V$$
(5)

$$2\frac{1}{3}\pi h_2^2 \left(3R - h_2^2\right) = 2\frac{1}{3}\pi h_1^2 \left(3R - h_1\right) + \alpha\varepsilon_L\left(\frac{P}{P + P_L}\right)(2R)^3$$
(6)

The new embedded height h_2 can be calculated from equation 6. The effective aperture of fracture b at any point during varying pore pressure at constant confined stress can be written as,

$$b = 2R - h_2 = b_0 - \Delta b \quad (7)$$

Here b_0 is the initial fracture aperture.

The change in aperture of the fracture Δb driven by these processes may be represented as,

$$\Delta b = -\Delta h_2 \quad (8)$$

For the cases where bulk in situ permeability k_0 is known at fracture aperture b_0 then the permeability evolution with change in aperture can be evaluated (Liu et al., 1997). This allows the evolution of fracture permeability to be followed for an arbitrary evolution of fracture aperture (Elsworth and Goodman, 1986; Piggott and Elsworth, 1993). It has been assumed that flow occurs in fractures only. The permeability of fracture k is modulated based upon its initial permeability k_0 as follows.

$$\frac{k}{k_0} = \left(1 + \frac{\Delta b}{b_0}\right)^3 \quad (9)$$

The formulation allows the evolution of normalized permeability to be represented with change in fracture aperture. The arbitrary shape factor (α) and cohesive strength (c) of coal are evaluated from the best fit as indexed by the coefficient of correlation (R^2).

4.2 Parameter Optimization

The mechanistic model developed (equation 9) has been used to describe the permeability evolution in propped fracture in coals on injection of CO_2. The model predicts the permeability with change in combined response to normal stress and sorptive gas pressure in the fractured core. The permeability evolution may be approximated by an arbitrary shape factor and cohesive strength of coal. The numerical values of Langmuir strain and Langmuir pressure are obtained from the literature for bituminous and anthracite coal (Kumar et al., 2012; Robertson, 2005; Wang et al., 2011). Here Langmuir strain is defined as the maximum swelling induced strain in coal due to gas pressure. The value of Langmuir strain and Langmuir pressure are 10% and 0.4 MPa for bituminous coal and 1% and 0.4 MPa for anthracite coal (Kumar et al., 2012). The initial permeability (k_0) and fracture aperture (b_0) have been chosen at first point of observation in permeability experiments in each coal.

MATLAB® curve fit toolbox was used to optimize the values of the parameters α and c. This function utilizes the lsqcurvefit algorithm to find the best possible set of values under prescribed constraints (MATLAB Curvefit Toolbox, 2009). The fitting parameters α and c have been obtained for each coal core. The model has been validated for each coal with experimental permeability evolution data in Figure 3.6.
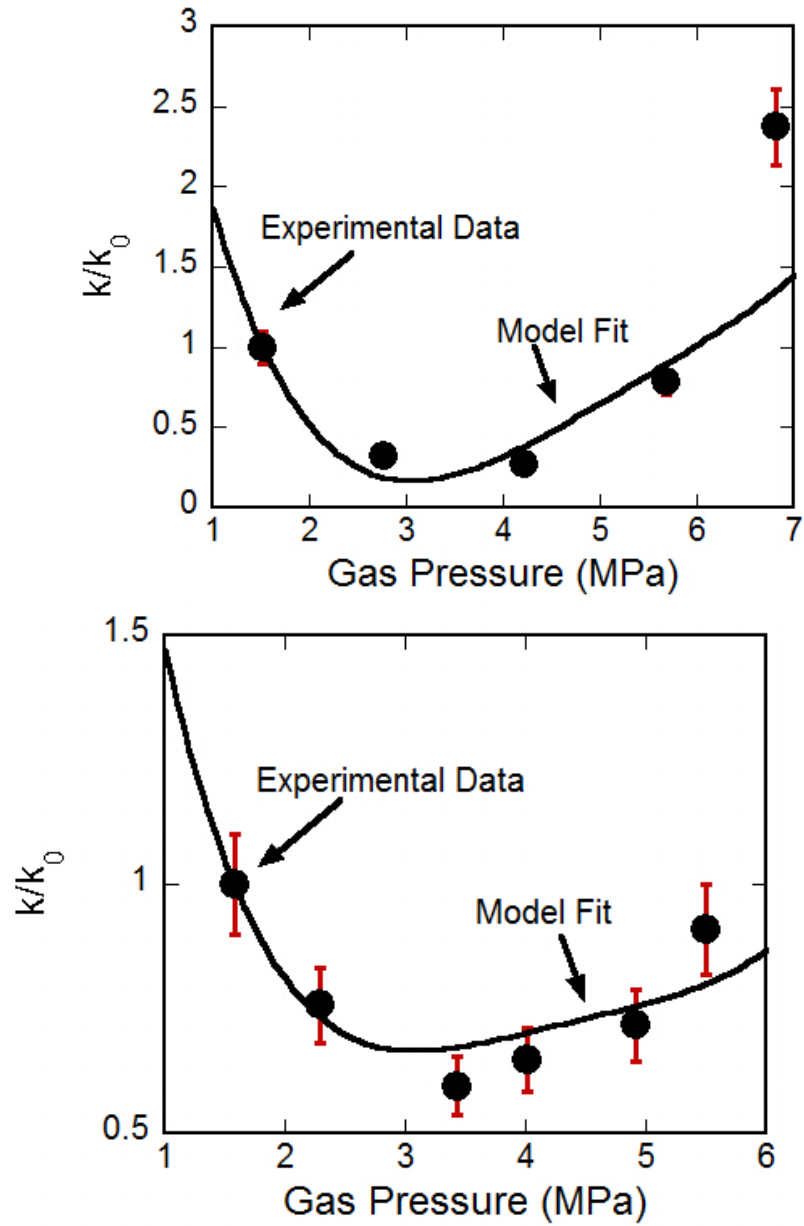
Figure 3.6: The evolution of permeability in propped fracture on injection of CO_2. The model fit is shown with black solid line a) bituminous coal b) anthracite coal. The uncertainty in permeability measurement is show by error bar (±10%) at each observation.

Table 3.2. The values of fitting parameters used in permeability evolution model in Figure 3.6.

Coal Type	α	c (MPa)
Bituminous	1.25	4
Anthracite	0.43	5

The bituminous coal sample has a larger shape factor than the Anthracite coal attributable to its inherent swelling ability on CO_2 exposure (Kumar et al., 2012; Wang et al., 2011). Commonly, the bituminous coal also has more open porosity relative to anthracite (Rogers, 1994) due to which injection gas can travel faster in bituminous coal matrix accessing more pores and inducing higher swelling strain resulting in higher shape factor. Often, the anthracite coal shows higher uniaxial compressive strength (UCS) than that of bituminous coal (Rogers, 1994). Therefore, the anthracite coal was expected to exhibit higher cohesive strength as indicated in Table 3.2. The values predicted from curve fitting lie within the range of values reported elsewhere (Martin and Maybee, 2000). Unfortunately, no direct comparison of cohesive strength values can be made due to the absence of published data for cohesive strength of these coals under the experimental conditions used in this work.

The permeability of propped fracture reduces as the gas pressure of the sorbing gas augments in steps at constant confining stress. The reduction in permeability is caused by the coal swelling and/or proppant embedment that reduce the pathways in the propped fracture. As the peak swelling strain is approached, the reduction in permeability

halts and permeability increases with gas pressure (Figure 3.6) making a "U-shape". The "U-shape" was observed in both bituminous and anthracite coal at different gas pressure corresponding to maximum swelling strain. The maximum swelling strain in bituminous coal is an order of magnitude higher than that of anthracite coal leading to larger permeability reduction bituminous coal. The maximum reduction in permeability is 27% and 6% for bituminous and anthracite coal respectively. The distinct difference in permeability-reduction is attributable to swelling which occurs due to CO_2 uptake capacity and swelling induced strain. The reduction in permeability halts when infiltrating gas pressure becomes approximately equal to the pressure at which maximum adsorption strain occurs. If the gas pressure is further increased then the fracture dilates leading to permeability increase (Figure 3.6).

This mechanistic model represents the modulation of propped fracture permeability where swelling and effective stress plays a major role. The excellent fit of the model to the permeability evolution observations in various ranks coal shows the model consistency and plausibility. To the best of our knowledge, no current model presents the mechanistic explanation to the permeability evolution in propped fracture on injection of sorbing gas.

4.3 Quantification of surface indentation

White light optical profilometry was utilized to quantify and characterize the surface of the polished coal. High magnification three-dimensional surface micrographs were obtained and stitched together to obtain a 7 mm × 4.5 mm area. The surface

characteristics are compared using micrographs before and after the experimental suite. Same core was used for propped and non-propped experiments.

The coal surface is relatively smooth from the polishing process but with the surface being slightly elevated at places (Figure 3.7). The coal consists of microlithotypes varying in their microhardness (Bratek et al., 2002; Das, 1972; Hower et al., 2008; Loustalet et al., 1994; Mukherjee et al., 1989; Nandi et al., 1977), sorption capacity (Laxminarayana and Crosdale, 2002; Richard, 2012; Weniger et al., 2012) and swelling strain (Kiyama et al., 2011; Yang and Zoback, 2011). The hard lithotypes (vitrain) remains elevated on the coal surface compared to the softer lithotypes (clarain) after polishing of the surface. This occurs due to differences in micro-hardness of different lithoptypes. The height differences are visually enhanced using false coloring where elevated features are shown by bright colors and other features are accordingly color coded. The topology changes are evident in the surface before and after the experimental suite (Figure 3.7). The surface roughness of polished fractures were 1.09 μm and 0.90 μm for bituminous and anthracite coal respectively. The smooth surface of the fracture was slightly rougher after exposure to 1.24 μm and 1.43 μm respectively probably due to a slight irreversible structural rearrangement within the coal with CO_2 uptake and loss. The infrequent depressed features are pits caused by proppant indentation most likely caused by a non-monolayer distribution of the sand. Coal softening would be expected to produce multiple evenly spaced pits. Thus, for the bituminous coal at these conditions no evidence of coal softening was observed. Thus, coal swelling and the management of the injection system should remain the research focus. Pre-existing pitting is likely due to

mineral grain removal during polishing. The histogram plots of feature height before and after the experimental suite is shown in Figure 3.8. The distribution of feature height is wider and smoother (Figure 3.8) for the fracture surface before the experimental suite indicating smooth surface prior to the experiments.

a　　　　　　　　　　　　　　　　　**b**
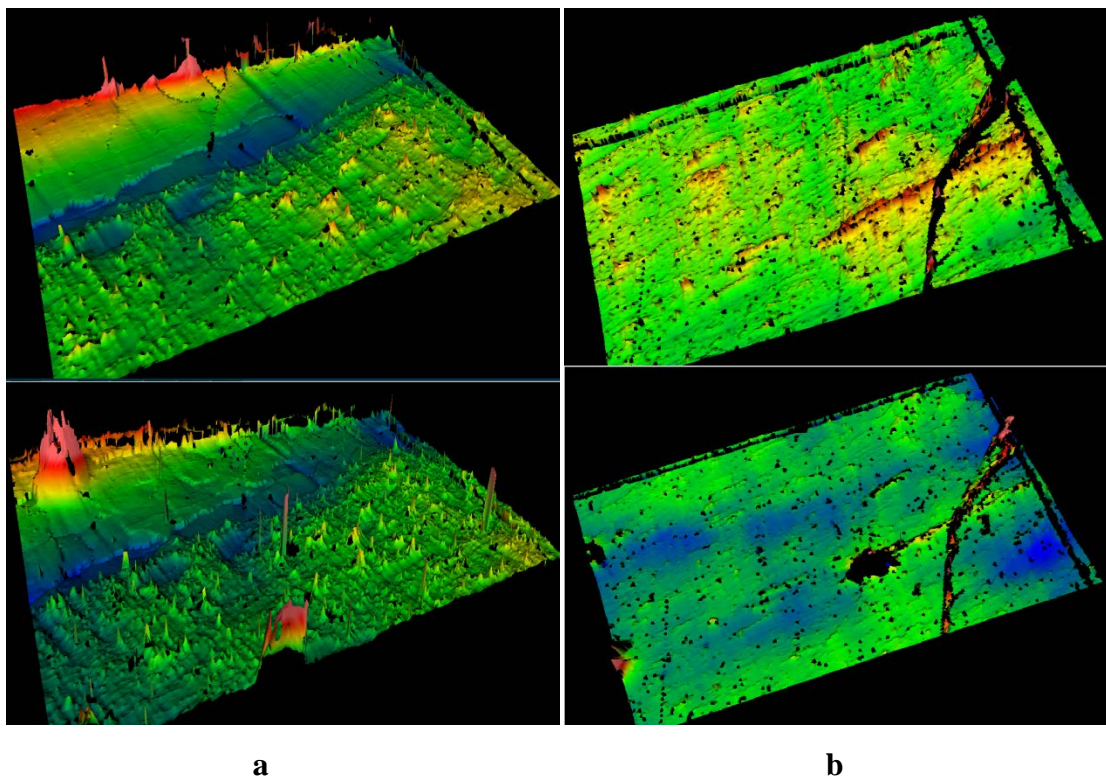
Figure 3.7: The aerial view of coal surface before (top) and after (bottom) the experiment a) bituminous b) anthracite. The vertical features are highly exaggerated (on the order of several microns) and are falsely colored. The red color represents highest elevated part while blue shows the depressed features on coal surface. The black regions indicate poorly reflecting deep pits which receives/sends poor signals during profilometer

scanning. The region of interest shown is 7 x 5 mm (i.e the vertical and horizontal scales differ by several orders of magnitude). scanning. The region of interest shown is 7 x 5 mm (i.e the vertical and horizontal scales differ by several orders of magnitude)

a

b
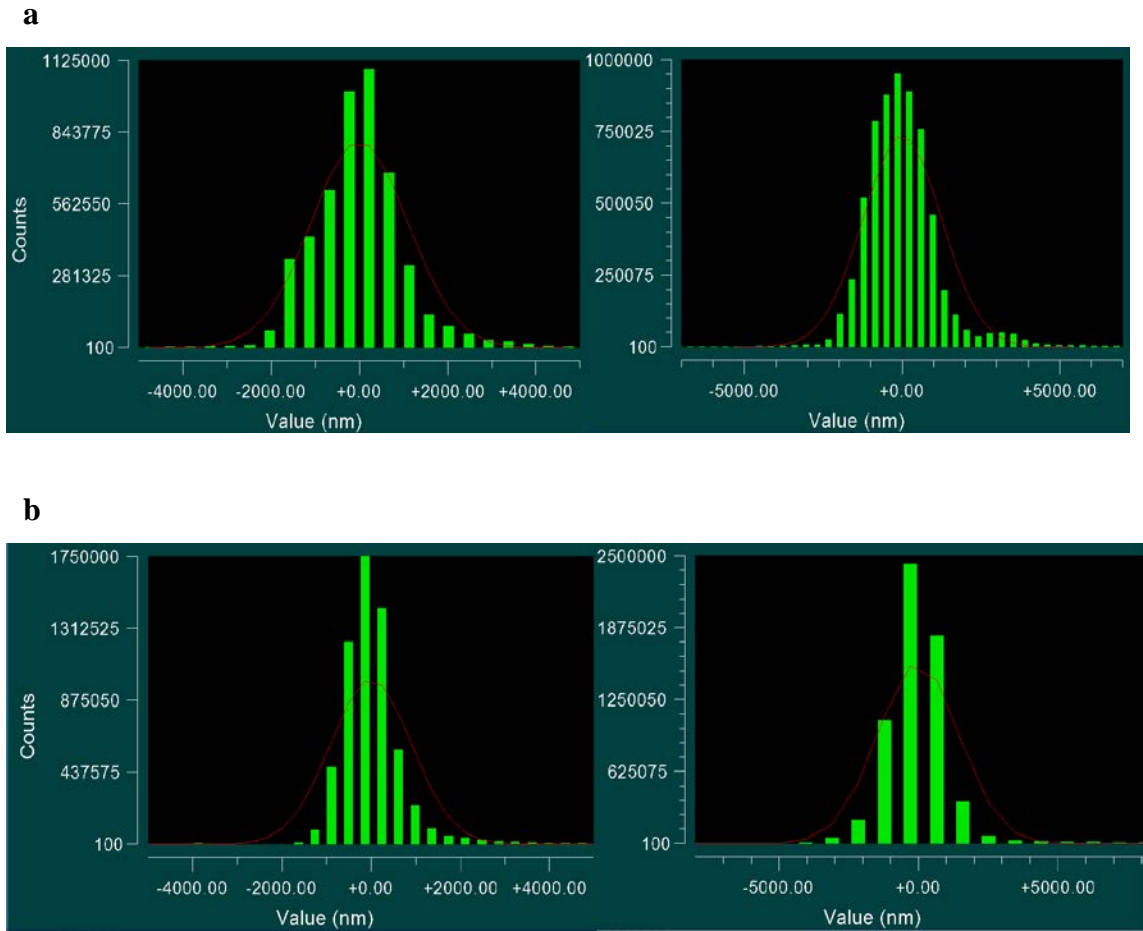
Figure 3.8: The surface histograms before (left) and after (right) the experimental suite for a) bituminous b) anthracite coal. The histograms represent the number of features of same height on y-axis with their characteristics height from the mean on x-axis. The negative height represents the depressed regions from mean surface height.

A suitable location was been chosen to quantify the surface indentation on the coal surface in anthracite coal. A single pit on fracture surface was analyzed using a 50X objective lens in optical profilometer. An area of 1.18 mm$\times$ 0.67 mm was captured at high magnification with dual light level in auto focus mode. Twenty small micrographs are attached to quantify the surface indentation by proppant grain. The micrographs show a deep pit surrounded by relatively elevated regions (Figure 3.9). The region colored in black indicates a deep and/or non-reflective surface, which was beyond the measurement capability of profilometer. The depth of the pit is 60 µm from the surface of the coal which is ~ $(1/3)^{rd}$ of the mean particle size of the proppant. Had coal softening occurred, it would have reduced the coal stiffness more uniformly, which would increase the areal density of pits on the fracture surface. On the contrary, the pits observed are infrequent and isolated, indicating insignificant contribution of coal softening under these conditions towards reduction in permeability. However, the uniformly distributed elevated features present on the fracture surface post the experiments (Figure 3.7) indicate coal swelling to be the likely contributor to the permeability reduction.
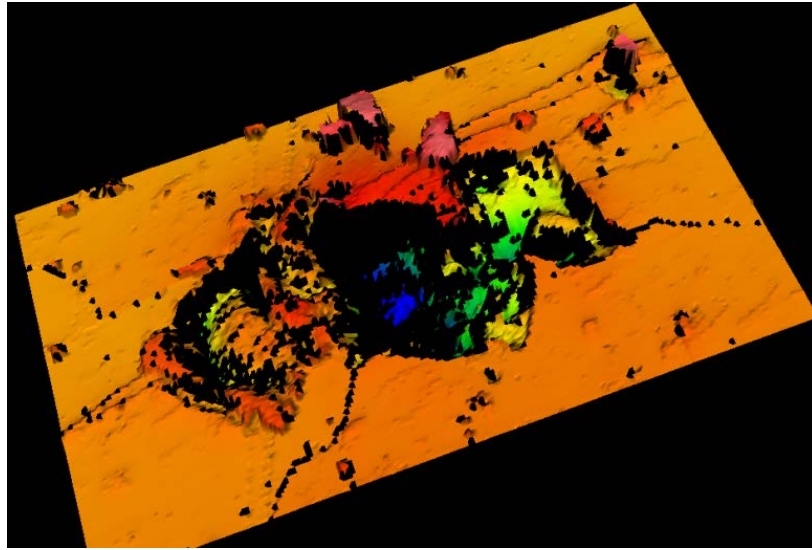
Figure 3.9: A false colored high resolution micrograph capturing an area of 1.18 mm× 0.67 mm on the fracture surface after the experimental suite. The region in black color is an example of surface indentation by proppant.

5 Conclusions

The permeability evolution was investigated for saw cut idealized fracture in bituminous and anthracite coal with injection of both non-sorptive (He) and sorptive gases under mechanically constrained condition. The permeability evolution for the same fracture was explored under propped conditions. We consider an extreme case of proppant placement in fracture i.e. a uniform monolayer. Also, the permeability evolution experiments were conducted on an artificial fracture in granite for non-propped and propped condition with helium injection at various pore pressures. The following observations and conclusions are proposed.

1. The helium permeability of non-propped and propped artificial fracture in granite decreases with effective stress. This decrease may be 2-3 times if the pore pressure stress increases from 4 MPa to 6 MPa. The permeability of propped fracture was 10-15 times higher than that of non-propped fracture in granite. Similar observations are made for artificial fracture in bituminous coal.

2. The increase in He permeability may be as high as ~10 fold in bituminous and ~5 fold in anthracite if monolayer proppant is sandwiched in the coal fracture. Similar increase is observed in the case of sorptive gas (CO_2) permeability.

3. The CO_2 permeability of non-propped artificial coal fracture increases with pore pressure in both coals. However, the permeability evolution with CO_2 exposure exhibits a "U-shape" pattern with pore pressure at constant confining stress in the propped fracture. The permeability decreases (likely due to coal swelling) and then increases (likely due to diminishing effective stresses) with effective stress. The permeability reduction with gas pressure is caused by coal swelling and coal softening was eliminated as a possible mechanism of permeability reduction.

4. A mechanistic model was developed for permeability evolution in propped fracture under CO_2 injection. Primarily, the permeability modulates as the swelling and effective stress varies with pore pressure. The model yields acceptable match with the experimental observations.

5. The roughness of fracture surface increases due to surface indentation and coal swelling. The pits created on fracture surface are significant ~ $(1/3)^{rd}$ compared to proppant size.

6 References

Alramahi, B., Sundberg, M.I., 2012. Proppant embedment and conductivity of hydraulic fractures in Shales, American Rock Mechanics Association, Chicago.

ASTM D7582, 2010. Standard test methods for proximate analysis of coal and coke by macro thermogravimetric analysis.

ASTM International D388, 2005. Standard classification of coals by rank. IHS, Pennsylvania, United States.

ASTM International D3302/D3302M-10, 2010. Standard test method for total moisture in coal. IHS, Pennsylvania, United States.

ASTM International D5671, 2011. Standard Practice for Polishing and Etching Coal Samples for Microscopical Analysis by Reflected Light. IHS.

Bai, M., Elsworth, D., 1994. Modeling of subsidence and stress-dependent hydraulic conductivity for intact and fractured porous media. Rock Mechanics and Rock Engineering 27, 209-234.

Brace, W.F., Walsh, J.B., Frangos, W.T., 1968. Permeability of granite under high pressure. Journal of Geophysical Research 73, 2225-2236.

Bratek, K., Bratek, W., Gerus-Piasecka, I., Jasienko, S., Wilk, P., 2002. Properties and structure of different rank anthracites. Fuel 81, 97-108.

Cooke, C.E., 1977. Hydraulic fracturing with a high-strength proppant. Journal of Petroleum Technology, 29, 1222-1226.

Das, B., 1972. Microhardness of Abnormally Metamorphosed Coal. Fuel 51, 52-53.

Elsworth, D., Yasuhara, H., 2010. Mechanical and transport constitutive models for fractures subject to dissolution and precipitation. Int. J. Numer. Anal. Methods Geomech. 34, 533-549.

Freeman, E.R., Anschutz, D.A., Rickards, A.R., Callanan, M.J., 2009. Modified API / ISO crush tests with a liquid-saturated proppant under pressure incorporating temperature, time, and cyclic loading: what does it tell us?, SPE Hydraulic Fracturing Technology Conference. Society of Petroleum Engineers, The Woodlands, Texas.

Hower, J.C., Trinkle, E.J., Raione, R.P., 2008. Vickers microhardness of telovitrinite and pseudovitrinite from high volatile bituminous Kentucky coals. International Journal of Coal Geology 75, 76-80.

Izadi, G., Wang, S., Elsworth, D., Liu, J., Wu, Y., Pone, D., 2011. Permeability evolution of fluid-infiltrated coal containing discrete fractures. International Journal of Coal Geology 85, 202-211.

Kiyama, T., Nishimoto, S., Fujioka, M., Xue, Z., Ishijima, Y., Pan, Z., Connell, L.D., 2011. Coal swelling strain and permeability change with injecting liquid/supercritical CO_2 and N_2 at stress-constrained conditions. International Journal of Coal Geology 85, 56-64.

Kumar, H., Elsworth, D., Liu, J., Pone, D., Mathews, J.P., 2012. Optimizing enhanced coalbed methane recovery for unhindered production and CO_2 injectivity. International Journal of Greenhouse Gas Control 11, 86-97.

Kumar, H., Pone, J.D.N., Mitchell, G.D., Halleck, P.M., Mathews, J.P., 2009. In Lithotype influences on (an idealized) coal cleat surface deformation by carbon dioxide

induced coal swelling, International Coalbed Methane and Oil Shale Symposium, Tuscaloosa, Alabama.

Lacy, L.L., Rickards, A.R., Ali, S.A., 1997. Embedment and fracture conductivity in soft formations associated with HEC, Borate and water-based fracture designs, SPE Annual Technical Conference and Exhibition. 1997, San Antonio, Texas, pp. 255-268.

LaFollette, R.F., Carman, P.S., 2010. Proppant diagenesis: results so far, SPE Unconventional Gas Conference. Society of Petroleum Engineers, Pittsburgh, Pennsylvania, USA.

Laxminarayana, C., Crosdale, P.J., 2002. Controls on methane sorption capacity of Indian coals. AAPG Bulletin 86, 201-212.

Lee, D.S., Elsworth, D., Yasuhara, H., Weaver, J.D., Rickman, R., 2010. Experiment and modeling to evaluate the effects of proppant-pack diagenesis on fracture treatments. Journal of Petroleum Science and Engineering 74, 67-76.

Loustalet, D., Oberlin, A., Moreau, M., 1994. Peculiar Process of Coal-Tar Pitch Carbonization (Textural and Physicochemical Characterization). Carbon 32, 1267-1275.

Mukherjee, A.K., Alam, M.M., Ghose, S., 1989. Microhardness Characteristics of Indian Coal and Lignite. Fuel 68, 670-673.

Nandi, B.N., Ciavaglia, L.A., Montgomery, D.S., 1977. The variation of the microhardness and reflectance of coal under conditions of oxidation simulating weathering. Journal of Microscopy 109, 93-103.

Piggott, A.R., Elsworth, D., 1993. Laboratory assessment of the equivalent apertures of a rock fracture. Geophys. Res. Lett. 20, 1387-1390.

Pope, C., Peters, B., Benton, T., Palisch, T., 2009. Haynesville Shale - one operators approach to well completions in this evolving play, SPE Annual Technical Conference and Exhibition. Society of Petroleum Engineers, New Orleans, Louisiana.

Richard, S., 2012. Relationships between CO2 sorption capacity by coals as measured at low and high pressure and their swelling. International Journal of Coal Geology 90–91, 156-161.

Robertson, E.P., 2005. Measurement and modeling of sorption-induced strain and permeability changes in coal. Idaho National Laboratory, Idaho.

Stoddard, T., McLennan, J., Moore, J., 2011. Fracture conductivity of a bauxite-propped geothermal system at in-situ conditions, Thirty-Sixth Workshop on Geothermal Reservoir Engineering Stanford University, Stanford, California.

Tao, S., Wang, Y., Tang, D., Xu, H., Lv, Y., He, W., Li, Y., 2012. Dynamic variation effects of coal permeability during the coalbed methane development process in the Qinshui Basin, China. International Journal of Coal Geology 93, 16-22.

Terracina, J.M., Turner, J.M., Collins, D.H., Spillars, S., 2010. Proppant selection and its effect on the results of fracturing treatments performed in shale formations, SPE Annual Technical Conference and Exhibition. Society of Petroleum Engineers, Florence, Italy.

Walsh, J.B., 1981. Effect of pore pressure and confining pressure on fracture permeability. International Journal of Rock Mechanics and Mining Sciences & Geomechanics Abstracts 18, 429-435.

Walsh, J.B., Grosenbaugh, M.A., 1979. A new model for analyzing the effect of fractures on compressibility. Journal of Geophysical Research 84, 3532-3536.

Wang, S., Elsworth, D., Liu, J., 2011. Permeability evolution in fractured coal: the roles of fracture geometry and water content. International Journal of Coal Geology 87, 13-25.

Weniger, P., Franců, J., Hemza, P., Krooss, B.M., 2012. Investigations on the methane and carbon dioxide sorption capacity of coals from the SW Upper Silesian Coal Basin, Czech Republic. International Journal of Coal Geology 93, 23-39.

Yang, Y., Zoback, M.D., 2011. The Effects of Gas Adsorption On Swelling, Visco-plastic Creep And Permeability of Sub-bituminous Coal. American Rock Mechanics Association.

Yasuhara, H., Elsworth, D., 2008. Compaction of a rock fracture moderated by competing roles of stress corrosion and pressure solution. Pure and Applied Geophysics 165, 1289-1306.

Yasuhara, H., Polak, A., Mitani, Y., Grader, A.S., Halleck, P.M., Elsworth, D., 2006. Evolution of fracture permeability through fluid–rock reaction under hydrothermal conditions. Earth and Planetary Science Letters 244, 186-200.

Chapter 4 : Permeability Evolution in Sorbing Media: Analogies between Organic-rich Shale and Coal

Abstract

We report measurements of permeability evolution in shales infiltrated separately by non-sorbing (He) and sorbing (CO_2) gases under varying gas pressures, confining stresses and deviatoric stresses. Experiments are completed on Pennsylvanian shales containing both natural and artificial fractures under non-propped and propped conditions. We use observations for permeability evolution in other sorbing media (coal, Kumar et al., 2012) to codify the response for shale. It is observed that for a naturally fractured shale, the He-permeability increases by ~15% as effective stress is reduced by increasing the gas pressure from 1 MPa to 6 MPa at constant confining stress of 10 MPa. Conversely, the CO_2-permeability reduces by a factor of two under similar conditions. Permeability of the core recovers to the original magnitude when the core is resaturated by a non-adsorbing gas, despite prior CO_2 exposure. A second core is split with a fine saw to create a smooth artificial fracture and the permeabilities measured for both non-propped and propped fractures. The He-permeability of a monolayer sand-propped artificial fracture is ~2-3 fold that of a non-propped fracture. Upon increasing the gas pressure, the He-permeability of the propped fracture increases under constant confining stress. Conversely, the CO_2-permeability of the propped fracture decreases by between one-half to one-third as the gas pressure increases from 1 to 4 MPa at a constant confining stress. We attribute the reduction in permeability to sorption-induced swelling in the organic material of the shale. The permeability of the non-propped shale fracture

increases with gas pressure, at constant confining stress, due to the absence of rock

bridges that commonly occur in naturally fractured samples. Although the permeability

evolution of non-propped and propped artificial fractures in shale are found to be similar

to those observed in coal, the extent of permeability reduction by swelling is much lower

in shale due to its lower organic content. The surface roughness and peak-to-valley

differential for the artificial fracture surfaces are quantified by optical profilometry.

Initial values of surface roughness and peak-to-valley differential height are 4.1 μm and

77.9 μm, respectively, which increases to 6.1 μm and 122.4 μm at completion of

experiments - indicating the significant influence of proppant indentation into the surface

of the fracture in shale. A mechanistic model representing permeability evolution in

sorbing media is applied to describe permeability evolution in shale. This model

characterizes the 'U-shaped' variation of permeability with gas pressure typical for

sorbing media and apparent for shales.

1 Introduction

Carbon dioxide injection in coal seams or shales may be an option for its geological sequestration (Kang et al., 2011; Nuttall et al., 2005; White et al., 2005). Gas shale plays in their matured state have similarities to coal due to their organic matter content, pore size distribution and stress regime (Pellenq et al., 2012). Furthermore, the porosity and permeability of shale reservoirs are similar to coalbed reservoirs (Shi and Durucan, 2010; Soeder, 1988). Shale formations with potential for natural gas production contain significant organic matter that may be as high as 10% on a w/w basis (Bruner and Smosna, 2011; Jenkins and Boyer II, 2008; Kang et al., 2011). These shales have four types of porous media: the non-organic matrix, the organic-matrix, any natural fractures and any hydraulically induced fracture (Wang and Reed, 2009). The non-organic portion is comprised of clay, minerals and heavy metals (Loucks et al., 2009). The organic matrix consists of carbon-rich matter as in the case of coal. The presence of organic matter creates a sorbing medium that imparts similar response un both coals and shales upon exposure to sorbing gases. Thus there is the potential to utilize the extensive understanding of coal behavior and modeling to as an analog to permeability evolution in shales. A significant portion of sorbing gas is stored in the adsorbed state in bituminous coalbed reservoirs (Laubach et al., 1998). Likewise, the organic matter present in shales provides storage capacity for sorbing gas in the organic pores (Wang and Reed, 2009). Although the mass of methane, stored as free gas in the fracture porosity, is significantly lower in shale reservoirs compared to conventional reservoirs, it is the adsorbed gas contributes to high storage capacity (Kang et al., 2011). Finally, micropore size

distributions (< 2 nm) observed in Pennsylvanian coals and Upper Devonian-Mississippian shales are similar although mesopore (2-50 nm) distributions are significantly different (Mastalerz et al., 2012).

Physico-sorption/desorption of the sorbing gas in the pores is expected to lead to physico-mechanical changes such as swelling or shrinkage and to correspondingly influence the evolution of permeability in shale reservoirs (Kang et al., 2011; Kumar et al., 2012; Wang et al., 2011) in a manner similar to coal. In both short term and long term, it is the permeability of the fractured porous medium and sorbing media response that controls CO_2 injectivity. Understanding of evolution of permeability is necessary for sequestration management in shale reservoirs. While the transport mechanisms and associated physic-mechanical changes have been studied extensively for coal, few data are available for shales.

Coal permeability is a function of net effective stress (Brace et al., 1968; Gash et al., 1993) with the permeability decreasing with an increase in effective stress (Bai et al., 1995; Durucan and Edwards, 1986; Min et al., 2009; Seidle et al., 1992; Somerton et al., 1975). Similarly, the permeability of shale varies with confining stress which may be attributed to the presence of microcracks (Dong et al., 2010). Similarly, shale permeability behaves with a power law dependency on effective stress (Dong et al., 2010). The desorption/adsorption response to gas infiltration also influences permeability evolution (Bustin et al., 2008; Cui et al., 2007; Harpalani and Chen, 1995; Kelemen and Kwiatek, 2009; Seidle and Huitt, 1995). Coal swells with the adsorption of CO_2 and develops compactive stresses if mechanically constrained (Day et al., 2010; Pone et al., 2010; Reucroft and Patel, 1986; Siemons and Busch, 2007). The reduction of coal

permeability is thus a consequence of swelling strain with CO_2 sorption (Durucan and Shi, 2009; Kiyama et al., 2011; van Bergen et al., 2006).

Expectations are that the change in gas pressure of a sorbing gas will induce swelling/shrinkage in the organic matrix of shale (Kang et al., 2011). For shales the swelling strain developed by a unit change in gas pressure is expected to be lower than that for coal due to the lower (~10% w/w) organic matter content in shale (Bruner and Smosna, 2011). Permeability evolution in shale is also complicated by complex geomechanical processes such as the transport of gas, adsorption, desorption, changing horizontal stresses, and vertical strains. Adsorption of CO_2 in micropores will result in matrix swelling therefore potentially closing the existing natural fractures and reducing injectivity (Sakhaee-Pour and Bryant, 2012). These dynamic changes in shale permeability are fundamentally similar to those for coal (Mastalerz et al., 2012). However, the increase in deviatoric stress beyond a threshold may lead to deformation bands in shale (Dong et al., 2010). The rearrangement of grains in the deformation bands can lead to the irreversible loss of porosity and concomitant reduction in permeability (Kumar et al., 2010). Such observations of permeability reduction beyond a threshold deviatoric stress indicate that the shale may exhibit stress path dependent permeability evolution (Perez et al., 2010).

Conceptual models for transport of sorbing gas in shale have been proposed (Fathi and Akkutlu, 2009; Kang et al., 2011). The injected CO_2 travels through the open fracture (natural and artificially induced) to the shale matrix. The concentration gradient drives the gas through the inorganic or organic matrix and reaches the organic matter where it is

144

adsorbed and therefore remains stored in the pores. The transport of gas in the inorganic matrix may result from transitional-slippage or diffusion-related mechanisms or a combination of both (Kang et al., 2011). The effect of mineral heterogeneity may also be coupled with conceptual models to predict the effect of macro-kinetics and macro transport on the potential reduction of ultimate recovery (Fathi and Akkutlu, 2009). Primary methane recovery remains poor without stimulating the shale gas reservoir. Therefore, shale gas reservoirs are often fractured using water slurry and cross-linked gels to develop a network of artificial fractures to enhance the permeability of the pay zone (Arthur et al., 2008; Boyer and Kieschniek, 2010; Veatch et al., 1989). Proppants are concurrently placed in the fractures to prevent aperture reduction due to closing upon the reduction in fracturing-fluid pressure. Enhanced gas recovery from shale reservoirs may also be achieved by injecting CO_2 (Nuttall, 2010) but it may further accelerate the fracture closure by inducing swelling in the organic matter of shale (Curtis, 2002), a phenomenon which is commonly observed in coal (Harpalani and Chen, 1995; Harpalani and Schraufnagel, 1990; White et al., 2005). However, evolution of permeability in proppant filled fractures under the application of stress and sorption induced swelling caused by CO_2 has not previously been evaluated.

Because the principal transport processes are similar, permeability evolution models developed for coal may be utilized to explain the evolution of permeability in shale. The following experiments were completed with sorbing and non-sorbing gases on open and propped fractures in shale to evaluate the evolution of permeability in shale.

2 Experimental Methods

Forced fluid-injection experiments were completed on a cylindrical core, axially saw-cut, then propped or non-propped with # 70-140 proppant. These samples were stressed to in situ conditions. He and CO_2 were used as permeants to investigate the role of swelling and effective stress on the dynamic evolution of permeability

2.1 Samples

The two cylindrical cores of shale, 2.5 cm diameter and 5 cm length, were sampled (drilled along bedding) from shale blocks collected in Pennsylvania. Shale density varied between 0.95 (A) and 1.58 gm/cm^3 (B) between the two sampled locations The He-porosity of the low-density shale (A) was 34% while the high-density sample (B) was 5% as determined using the pulse test technique. The fixed carbon, ash yield and moisture contents were 8%, 87%, 1% for sample A and 5%, 92%, 0.5% for sample B (ASTM International D7582, 2010).

The evolution of permeability was investigated by injecting He and CO_2 into an intact shale core. Shale gas reservoirs are typically fractured to enhance permeability and proppants concurrently placed into the fracture to retain the enhanced permeability. Here, an artificially saw-cut fractured core was prepared to evaluate the role of the fracture on permeability evolution. The fractured core was permeated using He and CO_2. Cores were

cut in half (axially) using a thin diamond coated blade to produce smooth opposing surfaces forming an idealized fracture. A uniform monolayer of 70-140 mesh proppant sand was sandwiched between the fracture surfaces to test the influence of propped fractures on permeability evolution. The cores were wrapped in aluminum foil to prevent any adsorption or diffusion of CO_2 through the rubber jacket during the permeability experiments. Surface roughness was quantified by optical profilometry both pre- and post-experimental sequences (Kumar et al., 2009; Rousseau et al., 2010).

2.2 Apparatus

A simple triaxial apparatus was used for the injection of various gases under predefined effective stress paths and the permeability measured concurrently (Figure 4.1). All experiments were completed in constant stress mode. The apparatus comprised a triaxial cell to confine the sample at prescribed stresses, an axial strain gauge to monitor the shrinkage or swelling in the axial direction, ISCO syringe pumps to apply stresses and to measure volume strains (axial and confining), pressure transducers to monitor the upstream and downstream reservoir pressures and a data acquisition system. Additional details of the equipment are described elsewhere (Kumar et al., 2012). The transient pulse test method was used to determine the permeability of the samples. The permeability was evaluated from the rate of pressure decay/gain in the upstream/downstream reservoirs (Brace et al., 1968) assuming that there was no sorption during the short duration (<10 min) experiments.
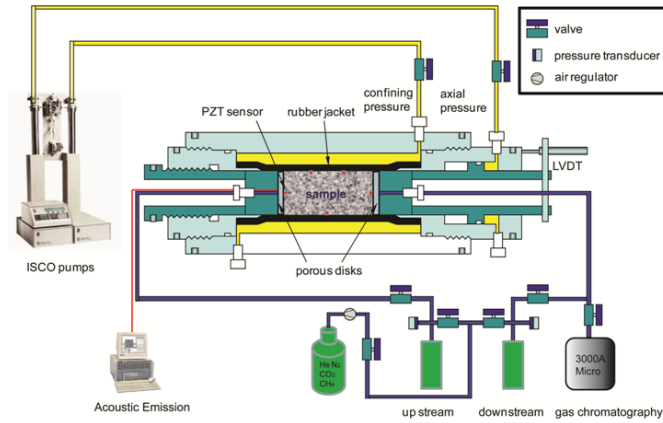
Figure 4.1: Schematic of transient pulse test permeability set-up.

2.3 Procedures

The shale cores were placed within the triaxial core holder and predefined stresses were applied. The experiments were conducted at a constant confining stress of 10 MPa (equivalent to an effective stress at ~1000 m or ~3500 feet depth). The respective roles of confining stress, deviatoric stress and sorption on the evolution permeability was explored using intact cores. The experiments consisted of sequential injection of He and CO_2. Also, a suite of experiments was conducted on saw-cut shale core, absent proppant, to explore the permeability evolution of an artificial fracture in response to injection of both inert (He) and sorbing (CO_2) gases. Table 4.1, provides the ranges of experimental variables and measured outputs.

Table 4.1: Suite of variables and prescribed ranges utilized in the experiments, for gas pressure P_p, permeability k, axial stress σ_1, confining stress σ_3, and axial strain ε_a.

Experimental Variables	Experimental Range	Measured Outputs
Temperature	Constant	N/A
Gas pressure	1 to 6 MPa	P_p
Axial stress σ_1	10,17 MPa	σ_1
Confining stress σ_3	10, 17 MPa	σ_3 ε_a
Gas type	He, CO_2	N/A

The following experimental sequence was followed for a shale sample containing a single artificial fracture under constant isotropic stress with incremental gas pressures:

1. *Non-propped fracture He permeability*: Helium was circulated in non-propped shale sample.

2. *Non-propped fracture CO_2 permeability*: The sample was permeated with CO_2 and permeability was measured by pulse test at different saturated conditions (gas pressures 1-6 MPa).

3. *Propped fracture He permeability*: The artificial fracture was propped with a monolayer of #70-140 sand. Helium was injected and the permeability was measured.

4.   *Propped fracture CO$_2$ permeability*: The sample was vented and

permeated using CO$_2$. The permeability was measured on the CO$_2$

saturated sample.

Pre- and post-experiment surface micrographs were captured using optical

interferometry. The micrographs contain surface roughness information including the

peak to pit height differential with high fidelity (resolution XX microns). The surface

micrographs were obtained pre- and post-experiments for a selected surface area

measuring 2.3 by 1.7 mm. The same core was utilized for both pre- and post-experiment

optical measurements. It is important to note that an intact sample was used to explore the

permeability evolution and then it was artificially fractured to explore permeability

evolution in the presence of this artificial fracture. The injection experiments were

repeated with the proppant-filled artificial fracture. Details of the optical profilometry

may be found elsewhere (Kumar et al., 2009).

2.4 Data Processing Methods

The transient pulse test method was utilized to evaluate shale permeability (Brace

et al., 1968). In a typical run, a shale core was packed and placed under axial and radial

stress in the triaxial apparatus as shown in Figure 4.1. A mild vacuum was applied to

evacuate the air from the combined sample and reservoir system. The core was saturated

with gas (He or CO$_2$) to an equilibrium pressure before applying a pressure pulse. A

pressure pulse was allowed to flow through the core from the upstream reservoir to the

downstream reservoir until the pressure reached equilibrium *i.e.* upstream and

downstream pressures were approximately equal. The applied pressure pulse was significantly smaller (<10%) than the initial gas pressure in the system – to avoid significantly altering effective stresses. We have assumed that there was insignificant additional adsorption with less than a 10% increment in gas pressure. The pressure loss in the upstream reservoir and pressure gain in the downstream reservoir were recorded with time. This process was repeated until the predetermined value of gas pressure was achieved. The pressure-time profile from the experiment was used to obtain permeability, k from equation 1 (Brace et al., 1968).

$$k = \frac{\gamma \cdot \mu \cdot L \cdot V_{up} V_{down}}{P_{eq} \cdot A \cdot (V_{up} + V_{down})}$$ (5)

where permeability k (m^2) is calculated from the decay parameter γ (s^{-1}) for a known gas viscosity μ (Pa.s), sample length L (m), equilibrium pressure at the end of the experiment P_{eq} (N/m^2) and cross sectional area of the specimen A (m^2) relative to upstream/downstream reservoir volumes $V_{up/down}$ (m^3), measured initial pressure $p_{up/down}{}^0$ (N/m^2) and transient upstream/downstream reservoir pressures $p_{up/down}$ (N/m$^{2.}$). The value of γ is the slope of the line obtained from a $\log\left(\frac{d(p_{up} - p_{down})}{(p_{up}{}^0 - p_{down}{}^0)}\right)$ versus time straight line plot from equation (2). This method yields a single value of permeability for a single pulse.

$$\gamma = \frac{\log\left(\frac{d(p_{up} - p_{down})}{(p_{up}{}^0 - p_{down}{}^0)}\right)_t}{dt}$$ (6)

Pressure-decay in the upstream reservoir and complementary pressure-gain in the downstream reservoir for a typical pulse test in moist coal with a non-adsorbing (He) gas

151

is shown in Figure 4.2. Pulse-decay data were reduced for $dP_o = p_{up^0} - p_{down^0}$, $dP_t = p_{up} - p_{down}$ and P_{eq}. A typical set of observations was used for the calculation of percentage error in the permeability. Further details of the analysis and error propagation may be found elsewhere (Kumar et al., 2012).

Gas slippage as quantified in the Klinkenberg effect is typically observed when the dimensions of flow channels are comparable to the mean free path of gas molecules causing the gas molecules to slip on the rock surface (Amyx et al., 1960; Klinkenberg, 1941). The observed reduction in permeability with increasing injection pressure at a constant confining stress may be attributed to slippage factor if the permeating media does not swell on exposure to the injected gas (Kumar et al., 2012; Zhu et al., 2007). The Klinkenberg slippage factor is a function of gas molecule slippage along the pore walls at low values of pore pressure (Rahmanian et al., 2010). We eliminated the possibility of the Klinkenberg effect as the size of the pores in the intact core was significantly larger than the mean free path of the gases (He and CO_2).

3 Parametric Evaluation of Permeability Evolution

Permeability experiments in shale for both He and CO_2 were carried out by injecting the gases under constant total stress of 10 MPa into intact and fractured shale cores while the gas pressures were varied within a range as given in Table 1. The following sections report observations and investigate the role of confining stress, deviatoric stress and sorption on permeability evolution in intact shale core, shale core containing artificial fracture and shale core containing propped artificial fracture.

152

3.1 Confining Stress

The shale core was permeated with He and gas pressures incremented under constant isostatic stresses of 10 MPa, 15 MPa and 20 MPa to measure the permeability. The confining stress was increased in steps by the injection of fluid into the triaxial cell (Figure 4.1). Shale permeability may vary with transitions in stress pathways (Dong et al., 2010). The axial and confining stresses were increased simultaneously and at the same rate in an effort to retain deviatoric stress relatively constant during loading. The permeability increased with gas pressure at all constant confining stresses (Figure 4.2). This is consistent with the opening of microfractures as effective stress decreases in an intact shale core. For example, the increase in permeability was ~15% as the gas pressure was increased from 1 MPa to 6 MPa at a constant confining stress of 10 MPa. Similar observations were made at higher confining stresses of 15 MPa and 20 MPa (Figure 4.2). These observations were consistent with shale permeability evolution data reported by others (Cho et al., 2012; Dong et al., 2010; Soeder, 1988).
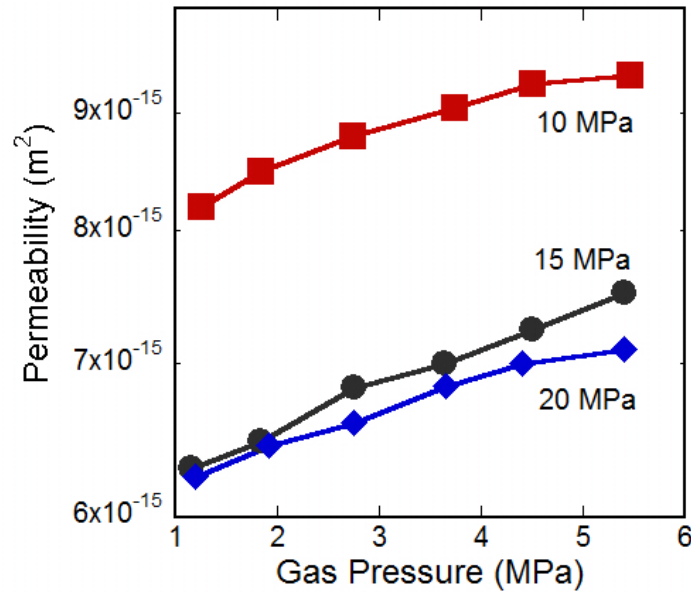
Figure 4.2: The permeability evolution of intact shale sample *A* on injection of helium at constant confining stresses of 10 MPa, 15 MPa and 20 MPa.

3.2 Sorptive Gas Injection

The role of gas sorption on shale permeability evolution was investigated by injecting CO_2 into the intact core at constant confining stress of 10 MPa (Figure 4.3). A reduction in permeability was observed with an increase in gas pressure for both low density (sample A) and high density (sample B) shale. The permeability at 1 MPa was approximately double the minimum permeability observed at ~4 MPa in sample A. However, the permeability reduction in sample B was relatively small (~20%) with a change in gas pressure from 1 MPa to 4 MPa. It is notable that the magnitudes of permeability reduction were different for two samples which may be attributed to their compostional (organic matter, clay, heavy minerals) and lithologic differences.

This permeability reduction was the result of the dominant swelling response of the organic component of the organic-rich shale relative to the dilation of natural fractures. This occurs for gas pressures below approximately double the Langmuir pressure. At gas pressures above this double-Langmuir threshold permeability reduction halted and the permeability then increased (Kumar et al., 2010). These findings are consistent with observations of permeability evolution concurrent with injection of a sorbing gas (CH_4) in a gas shale sample collected from Alberta, Canada (Letham, 2011). Similar behavior is also reported for various coals upon injection of CH_4 and CO_2 (Kumar et al., 2012; Pini et al., 2009; Wang et al., 2012). The permeability of the low-density sample was one-hundred times larger than that of the high-density shale sample. However, the behavior exhibited by both samples upon injection of CO_2 was similar (Figure 4.3). The sample was evacuated using a mild vacuum at the completion of the CO_2 permeability test and He was injected to evaluate the post CO_2 flow permeability of the core. The He permeability after the CO_2 flow was a fraction of the original He permeability (not shown). The He permeability partly recovered as the desorption of CO_2 continued with He injection. These observations are analogous to the permeability evolution in bituminous coal (Kumar et al., 2012).
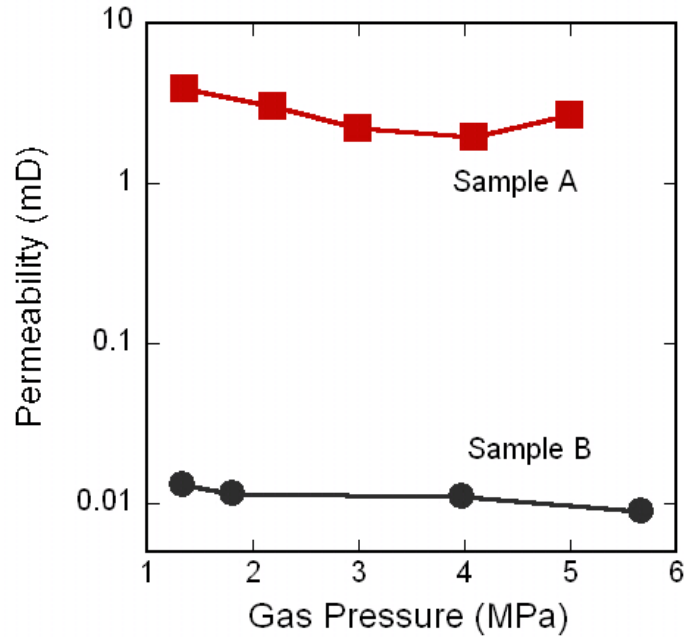
Figure 4.3: The permeability evolution in two shale samples (A and B) on injection of CO_2. The observations were made in the order of incremental gas pressures at constant confining stress of 10 MPa.

3.3 Non-propped and propped artificial fracture

The shale sample with an artificial fracture was permeated with He and CO_2 and the permeability evolution determined for the idealized non-propped and propped fracture. A monolayer of the proppant was laid as uniformly as possible on the surface of the shale and the permeability of the propped artificial fracture determined. The permeability evolution was measured at a constant confining stress of 10 MPa with varying gas pressures (Figure 4.4). The He permeability of the propped fracture was ~2-3 times higher than that of the non-propped fracture (Figure 4.4). The permeability of the artificial fracture increased exponentially with decreasing effective stress in both non-

156

propped and propped cases. The permeability increased by ~30% in the non-propped

fracture compared to ~100% in the propped fracture with gas pressure increasing from ~1

to ~5 MPa. The rate of change of permeability with gas pressure was greater in the

propped fracture relative to that in non-propped fracture (Figure 4.4). The permeability

evolution in non-propped and propped artificial fractures in bituminous and anthracite

coal is known to exhibit similar behavior (Kumar et al., 2012).

The CO_2 permeability evolution of non-propped and propped artificial fractures in

shale was next evaluated. The CO_2 permeability of the non-propped fracture increased

with an increase in gas pressure (Figure 4.4). The increase in permeability of the propped

fracture was as high as ~5 fold that of the non-propped fracture depending upon the

conditions under which permeability was evaluated. Interestingly, the permeability

evolution in the propped fractures exhibited behavior similar to that of intact coal (Kumar

et al., 2012). The permeability evolution of the propped fracture in shale upon injection

of CO_2 is shown in Figure 4.4. Although, the permeability evolution for this sample did

not show the typical "U-shaped" response of permeability versus gas pressure (Figure

4.4) observed in our other work (not shown here) this is likely specific to this particular

sample and under these specific conditions (Kumar et al., 2010).
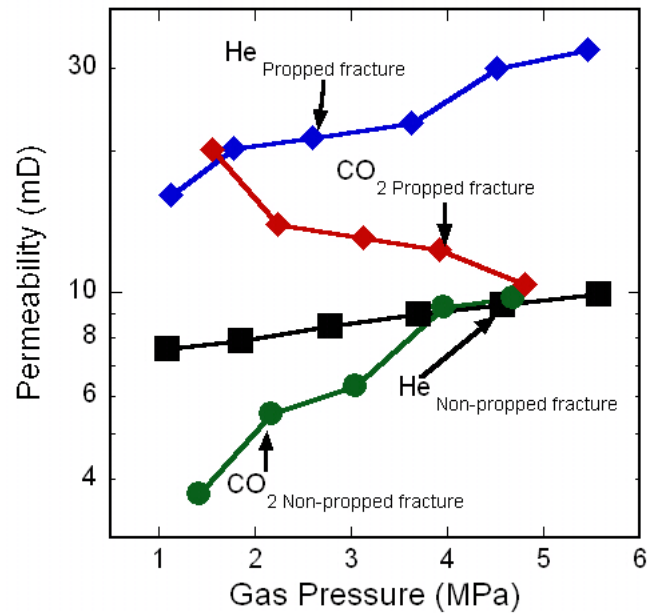
Figure 4.4: The permeability evolution of non-propped and propped fracture on injection of He and CO_2. The gas pressure is augmented to higher values at constant confining stress of 10 MPa. The curves are indicated in the figure.

3.4 Observations with white light optical

White light optical profilometry was utilized to quantify and characterize the surface of the shale both pre- and post-experimental sequences. The advanced facility of optical profilometry allowed capture of a significant portion of the features on the fracture surface even in the absence of a reflective surface. High magnification three dimensional surface micrographs (~300) were acquired and stitched together to obtain a micrograph covering a 2.3 mm × 1.7 mm patch. Surface characteristics were compared both before and after the experimental suite.

Deep and wide interconnected pores were uniformly distributed on the shale fracture surface (Figure 4.5a). The permeability of the intact shale sample was in the range 1-10 mD (Figure 4.2) also indicating a well-developed interconnected pore-network. In the micrographs, feature height is color-coded using false-coloring. Elevated features are shown in bright colors with depressions in dark colors. Changes in surface topography are evident in the surface after the experimental suite (Figure 4.5). The surface roughness and peak-to-valley differential for the fracture surface is 4.1μm and 77.9μm before the experiments and increases to 6.1μm and 122.4μm after. We hypothesize that the smooth surface of the fracture is indented by the proppant particles that creates small pits that in turn result in increased surface roughness and peak-to-valley differential. This in turn reduces the effective fracture aperture and concomitantly reduces the permeability

a   b
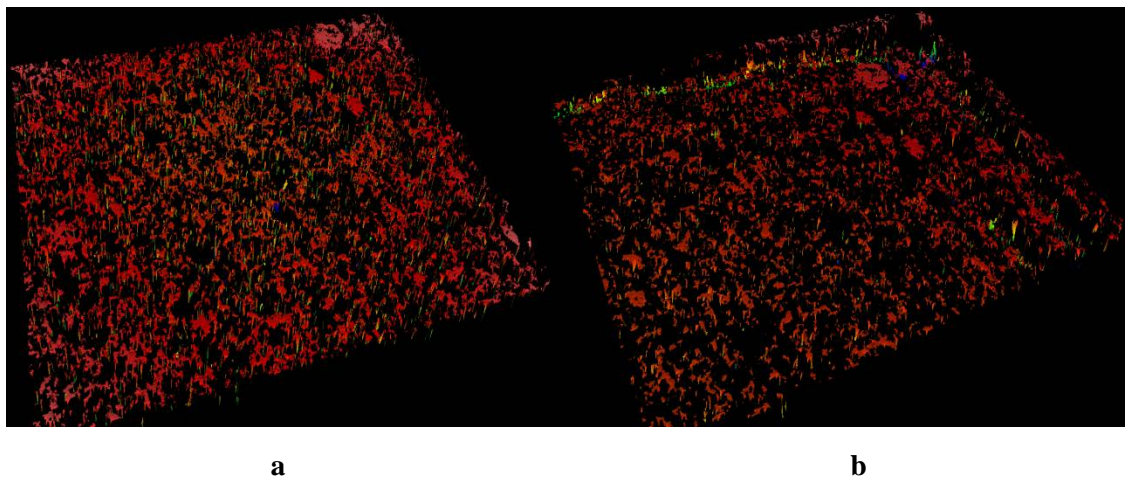
Figure 4.5: The aerial view of shale surface a) before (left) b) after (right) the experiment. The features are falsely colored according to their height. The vertical

features are highly exaggerated (on the order of several microns) and are falsely colored. The red color represents highest elevated part while blue shows the depressed features on the surface. The black regions indicate poorly reflecting deep pits which receives/sends poor signals during profilometer scanning. The region of interest shown is 2.3 x 1.7 mm (i.e the vertical and horizontal scales differ by several orders of magnitude)

4 Utilizing Mechanistic Models Reported for Coal in Shale

There are several models for permeability evolution in coal. They may be divided between strain based, stress based and empirical models (Palmer, 2009). Here we adapt a stress-based mechanistic model describing permeability evolution in coal (Kumar et al., 2012) to explore permeability evolution in shale upon injection of a sorbing gas. Furthermore, we used a mechanistic model, developed for permeability evolution in propped artificial fractures in coal (Kumar et al., 2013) to explain similar permeability observations in artificially fractured shale.

4.1 Permeability evolution in intact shale core

The evolution of permeability upon injection of CO_2 in various rank of coals is observed to vary with stress, pressure and moisture content (Kumar et al., 2012). These represent the principal features that impact permeability evolution in swelling media (e.g. equation (3)).

$$\frac{k}{k_0} = \left\{ \left(1 + \frac{C.p}{p+P_L}\right)^3 + e^{-\beta\sigma'} \right\} * e^{-\delta S_w} \tag{3}$$

160

where permeability k, initial permeability k_0, gas pressure p, Langmuir pressure P_L and assumed fitting constant C, effective stress σ', moisture content S_w and scaling parameters β and δ define the response. The scaing parameter C is defined as $C = \left(\frac{\varepsilon_L s^2}{ab_0} \right)$ where initial fracture aperture b_0, fracture length a, fracture spacing s, and peak Langmuir strain ε_L, represent the response. We have applied this mechanistic model to describe permeability observations that result upon injection of CO_2 in the two shale samples (A & B) used for this study. The fitting parameters for C, P_L, β and δ in this model are strain index, Langmuir pressure, stiffness index and interaction index, respectively. The shale samples used for this study were dry therefore the water content $(S_w \cong 0)$ is assumed to be zero. This assumption eliminates one parameter (δ) in the model. The remaining parameters $(C, P_L, \beta$ and) are recovered using an optimization against the permeability observations. The details of the optimization may be found elsewhere (Kumar et al., 2012).

The normalized permeability evolution data upon injection of CO_2 in intact shale samples (A & B) is shown (Figure 4.6). The normalizing factor used for these observations is the base magnitude of He permeability at null confining stress *i.e.* k_0. The values of k_0 were 1.09×10^{-14} m^2 and 3.16×10^{-17} m^2 for samples A and B, respectively. The goodness of fit was 92.1% and 86.6% for sample A and B indicating that the trend predicted by the proposed model demonstrated acceptable fits to the experimental values (Figure 4.6). The values of the fitting parameters are shown in Table 4.2. The absence of CO_2 adsorption and swelling induced strain measurement data on Pennsylvanian shale

restrict us from any direct parametric comparison. However, we present the congruence of fitting parameters below.

1. **Parameter *C***: The Langmuir strain may be expressed as $\varepsilon_L = \left(\frac{Cab_0}{s^2}\right)$. The larger values of C indicate higher values of maximum swelling induced strain (ε_L). The swelling induced strain in sample A (lower density shale) was ~3 fold that of sample B (higher density shale) if other parameters (a, b_0 and s) were assumed to be same for the two samples. This may be attributed to the higher organic matter content of sample A compared to sample B.

2. **Parameter *P_L***: Langmuir pressures P_L for samples A and B were 3.0 MPa and 0.5 MPa, respectively. Minimum permeability occurs at ~3.5 MPa for sample A while sample B did not show a point of inflexion in the observed gas pressure range.

3. **Parameter *β***: The parameter β for sample B was ~10-15 fold that of sample A. This indicates that sample B is stiffer than the sample A. Consequently, the permeability of sample B is less affected by changes in effective stresses. These findings are consistent with the permeability observation made above.

It is important to note that the variation in values of the parameters (P_L and ε_L) may yield different production characteristics.
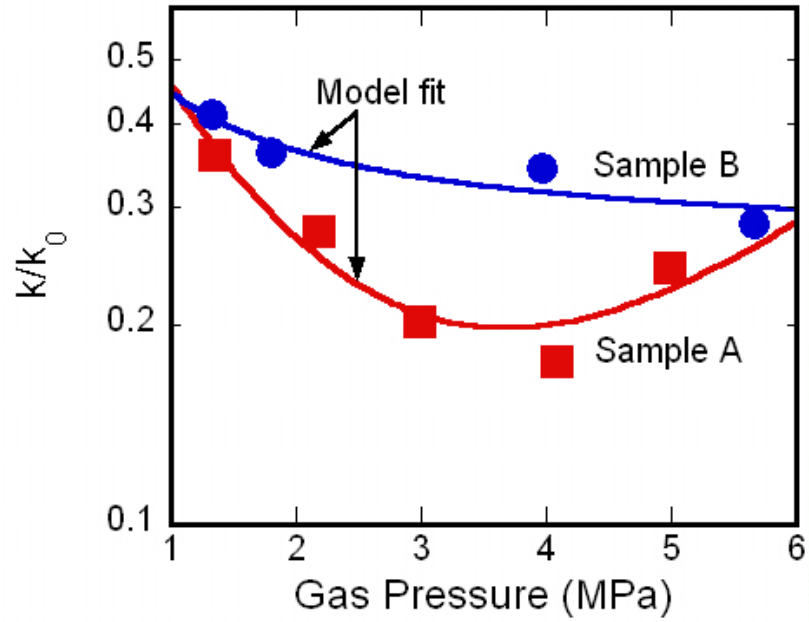
Figure 4.6: Analytical fits to the mechanistic model for the observations of permeability evolution upon injection of CO_2 in the two intact shale samples. The low-pressure portion (<3.5 MPa) of the curve is dominated by swelling response while the high-pressure portion (>3.5 MPa) is dominated by dilation promoted by diminishing effective stresses.

Table 4.2: Typical value of the fit parameters. See text for the definition of fit parameters.

Sample	Fit Parameters		
	C	P_L	β
A	1.02	3.00	0.34
B	0.36	0.53	4.99

4.2 Permeability evolution of propped artificial fracture in shale core

A mechanistic model for permeability evolution in a propped artificial fracture in coal is applied to represent the response in shale. This model assumes that the proppant grains act as "bridges" that partially embed into the shale matrix. Correspondingly, the permeability of a propped artificial fracture is much higher than the shale matrix but also much more sensitive to changes in pressure. This is because the void volume available for flow (CO_2) is modulated with both overburden stress and swelling, with this in turn affecting the permeability. The details of the model can be found elsewhere (Kumar et al., 2013).

The embedded height (h_1) of a hard sphere (proppant) pressed against a flat surface (shale fracture surface) can be represented as,

$$h_1 = R\left(1 - \sqrt{1 - \frac{\sigma'}{\pi c}}\right). \quad (4)$$

Here R is the radius of the proppant grain, σ' is the effective stress and c is the cohesive strength of the shale. The total volume V_1 of the proppant grain embedded into the two fracture surfaces can be evaluated as,

$$V_1 = 2\frac{1}{3}\pi h_1^2 (3R - h_1). \quad (5)$$

Considering a cubical unit of shale of side *2R* containing a proppant grain. The volumetric strain developed in this unit due to sorption-induced swelling may be written as,

$$\Delta V = \alpha \varepsilon_L \left(\frac{P}{P + P_L} \right) (2R)^3 \quad . \quad (6)$$

Here ΔV is the volumetric strain developed through swelling, α is an arbitrary shape factor, P is the gas pressure present within the fracture and P_L is the Langmuir pressure.

If h_2 is the resultant new embedded height due to the combined effects of stress and swelling then the change in embedded volume can be represented as,

$$2\frac{1}{3}\pi h_2^2 \left(3R - h_2^2 \right) = V_1 + \Delta V \quad (7)$$

or

$$2\frac{1}{3}\pi h_2^2 \left(3R - h_2^2 \right) = 2\frac{1}{3}\pi h_1^2 \left(3R - h_1 \right) + \alpha \varepsilon_L \left(\frac{P}{P + P_L} \right) (2R)^3 \quad . \quad (8)$$

Thus the new embedded height h_2 can be evaluated from equation (8). The effective aperture of the fracture, b, at any point during the varying of pore pressure at constant confining stress can be written as,

$$b = 2R - 2h_2 = b_0 - \Delta b \quad (9)$$

where b_0 is the initial fracture aperture.

Thus, the change in aperture of the fracture Δb driven by these processes may be represented as,

$$\Delta b = -2\Delta h_2 \quad . \quad (10)$$

For the cases where bulk in situ permeability k_0 is known at fracture aperture b_0 then the permeability evolution with change in aperture can be evaluated (Liu et al.,

165

1997). This allows the evolution of fracture permeability to be followed for an arbitrary evolution of fracture aperture (Elsworth and Goodman, 1986; Piggott and Elsworth, 1993). It is assumed that flow occurs in the fractures only. The permeability of the fracture, k, is modulated based upon its initial permeability, k_0, as,

$$\frac{k}{k_0} = \left(1 + \frac{\Delta b}{b_0}\right)^3.$$ (11)

This formulation allows the evolution of normalized permeability to be represented with the change in fracture aperture as a combined response to both normal stress and sorptive gas pressure in the fractured core. The arbitrary shape factor (α) and cohesive strength (c) of shale are evaluated from the best fit as indexed by the coefficient of correlation (R^2). As noted in section 4.1, the magnitudes of the Langmuir strain and Langmuir pressure are 1.5% and 4MPa respectively. The initial permeability (k_0) and fracture aperture (b_0) are chosen from the first point of observation in the permeability experiments and the MATLAB® curve fit toolbox used to optimize the values of the parameters α and c. The values predicted from curve fitting for α and c are 2 and 10 MPa. Unfortunately, no direct comparison of cohesive strength values can be made due to absence of any published data for the cohesive strength of these shales however the value of c lies within the expected values reported elsewhere (Chen et al., 2003).
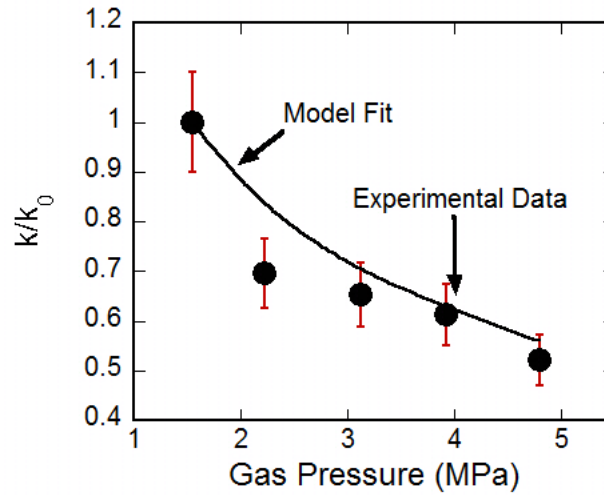
Figure 4.7: The evolution of permeability in a propped fracture in shale upon injection of sorbing gas CO_2. Uncertainty in the permeability magnitude is within $\pm 10\%$ as indicated by error bars. The model fit is shown by the solid line.

5 Conclusions

Experimental measurements of permeability evolution are reported for shale cores infiltrated by He and CO_2. The permeability was measured under various confining stresses (10, 15 and 20 MPa) and gas pressures of non-sorbing (He) and sorbing gas (CO_2). The permeability evolution was explored for non-propped and propped artificial fracture in the shale core by injecting both sorptive and non-sorptive gases at prescribed and constant confining stresses. Optical profilometery was used to quantify the change in surface roughness of the fracture resulting from proppant indentation. The observed evolution of permeability in shale is compared with similar observations for coal. A mechanistic model for permeability evolution developed for coal is successfully applied

to permeability observations collected for shale. The following conclusions are drawn from this study.

1. The He-permeability of shale increases with gas pressure at constant confining stress. The He-permeability increases by ~15% as the gas pressure is varied from 1 MPa to 6 MPa at a constant confining stress of 10 MPa. The permeability decreases with confining stress (10 MPa >15 MPa >20 MPa).

2. The adsorption of CO_2 in shale may reduce the permeability by a factor of two, The permeability may reset to the original magnitude if sufficient time is allowed for the sample to release the sorptive gas.

3. The permeability of shale decreases with gas (CO_2) pressure and the reduction in permeability with gas pressure halts at a critical pressure corresponding to the point at which maximum adsorption is achieved. Beyond this pressure threshold (~double the Langmuir pressure) the permeability increases as a consequence of elevated influence of the diminishing effective stress corresponding to a typical "U-shaped" form of permeability with gas pressure (Kumar et al., 2013).

4. The He-permeability of the propped fracture increases ~2-3 fold that of the non-propped fracture. The He-permeability increases with gas pressure at a constant confining stress. The CO_2-permeability of the propped fracture may decrease by as much as a factor of two as the gas pressure is increased from 1 MPa to 4 MPa at constant confining stress. However, the permeability of the non-propped fracture increases with gas pressure.

5. The surface roughness and peak-to-valley differential for the fracture surface are 4.1 μm and 77.9 μm, respectively, before the experiments and increase to 6.1 μm and

122.4 μm at the conclusion of the experimental suite, indicating the significant influence of proppant indentation on the fracture surface.

6. Permeability evolution trends in shale are shown to be comparable with those for other sorbing media – such as coal. Correspondingly, permeability evolution models developed for coal may be utilized to both explain and to quantify permeability evolution in shale. An excellent match exists between experimental data and the model for intact, non-propped fractured and propped fractured shale cores.

Table 4.3: Factors influencing permeability evolution in high organic content and high swelling materials (e.g. coal) relative those influencing the response of lower organic content shales.

Type	Coal-Gas	Shale-Gas
Relative carbon content	High	Low
Bound gas content	Low	High
Sorptive strains	High	Low
Fracture network geometry	Small spacing	Large spacing
Comparative permeability	High/Open fractures	Low/Tight fractures
Permeability sensitivity to deformation	Low	High
Linkage: Permeability-to-sorption	Significant	Significant
Stiffness	Low	High
Strength	Low	High

The surprisingly significant influence of swelling strains on the evolution of permeability in both non-propped and probed fractures is surprising, when considering

the low mass percentage of organic material present in shales (<20%) relative to coals

(>90%). Since sorption-induced changes in permeability result from the swelling strains

induced within the organic fraction, their magnitude should scale with the organic

fraction. A reduced mass-based fraction of organic material, and hence reduced

magnitude of induced strain, may still result in a significant change in permeability if

both the initial permeability of the shales low and the initial fracture spacing is high –

both in relation to high organic fraction coals – as noted in Table 3. As fracture spacing

increases, the scaled swelling displacement resulting from a given uniform strain, but

concentrated onto a single fracture (Δb), increases. Thus, the resulting change in

permeability that scales as $k/k_0 \sim (1 + \Delta b/b_0)^3$ may still be significant even if the

magnitude of the swelling strain (ϵ_L) is significantly smaller in shale than in coal.

5 References

Amyx, J.W., Bass, D.M., Whiting, R.L., 1960. Petroleum Reservoir Engineering:Physical Properties. New York : McGraw-Hill.

Arthur, J.D., Bohm, B., Layne, M., 2008. Hydraulic Fracturing Considerations for Natural Gas Wells of the Marcellus Shale, The Ground Water Protection Council, 2008 Annual Forum, Cincinnati, Ohio.

ASTM International D7582, 2010. Standard test methods for proximate analysis of coal and coke by macro thermogravimetric analysis. IHS, Pennsylvania.

Bai, M., Roegiers, J.-C., Elsworth, D., 1995. Poromechanical response of fractured-porous rock masses. Journal of Petroleum Science and Engineering 13, 155-168.

Boyer, C., Kieschniek, J., 2010. Producing gas from its source, Oilfiled Review Schlumberger.

Brace, W.F., Walsh, J.B., Frangos, W.T., 1968. Permeability of granite under high pressure. Journal of Geophysical Research 73, 2225-2236.

Bruner, K.R., Smosna, R., 2011. A comparative study of the Mississippian Barnett Shale, Fort Worth Basin, and Devonian Marcellus Shale, Appalachian Basin, in: Soeder, D.J. (Ed.). US-DOE.

Bustin, R.M., Cui, X., Chikatamarla, L., 2008. Impacts of volumetric strain on CO_2 sequestration in coals and enhanced CH_4 recovery. AAPG Bulletin 92, 15-29.

Cho, Y., Ozkan, E., Apaydin, O.G., 2012. Pressure-Dependent Natural-Fracture Permeability in Shale and its Effect on Shale-Gas Well Production, SPE Annual

Technical Conference and Exhibition. Society of Petroleum Engineers, San Antonio, Texas, USA.

Cui, X., Bustin, R.M., Chikatamarla, L., 2007. Adsorption-induced coal swelling and stress: Implications for methane production and acid gas sequestration into coal seams. J. Geophys. Res. 112, B10202.

Curtis, J.B., 2002. Fractured Shale-Gas Systems. AAPG Bulletin 86, 1921-1938.

Day, S., Fry, R., Sakurovs, R., Weir, S., 2010. Swelling of coals by supercritical gases and its relationship to sorption. Energy & Fuels 24, 2777-2783.

Dong, J.-J., Hsu, J.-Y., Wu, W.-J., Shimamoto, T., Hung, J.-H., Yeh, E.-C., Wu, Y.-H., Sone, H., 2010. Stress-dependence of the permeability and porosity of sandstone and shale from TCDP Hole-A. International Journal of Rock Mechanics and Mining Sciences 47, 1141-1157.

Durucan, S., Edwards, J.S., 1986. The effects of stress and fracturing on permeability of coal. Mining Science and Technology 3, 205-216.

Durucan, S., Shi, J.-Q., 2009. Improving the CO2 well injectivity and enhanced coalbed methane production performance in coal seams. International Journal of Coal Geology 77, 214-221.

Fathi, E., Akkutlu, I., 2009. Matrix heterogeneity effects on gas transport and adsorption in coalbed and shale gas reservoirs. Transport in Porous Media 80, 281-304.

Gash, B.W., Volz, R.F., Potter, G., Corgan, J.M., 1993. In The effect of cleat orientation and confining pressure on cleat porosity, permeability and relative permeability in coal, International Coalbed Methane Conference, University of Alabama, Tuscaloosa, Alabama, pp. 247-255.

Harpalani, S., Chen, G., 1995. Estimation of changes in fracture porosity of coal with gas emission. Fuel 74, 1491-1498.

Harpalani, S., Schraufnagel, R.A., 1990. Shrinkage of coal matrix with release of gas and its impact on permeability of coal. Fuel 69, 551-556.

IPCC, 2005. Special report in carbon dioxide capture and storage, Cambridge.

Jenkins, C.D., Boyer II, C.M., 2008. Coalbed- and Shale-Gas Reservoirs. SPE Journal of Petroleum Technology 60.

Kang, S.M., Fathi, E., Ambrose, R.J., Akkutlu, I.Y., Sigal, R.F., 2011. Carbon dioxide storage capacity of organic-rich shales. SPE Journal 16, pp. 842-855.

Kelemen, S.R., Kwiatek, L.M., 2009. Physical properties of selected block Argonne Premium bituminous coal related to CO_2, CH_4, and N_2 adsorption. International Journal of Coal Geology 77, 2-9.

Kiyama, T., Nishimoto, S., Fujioka, M., Xue, Z., Ishijima, Y., Pan, Z., Connell, L.D., 2011. Coal swelling strain and permeability change with injecting liquid/supercritical CO_2 and N_2 at stress-constrained conditions. International Journal of Coal Geology 85, 56-64.

Klinkenberg, L.J., 1941. The Permeability Of Porous Media To Liquids And Gases. American Petroleum Institute, pp. 200-213.

Kumar, H., Elsworth, D., Liu, J., Pone, D., Mathews, J.P., 2012. Optimizing enhanced coalbed methane recovery for unhindered production and CO_2 injectivity. International Journal of Greenhouse Gas Control 11, 86-97.

Kumar, H., Elsworth, D., Liu, J., Pone, D., Mathews, J.P., 2013. A mechanisic model for permeability evolution of propped artificial fracture in coals. In preparation.

173

Kumar, H., Elsworth, D., Marone, C.J., Mathews, J., 2010. Permeability evolution of shale and coal under differential sorption of He, CH4 and CO2, American Geophysical Union, Fall Meeting 2010, San Francisco.

Kumar, H., Pone, J.D.N., Mitchell, G.D., Halleck, P.M., Mathews, J.P., 2009. In Lithotype influences on (an idealized) coal cleat surface deformation by carbon dioxide induced coal swelling, International Coalbed Methane and Oil Shale Symposium, Tuscaloosa, Alabama.

Laubach, S.E., Marrett, R.A., Olson, J.E., Scott, A.R., 1998. Characteristics and origins of coal cleat: A review. International Journal of Coal Geology 35, 175-207.

Letham, E.A., 2011. Matrix permeability measurements of gas shales: gas slippage and adsorption as sources of systematic error, Geological Science, Vancouver.

Loucks, R.G., Reed, R.M., Ruppel, S.C., Jarvie, D.M., 2009. Morphology, genesis and distribution of nanometer-scale pores in Siliceous mudstones of the Mississippian Barnett shale Journal of Sedimentary Research 79, 848-861.

Mastalerz, M., He, L., Melnichenko, Y.B., Rupp, J.A., 2012. Porosity of Coal and Shale: Insights from Gas Adsorption and SANS/USANS Techniques. Energy & Fuels 26, 5109-5120.

Min, K.-B., Rutqvist, J., Elsworth, D., 2009. Chemically and mechanically mediated influences on the transport and mechanical characteristics of rock fractures. International Journal of Rock Mechanics and Mining Sciences 46, 80-89.

Nuttall, B.C., 2010. Reassessment of CO2 sequestration capacity and enhanced gas recovery potential of middle and upper Devonian black shales in the Appalachian

Basin, MRCSP Phase II Topical Report. Kentucky Geological Survey, Lexington, Kentucky, pp. 1-48.

Nuttall, B.C., Eble, C.F., Drahovzal, J.A., Bustin, A.M.M., 2005. Analysis of Devonian black shales in Kentucky for potential carbon dioxide sequestration and enhanced natural gas production. Kentucky Geological Survey, Lexington, Kentucky.

Palmer, I., 2009. Permeability changes in coal: Analytical modeling. International Journal of Coal Geology 77, 119-126.

Pellenq, R.J.-M., Brochard, L., Damme, M.V., Ulm, F.-J., 2012. From the Fundamentals of Porous Carbons Poromechanics to Applications for CO2 Sequestration and Gas-Shale AIChE, Pittsburgh.

Perez, E., Kaproth, B.M., Haines, S., Saffer, D., 2010. Laboratory measurements of permeability reduction in naturally occurring shear bands formed in unlithified sands, 106th Annual Meeting, and Pacific Section, American Association of Petroleum Geologists. Geological Society of America Anaheim, California, p. 84.

Pini, R., Ottiger, S., Burlini, L., Storti, G., Mazzotti, M., 2009. Role of adsorption and swelling on the dynamics of gas injection in coal. J. Geophys. Res. 114, B04203.

Pone, J.D.N., Halleck, P.M., Mathews, J.P., 2010. 3D characterization of coal strains induced by compression, carbon dioxide sorption, and desorption at in-situ stress conditions. International Journal of Coal Geology 82, 262-268.

Rahmanian, M.R., Solano, N., Aguilera, R., 2010. Storage and output flow from shale and tight gas reservoirs, SPE Western Regional Meeting. Society of Petroleum Engineers, Anaheim, California, USA.

Reucroft, P.J., Patel, H., 1986. Gas-induced swelling in coal. Fuel 65, 816-820.

Sakhaee-Pour, A., Bryant, S., 2012. Gas permeability of shale. SPE Reservoir Evaluation & Engineering 15, pp. 401-409.

Seidle, J.P., Jeansonne, M.W., Erickson, D.J., 1992. Application of matchstick geometry to stress dependent permeability in coals, SPE Rocky Mountain Regional Meeting. SPE, Casper, Wyoming.

Seidle, J.R., Huitt, L.G., 1995. Experimental measurement of coal matrix shrinkage due to gas desorption and implications for cleat permeability increases, International Meeting on Petroleum Engineering. Society of Petroleum Engineer.

Shi, J.-Q., Durucan, S., 2010. Exponential Growth in San Juan Basin Fruitland Coalbed Permeability With Reservoir Drawdown: Model Match and New Insights. SPE Reservoir Evaluation & Engineering 13, pp. 914-925.

Siemons, N., Busch, A., 2007. Measurement and interpretation of supercritical CO_2 sorption on various coals. International Journal of Coal Geology 69, 229-242.

Soeder, D.J., 1988. Porosity and Permeability of Eastern Devonian Gas Shale. SPE Formation Evaluation 3, 116-124.

Soeder, D.J., 2011. Petrophysical characterization of the Marcellus & other gas shales, AAPG Eastern Section Meeting. NETL, US-DOE, Arlington, Virginia.

Somerton, W.H., Söylemezoglu, I.M., Dudley, R.C., 1975. Effect of stress on permeability of coal. International Journal of Rock Mechanics and Mining Sciences & Geomechanics Abstracts 12, 129-145.

van Bergen, F., Pagnier, H., Krzystolik, P., 2006. Field experiment of enhanced coalbed methane-CO_2 in the upper Silesian basin of Poland. Environmental Geosciences 13, 201-224.

Veatch, R.W.J., Moschovidis, Z.A., Fast, C.R., 1989. An Overview of Hydraulic Fracturing-Recent Advances in Hydraulic Fracturing. Society of Petroleum Engineers.

Wang, F.P., Reed, R.M., 2009. Pore networks and fluid flow in gas shales, SPE Annual Technical Conference and Exhibition. Society of Petroleum Engineers, New Orleans, Louisiana.

Wang, S., Elsworth, D., Liu, J., 2011. Permeability evolution in fractured coal: the roles of fracture geometry and water content. International Journal of Coal Geology 87, 13-25.

Wang, S., Elsworth, D., Liu, J., 2012. A mechanistic model for permeability evolution in fractured sorbing media. J. Geophys. Res. 117, B06205.

White, C.M., Smith, D.H., Jones, K.L., Goodman, A.L., Jikich, S.A., LaCount, R.B., DuBose, S.B., Ozdemir, E., Morsi, B.I., Schroeder, K.T., 2005. Sequestration of Carbon Dioxide in Coal with Enhanced Coalbed Methane RecoveryA Review, Energy & Fuels 19, 659-724.

Zhang, J., Scherer, G.W., 2012. Permeability of shale by the beam-bending method. International Journal of Rock Mechanics and Mining Sciences 53, 179-191.

Zhu, W.C., Liu, J., Sheng, J.C., Elsworth, D., 2007. Analysis of coupled gas flow and deformation process with desorption and Klinkenberg effects in coal seams. International Journal of Rock Mechanics and Mining Sciences 44, 971-980.

Chapter 5 : Summary and Conclusions

This study was a step to understand the permeability evolution in sorbing media such as coal and shale. The permeability evolution laboratory experiments were conducted on naturally fractured and artificially fractured cylindrical samples of various ranks coal and shale. The samples at various were infiltrated with helium, methane and carbon dioxide at various gas pressures under constant confining stress. The mechanistic models were developed for the predictions of permeability evolution under the experimental conditions. A finite element coupled reservoir simulator was developed to investigate the permeability evolution, permeability variability, methane production and CO_2 fractions in the reservoir during its life. Also, the permeability evolution was studied for non-propped and propped artificial fractured in coal and a mechanistic model was proposed to predict the permeability evaluation. Similar experiments are repeated for organic low density shale from Pennsylvania. The mechanistic models developed for coals were successfully utilized to predict the permeability in shale. The key conclusions from this study are following:

1. The permeability of a bituminous coal modulates as a function of effective stress, sorptive gas pressure and moisture saturation. A mechanistic model developed in this work successfully predicts the permeability evolution. An optimized injection schedule which prevents the permeability reduction during CO_2-ECBM is explored.

2. The results from finite element model indicate that the injection of CO_2 in coalbed reservoir increases its production. Although, the injection of CO_2 at

higher pressures yields highest production and maximum injectivity but the production stream contains higher mole fractions of CO_2 compared to low pressure or no CO_2-injection scenario. The injection of CO_2 in a heterogeneously permeable reservoir reduces its permeability variability with time as indicated by coupled reservoir simulations.

3. The permeability of artificially fractured coal increases with injection pressure (helium and carbon dioxide) on constant confining stress. The permeability of the artificial increases significantly compared to non-propped fracture if a monolayer of proppant is sandwiched in the fracture. The evolution of permeability in propped artificial fracture can be explained by a mechanistic model developed here. The reduction in permeability of propped artificial fracture is caused by swelling.

4. The permeability evolution in organic shale on injection of helium and carbon dioxide trends alike coal and the mechanistic models developed for coal may be applied for the prediction of permeability evolution in shale.

This study recommends potential areas for future research which are as following

1. The recovery of methane from a saturated core in the presence of varying moisture/water saturations may vary on injection of CO_2. The injection rate, gas type, water saturation, applied stresses and temperature should be investigated for exploring ultimate recovery.

2. Non-ideality of gases at higher pressure and non-isothermal conditions in the reservoir may change the recovery therefore needs investigation. A three

dimensional finite element may better represent the permeability

heterogeneity therefore it should be utilized for simulations.

3. The permeability evolution in propped artificial fractures may depend upon

size, shape and crushing-strength proppant and its placement in the fracture

therefore needs further investigation.

HEMANT KUMAR

Nationality:	India
Birth Details:	July 1, 1984, Mathura, Uttar Pradesh, India
Address:	411 Waupelani Drive B215 State College, PA, 16801
Electronic:	kumarhemant@live.com

EDUCATION

2010-2014	Ph.D. in Energy and Mineral Engineering with option in Petroleum and Natural Gas Engineering, Penn State University, USA
2008-2010	M.S. in Energy and Mineral Engineering, Penn State University, USA
2001-2004	B.Tech. in Mining Engineering, Indian Institute of Technology-Banaras Hindu University (IIT-BHU), Varanasi, India

SELECT AWARDS

2007	Undergraduate Merit Award in Mining Engineering, IIT-BHU

PROFESSIONAL DETAILS

2011	Reservoir Engineer, Internship, ExxonMobil Upstream Research Centre, Houston, TX, USA
2008	Technical Services Engineer, Orica Mining Services, Kolkata, India
2007	Associate Software Engineer, Covansys India Pvt. Ltd., Chennai, India

RESEARCH INTERESTS

Mathematical Modeling, Reservoir Simulation and Experimental Studies on flow and transport response of fractured sorbing media with applications to coal and shale gas reservoir, enhanced gas recovery and carbon sequestration.

PUBLICATIONS

Select Articles

1. Kumar, H., Elsworth, D., Mathews, J.P., Marone, C., 2013. Permeability evolution analogies in sorbing media: An example from coal and shale. In preparation to Geofluids.
2. Kumar, H., Elsworth, D., Liu, J., Pone, D., Mathews, J.P., 2013. A mechanisic model for permeability evolution of propped artificial fracture in coals. In preparation to Journal of Petroleum Science and Engineering.
3. Kumar, H., Elsworth, D., Liu, J., Pone, D., Mathews, J.P., 2013. Effect of CO_2 injection on homogeneously and heterogeneously permeable coalbed reservoirs. In preparation to Fuel.
4. Kumar H., Elsworth D., Liu J., Pone D., Mathews J., Optimizing ECBM recovery for unhindered production and CO_2 injectivity (International Journal of Greenhouse Gas Control, v11, 2012)
5. Kumar H., Lester E., Kingman S., Bourne R., Claudio A., Aled. J., John R., Halleck P., Mathews J., Inducing fractures and increasing cleat apertures in a bituminous coal under isostatic stress via application of microwave energy (International Journal of Coal Geology, v 88, 2011)

Conference Proceedings

Seven papers published in international proceedings.